Analysis of performance and results of a Steam Jet Ejector Chiller (Solar Cooling)

Master of Science Thesis – MSc. Energy & Environment

Karlsruher Institut für Technologie – Instituto Tecnológico de Buenos Aires

In cooperation with Hochschule Karlsruhe für Technik und Wirtschaft

Author: **Nicolás Carbonare** (1797915)

Tutors:

- Dr. Ferdinand Schmidt (KIT)
- Dipl.-Ing Tunay Özcan (HSKA)

Examiners:

- Prof. Dr. Ing. Martin Gabi (KIT)
- Dra. Ing. Cecilia Smoglie (ITBA)
- Prof. Dr. Ing. Michael Kauffeld (HSKA)

Karlsruhe, May 2016

Abstract

English

The German Government has the objective the reduce by 11% the electrical energy consumption until 2020. Cooling facilities represent 14% of this consumption and bring huge savings potential. Solar thermal cooling and heating facilities promise primary energy savings compared to electric vapor compression chiller systems. The aim of this study is to analyze the results of the ProSolar Project, performed by the Hochschule Karlsruhe für Technik und Wirtschaft (HSKA). The project, that formally ended in October 2015, has led to the opportunity to build a solar cooling prototype, with the cooperation of Ritter Solar GmbH, GEA Wiegand and Fraunhofer UMSICHT. The objective was the development of a cooling and heating facility (steam jet ejector) with a low primary energy consumption, as it does not involve fossil fuels and only requires auxiliary electricity. The operational performance during the Summer 2015 period is analyzed and the results and overall system performance are compared with other solar cooling facilities in Europe (small and large scale). Advantages and drawbacks are highlighted and future possibilities based on the operational experience gained are also mentioned.

Deutsch

Die Bundesregierung hat das Ziel ausgegeben, den Verbrauch elektrischer Energie bis zum Jahr 2020 um 11 % zu senken. Kälte- und Klimaanlagen verbrauchen in etwa 14 % dieser Energie und verfügen über hohe Einsparpotentiale. Solare Heizungs- und Kühlungsanlagen versprechen Einsparungen der Primärenergie, auch im Vergleich zu konventionellen Kompressionskälteanlagen. Das Ziel der Masterarbeit ist die Analyse der Ergebnisse des ProSolar Projekts, das von der Hochschule Karlsruhe für Technik und Wirtschaft (HSKA) durchgeführt wurde. ProSolar wurde im Oktober 2015 in Kooperation mit Ritter Solar GmbH, GEA Wiegand und Fraunhofer UMSICHT in Betrieb genommen. Ziel des Projekts war die Entwicklung eine niedrig-Energien Prototypen (Dampfstrahlkältemaschine), ohne den Einsatz fossiler Brennstoffe und einem möglichst geringen Anteil an Hilfsenergie. Der Betrieb der Anlage wird für den Sommer 2015 analysiert und die Leistung wird mit weiteren Kälteanlagen

in Europa verglichen. Vor- und Nachteilen werden beschrieben und zukünftige Verbesserungsmöglichkeiten werden zudem erwähnt.

Español

El gobierno alemán tiene como objetivo lograr un 11% de reducción de consumo eléctrico hasta el año 2020. En este escenario, las instalaciones de acondicionamiento de aire representan el 14% de este consumo total, con un enorme potencial de ahorro. Instalaciones a partir de energía solar prometen ahorrar energía primaria en comparación con sistemas convencionales a compresión. El objetivo de este estudio es analizar los resultados del proyecto ProSolar, llevado a cabo por la Hochschule Karlsruhe für Technik und Wirtschaft (HSKA). El mismo finalizó en octubre 2015 y permitió construir un prototipo solar con la cooperación de Ritter Solar GmbH, GEA Wiegand y Fraunhofer UMSICHT, cuyo objetivo fue funcionar sin combustibles fósiles y con electricidad auxiliar. Se analizará el rendimiento operativo y los resultados arrojados en el verano 2015, comparando los mismos con otras instalaciones en Europa, a mayor o menor escala. Ventajas y desventajas serán destacadas y las posibilidades futuras a partir de la experiencia obtenida también serán mencionadas.

Declaration of Authorship

I declare that I have developed and written the enclosed Master Thesis completely by myself, and have not used sources or means without declaration in the text. Any thoughts from others or literal quotations are clearly marked. The Master Thesis was not used in the same or in a similar version to achieve an academic grading or is being published elsewhere.

Karlsruhe, 17.05.2016

Place, Time

Signature

Table of Contents

List of Figures

List of Tables

List of Abbreviations

Abbreviation	Name
PEC	Primary Energy Consumption
PER	Primary Energy Ratio
LiBr	Lithium Bromide solution
PCM	Phase-change Materials
PCS	Phase-change Slurries
FPC	Flat Plate Collectors
GWP	Global Warming Potential
EER	Energy Efficiency Ratio
TDHP	Thermally Driven Heat Pumps
PE	Polyethylene
PV	Photovoltaics
DHW	Domestic Hot Water
COP	Coefficient of Performance
COPth	Thermal Coefficient of Performance
COPel	Electrical Coefficient of Performance
SJE	Steam Jet Ejector
SJEC/DSKM	Steam Jet Ejector Chiller
ABS	Absorption Chiller
HSKA	Hochschule Karlsruhe für Technik und Wirtschaft
ITBA	Instituto Tecnológico de Buenos Aires
KIT	Karlsruher Institut für Technologie
VTC	Vacuum Tube Collector
VBA	Visual Basic for Applications
SPS	Speicherprogrammierbare Steuerung - see PLC
PLC	Programmable Logic Controller
MAG	Membran Ausdehnung Gefäß (Expanding Membrane Vessel)
KPI	Key Performance Indicators
HS	Heat Storage

Nomenclature

Symbol	Variable	Measure
c	Heat Capacity	kJ/m2/K
I	Insolation Collector	W/m2
m0	Suction mass flow	kg/h
m1	Motive mass flow	kg/h
Q0	Cold Capacity	kW
Q2	Motive Heat	kW
Q1	Waste Heat (in cooling mode)	kW
QPTC	Heat Energy of PTC	kWh/m2/a
p0	Suction pressure	Pa
p1	Motive pressure	Pa
pc	Condenser pressure	Pa
T0	Temperature of the cold operation for the Carnot heat pump and	K
	Evaporator Temperature	°C
T	Temperature	K
T1	Temperature of the heat sink for the Carnot heat engine and	K
	Temperature of the heat sink for the Carnot refrigeration system	K
T2	Carnot refrigeration system, low temperature level	K
Ta	Ambient temperature	°C
Tc	Condenser Temperature	°C
Tcol	Collector Temperature	°C
Tdrum	Steam Drum (Generator) Temperature	K
Tr	Room Temperature	°C
t	Time	h
W	Work (Carnot cycles)	kW
Wpump	Electricity input to the pump	kW
ηcol	Efficiency collector	%
ηpv	Efficiency photovoltaic panel	%
ηtot	Total efficiency	%
εcool	Refrigeration cycle efficiency	%
ξ	Process Quailty	%
I	Solar irradiation	kW/m2
Apv	Surface of solar PV cells	m2
Acol	Surface of solar collector	m2
FR	Collector Heat Removal Coefficient (for FPC)	-
UL	Collector Overall Heat Losses (for FPC)	W/m2
τ	Coefficient of transmission	-
α	Coefficient of absorption	-
WBT	Wet Bulb Temperature	°C
DBT	Dry Bulb Temperature	°C

Bibliography

"Cooling heating and power for industry: a market assessment. Resource Dynamics Corporation" (2003) US Department of Energy, Washington DC, USA. http://www.eere.energy.gov/de/pdfs/chp_industry_market_assessment_0803.pdf

ASTM G 173-03 - "*Standard Tables for Reference Solar Spectral Irradiances: Direct Normal and Hemispherical on 37° Tilted Surface,*" ASTM International, 2003.

Bauer, Irmgard (2014) – *"Solarthermische Dampferzeugung"* – Ritter Gruppe – ProSolarDSKM Project, Karlsruhe, Germany.

Bejan, Adrian (2006) – *"Advanced Engineering Thermodynamics"* – Duke University, Durham, North Carolina, USA. John Wiley & Sons, Inc.

J. Deng, R.Z. Wang, G.Y. Han (2010) – *"A review of thermally activated cooling technologies for combined cooling, heating and power systems"* - Institute of Refrigeration and Cryogenics, Shanghai Jiao Tong University, Shanghai, China and Department of Aerial Four Stations, Xuzhou Air Force College, Xuzhou, China.

Dietzmann, Thilo (2014) – "Dampfstrahl-Kühlanlagen" – GEA Wiegand GmbH – ProSolarDSKM Project, Karlsruhe, Germany.

Eicker, Ursula (2012) – "Solar Thermal or Photovoltaic cooling?" – Presentation Intersolar Europe 2012– Research Center Sustainable Energy ZAFH.NET – University of Applied Sciences, Stuttgart, Germany.

Helm, Martin; Hagel, Kilian; Hiebler, Stefan; Schweigler, Christian (2009) - *"Solar Heating and Cooling with Absorption Chiller and latent Heat Storage"* - Bavarian Center for Applied Energy Research (ZAE Bayern), Garching, Germany.

Helm, Martin; Hagel, Kilian; Hiebler, Stefan; Pfeffer, Werner; Hiebler, Stefan; Schweigler, Christian (2013) - *"Schlussbericht: Solares Heizen- und Kühlen mit Absoprtionskältemaschine und Latentwärmespeicher."* - Bavarian Center for Applied Energy Research (ZAE Bayern), Garching, Germany.

Henning, Hans-Martin; Morgenstern, Alexander; Wiemken, Edo (2014) – *"Kolloquium Solare Kühlung im Rahmen des BMBF-Verbundprojekts ProSolarDSKM"* - Fraunhofer ISE Freiburg and Hochschule Karlsruhe, ProSolarDSKM Project, Karlsruhe, Germany.

Jähnig, Dagmar; Thuer, Alexander (et. Al. 2011) – "D-A3b: Monitoring Results. A technical report of subtask A (Pre-engineered systems for residential and small commercial applications)". Austrian Institute of Technology (AIT), Giefinggasse 2, A-1210 Vienna, Austria.

Jähnig, Dagmar (2010) – *"D-A1: Market Available Components for Systems for Solar Heating and Cooling with a Cooling Capacity < 20 kW. A technical report of subtask A".* AEE INTEC, Gleisdorf, Austria.

Joemann, Michael (2014) – "Zusammenspiel aller Komponenten. Erste Ergebnisse mit der Gesamtanlage" – Fraunhofer UMSICHT – ProSolarDSKM Project, Karlsruhe, Germany.

Kim, D.S.; Infante Ferreira, C.A. (2007) - *"Solar refrigeration options – a state-of-the-art review".* Arsenal Research, Sustainable Energy Systems, Vienna, Austria and Delft University of Technology, Engineering Thermodynamics, CA Delft, Netherlands.

Krause, Michael (et. Al. 2010) – "State of the art – Survey on new solar cooling developments. A technical report of subtask C". Solar Cooling & Heating Programme. Solar Air-Conditioning and Refrigeration. International Energy Agency (IEA) - Task 38. Paris, France.

Kühn, Annett (2013) – *"Thermally Driven Heat Pumps for Heating and Cooling"* - Universitätsverlag der TU Berlin, Berlin, Germany.

Malenkovic, Ivan (2012) - *"Definition of Performance figures for solar and heat pump systems: Technical Report 5.1.3".* Austrian Institute of Technology, Vienna, Austria.

Schmidt, Ferdinand (2015) – *"Energy and Indoor Climate Concepts for High Performance Buildings"* Literature – ENTECH – Karlsruher Institut für Technologie, Karlsruhe, Germany.

Pridasawas, Wimolsiri (2006) - "*Solar-Driven Refrigeration Systems with Focus on the Ejector Cycle*" – Doctoral Thesis - Royal Institute of Technology, KTH – Stockholm, Sweden.

Pollerberg, Clemens; Ahmed Hamza H. Ali; Dötsch, Christian (2008) – *"Solar driven steam jet ejector chiller"* - Fraunhofer Institute for Environmental, Safety and Energy Technology

UMSICHT, Oberhausen, Germany and Department of Mechanical Engineering, Faculty of Engineering, Assiut University, Egypt.

Riepl, Manuel (et. Al. 2012) – "Operational performance results of an innovative solar thermal cooling and heating plant" – ZAE Bayern – Garching, Germany.

Weiss, Werner; Biermayr, Peter (2008) – "*Potential of Solar Thermal in Europe*" – RESTMAC Project, European Solar Thermal Industry Federation Federation (ESTIF), Bruxelles, Belgium.

Annex Sources

Incropera, Frank P (2007) - "Fundamentals of heat and mass transfer". 6th edition. John Wiley & Sons. United States of America.

Kumana, Jimmy D.; Kothari, Samir P.; Henningson, Durham, and Richardson, Inc. (1982) - *"Predict Storage Tank Heat Transfer Precisely Use this procedure to determine the rate of heat transfer from a vertical storage tank when shortcut methods are inadequate."* Chemical Engineering Magazine.

Lammers, Enrico (2011) - *"Heat loss calculation in a vertical and horizontal storage and in a pipeline"*. Pro6com Engineered Solutions.

National Institute of Standards and Technology (NIST)– Engineering Statistics Handbook http://www.itl.nist.gov/div898/handbook/mpc/section5/mpc55.htm - United States of America.

WeatherSpark.Com – Average Weather conditions for the región of Karlsruhe – Baden-Baden. https://weatherspark.com/averages/28657/Baden-Baden-Karlsruhe-Baden-Wurttemberg-Germany

White, Frank M. (2009) – "*Fluid Mechanics*". 7th edition. McGraw-Hill Series. University of Rhode Island, United States of America.

1. Introduction

After the oil World crisis in the mid 70s and the accident in Chernobyl, Ukraine in 1986 began discussions about the energy consumption and its future consequences. The immediate result was the signature of the Kyoto Protocol on 1997, raising the global concerns about the environmental impact of human activities (in the frame of the United Nations Framework Convention on Climate Change). The objective was to fight global warming reducing greenhouse gases emissions.

The appearence of renewable energies made a huge contribution to these efforts, ont only by making possible the power generation through clean sources, but also as non expirable, such as solar radiation or wind energy. Research was carried out with the development of these technologies throughout the last 40 years. Solar energy conversion consists of a large family of different technologies, with a broad range of applications. Whereas solar technologies can deliver heat, cooling, natural lighting, electricity, and fuels, this work concentrates on the use of solar energy in cooling applications.

The interest on the development of these technologies arises while looking at the energy demand profiles. The next figure shows the energy demand in Germany on 2006, divided into heat and electricity (Source: Weiss (et. Al. 2008)).

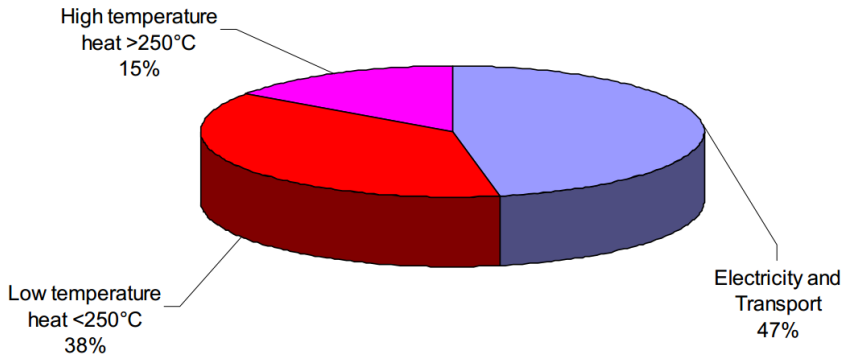

Figure 0-1: Energy Demand in Germany 2006 (Total 2600 TWh).

As it can be seen, the low temperature heat represents 38% of the total energy consumption. This is the sector that shows potential energy savings through the implementation of solar energy. What is more, the next graphic (Source: Weiss (et. Al. 2008)) shows the energy consumption for Germany from heating and cooling.

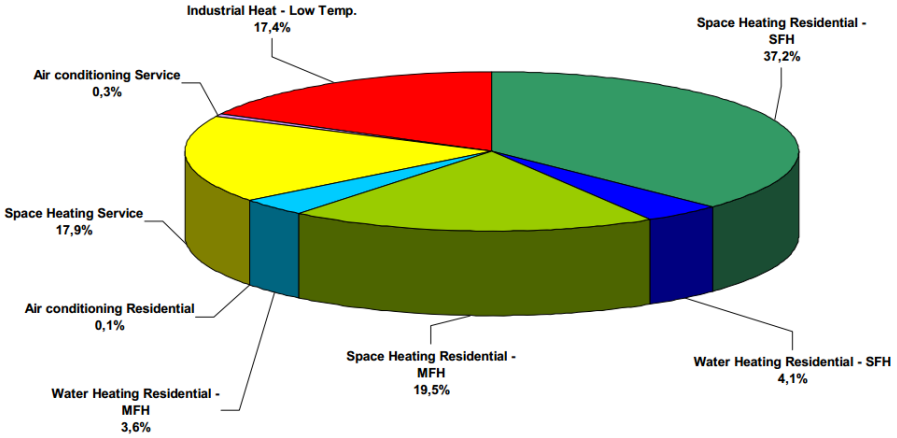

Figure 0-2: Heating and cooling energy demand in Germany 2006 (Total 980 TWh).

A total of 980 TWh are consumed in Germany from heating and cooling. Residential consumption represents the 65% of these demand. Only focusing on heating and cooling systems, the energy demanded is 57% of the total.

In this direction, the Hochschule Karlsruhe (HSKA) developed the Prosolar DSKM Project, in order to develop a potential solar heating and cooling system, based on a steam jet ejector chiller and driven with 100% renewable energy (only auxiliary electricity). The project was funded by the Bundesministerium für Bildung und Forschung (Förderkennzeichen 01 RI 0908) and companies and institutes GEA Wiegand, Ritter Solar und Fraunhofer-Institut für Umwelt-, Sicherheits- und Energietechnik UMSICHT took part in the project and helped in the development of the proposed solution.

The system consists of a nominal 82 KW steam jet ejector chiller driven with 400 m^2 vacuum tube solar collectors, and assisted by a wet open cooling tower, in order to air-condition a 3130 m^2 building (LB Building of the HSKA). The development of heat and cold energy storages was proposed and carried out, in order to serve as buffer in operational oscillations and to fulfill with the designed conditions.

The aim of this work is to study the operational results of the facility during its first full summer of operation, on the year 2015. The results and performance indicators are calculated and the operation is analyzed. A comparison with similar facilities of different approaches is carried out to benchmark the current situation of the HSKA Installation and to identify potential future improvement opportunities.

2. Solar Cooling Technologies

In this chapter the basic elements to understand a solar cooling technology will be introduced, making special focus in the three methods that are subject of this study. A short comparison of the methods is carried out at the end of it.

2.1 Introduction

The main concept of solar cooling technologies is based on using the solar radiation as the driving force for air conditioning. There are several systems that were developed during the last decades around this idea, which are usually utilized during winter for cooling and summer for heating. The next figure presents an overview of these mentioned technologies:

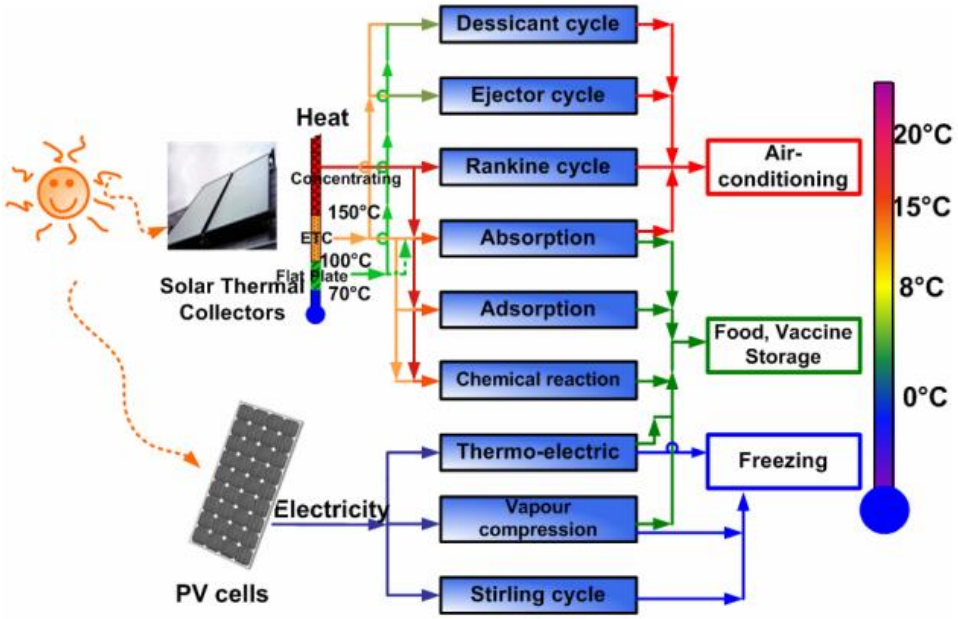

Figure 0-1: Solar cooling Technologies. Source: Pridasawas (2006).

Here are presented two main possibilities. The first one involves the use of solar collectors and provides a thermal compression instead of a mechanical compression. With this technology nowadays it is difficult to reach below zero temperatures, which is a big limitation for some specific applications. In the case of air conditioning, it is usually cold enough to produce a cycle. During winter it is possible to perform the heating (or also domestic how water (DHW)) utilizing directly the heat obtained with the solar collector to produce steam. A big advantage of these technologies is that it creates independence from the power grid, as it requires only electricity for the operation of pumps and fans. However, they usually need a back-up system to reach a regular operation.

In contrast with thermal compression, it is also possible to use mechanical compression for air conditioning. This technology is proven all over the World, as it has been used for the last decades as the main system commercially available for air conditioning. However, the mechanical compressor requires a big amount of electrical power to run, leading to an increasing energy consume. The focus here is to supply the electricity with solar photovoltaic (PV) panels, and using the mechanical compression to perform both cooling (chillers) and heating (heat pump). However, the PV panels and conventional chillers usually lead to a load mismatch in the power grid. Next figure summarizes both possibilities.

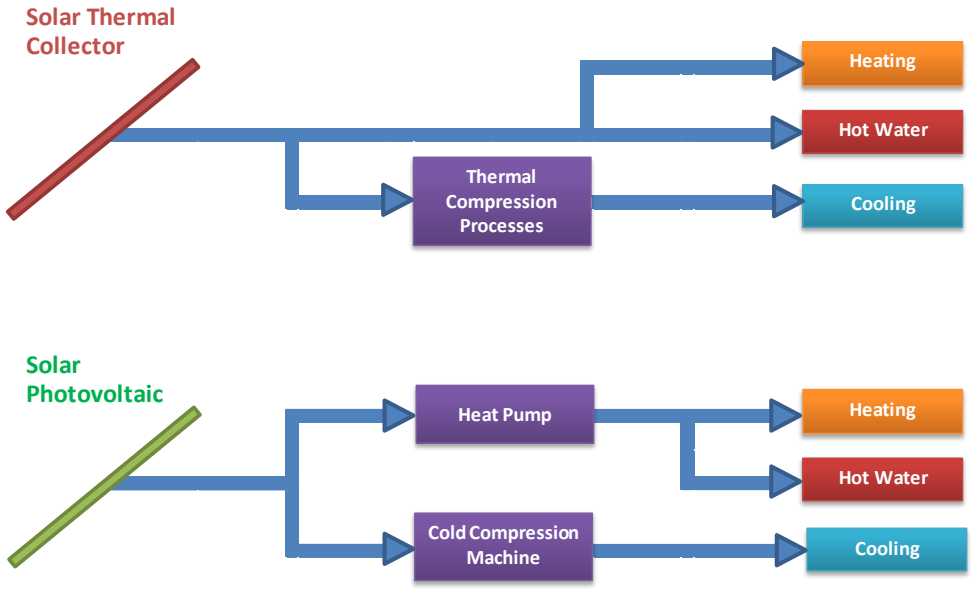

Figure 0-2: Solar technologies.

Therefore, this study will focus on three selected technologies to analyze and compare the results in difference pilot plants and research studies. Steam Jet Ejector, Absorption pump and solar PV + conventional chiller were the technologies selected. They will be described more in detail in the following sections.

2.2 Solar Energy

In this subsection, an introduction to the principle of work of different solar panels will be carried out. Efficiencies and performance indicators will be presented as well.

A solar collector is a device that captures the solar radiation (absorption of sunlight) and transforms it into heat. There are different existing configurations, in order to optimize the capture of the radiation and raise the performance of these systems, depending of the different applications. Per definition, any collector efficiency is calculated as the ratio between the useful heat obtained and the solar gains, represented by the solar irradiation I and the total collector surface.

$$\eta_{col} \equiv \frac{Q_{useful}}{I \; x \; A_{col}} \qquad (2.1)$$

Among the several types of available collectors in the market, only focus on the collectors of main interest will be made.

Flat Plate Collectors (FPC) are the simplest ones. The sun radiation is filtered by a glass cover and absorbed by a flat plate, usually welded to the tubes, where the water flows. It is important to add an insulation to reduce the heat losses. The next figure illustrates the basic construction described:

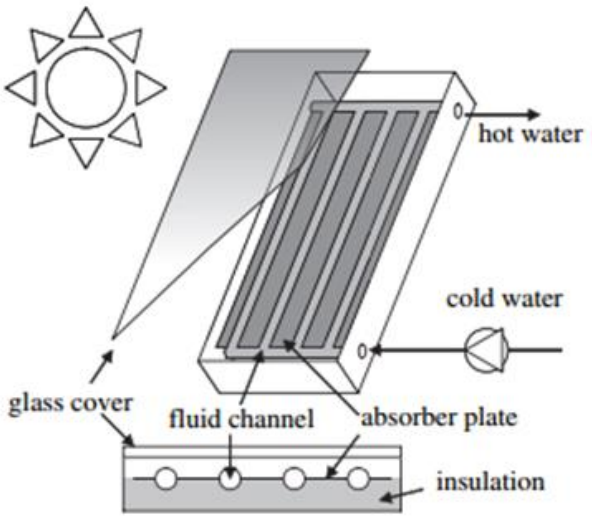

Figure 0-1: Flat plate collector. Source: Kim, Infante Ferreira (et. Al. 2007).

The thermal efficiency of these collectors is represented by the following equation,

$$\eta_{FPC} = F_R\tau\alpha - F_R U_L \frac{(T_{col} - T_a)}{I} \quad (2.2)$$

where F_R is the heat removal factor, U_L is the overall heat loss coefficient, Tcol is the collector average temperature, α is the absorption coefficient of the plate and τ is the transmission coefficient of the glazing. This equation shows a linear relationship between the temperatures and the efficiency, assuming all properties as constant. The first term of the equation is then considered constant and it is called Optical Efficiency.

Another collector type of interest will be the Vacuum Tube Collectors (VTC). The main design is based on glass tubes concentric with the copper tubes (fluid channel), using vacuum as isolator. In standard conditions, they present higher efficiencies in comparison with FPC. The next figure illustrates its basic construction.

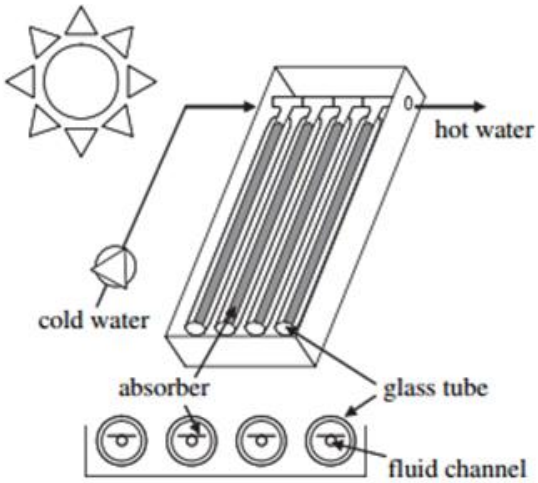

Figure 0-2: Vacuum Tube collector. Source: Kim, Infante Ferreira (et. Al. 2007).

The efficiency of these is given by the following equation,

$$\eta_{VTC} = \eta_0 - k1\frac{(T_{col} - T_a)}{I} - k2\frac{(T_{col} - T_a)^2}{I} \quad (2.3)$$

where η_0 represents the optical efficiency, and k1 and k2 are heat losses. The technical background is the same as the FPC equation, although in this particular case they are grouped into constants. This occurs in an attempt to follow Clemens Pollerberg (2008) research on solar collectors for solar cooling techniques, who studied them and calculated empirically these constants for these collectors.

Parameter	Value PTC	Value VTC	Unit
Optical efficiency, η_0	0.6	0.64	Dimensionless
Linear heat loss, $k1$	0.1	0.688	$W/m^2/K$
Quadratic heat loss, $k2$	0.0075	0.004	$W/m^2/K^2$
Heat capacity, c	7.5	13.06	$kJ/m^2/K$

Figure 0-3: Parameters of the efficiency equation Source: Pollerberg (2008).

The heat capacity *c* is higher in VTC than in PTC, which means that changes in solar irradiation are less sensitive in VTC (higher power output).

Photovoltaic cells (PV) are used to convert solar energy to electricity. They take advantage of the photoelectric effect to produce it. When light shines on a PV cell, it may be reflected, absorbed, or transmitted, but only the absorbed generates electricity. The energy of the absorbed light is transferred to electrons in the atoms of the PV cell semiconductor material. With their newfound energy, these electrons escape from their normal positions in the atoms and become part of the electrical current, in a circuit. Although the design of these cells depend strongly on the use of it and it is not a subject of study of this thesis, the next figure shows a basic design of a photovoltaic system.

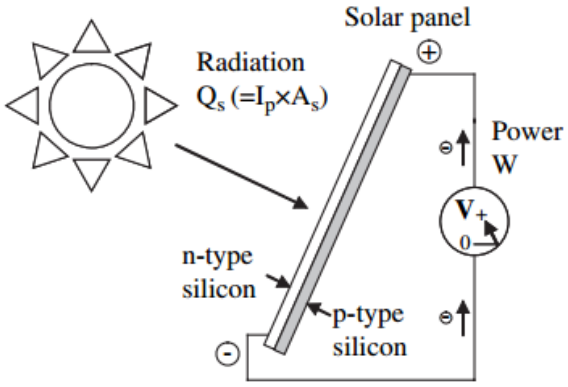

Figure 0-4: Photovoltaic system. Source: Kim, Infante Ferreira (et. Al. 2007).

2.3 Thermodynamic Fundamentals of Cooling processes

Firstly, any cooling system has the Carnot Refrigeration Cycle as the ideal thermodynamic reference cycle for its development. The main concept is to take heat from a cold source (operating at T_0) and to transfer it to the ambient (working at T_1). As this is driven from a cold source to a heat sink (ambient), it needs useful work to be performed (W). In conventional chillers, this power is supplied by the mechanical compression, the heat removal Q_0 takes

place during the expansion and the heat transfer to the environment, during the condensation. The following figure illustrates a ph-diagram of this cycle.

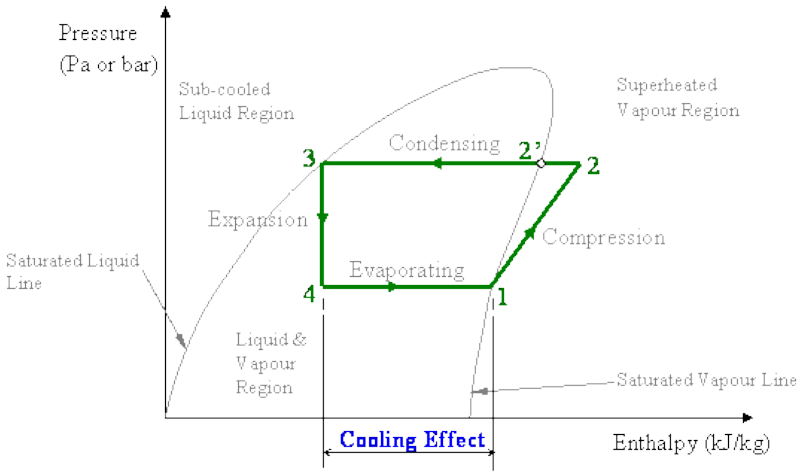

Figure 0-1: ph Diagram. Source: http://www.arca53.dsl.pipex.com/

The conventional refrigeration cycle is illustrated as a heat pump in the figure 2-4. It is also defined the efficiency of the cycle, as dividing what is obtained (heat removal Q_0) over what is spent for it (useful work W).

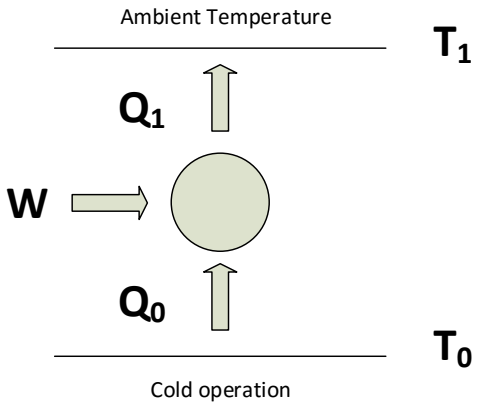

$$\varepsilon_{cool} = \frac{Q_0}{W}$$

Figure 0-2: Conventional refrigeration cycle.

Moreover, here are presented the Thermally Driven Heat Pumps (TDHP). As stated by Annett Kühn (et. Al. 2013), "Thermally driven heat pumps (TDHP) work at three temperature levels. Driving heat Q_2 is supplied at a high temperature level. Useful cold (cooling operation) or low temperature heat (heating operation) Q_0 is supplied at a low temperature level. The sum of the heat supplied is released at a medium temperature level. Q_1 is the useful heat in heating operation. In cooling operation, it is usually released to the environment. However, medium

and low temperature heat can also be used simultaneously for heating and cooling purposes". This is like operating a Heat Engine and a Heat Pump in the same system. Therefore, the useful work obtained by the heat engine (solar collector) is used to drive the heat pump and perform the cooling. The next figure illustrates what is explained above.

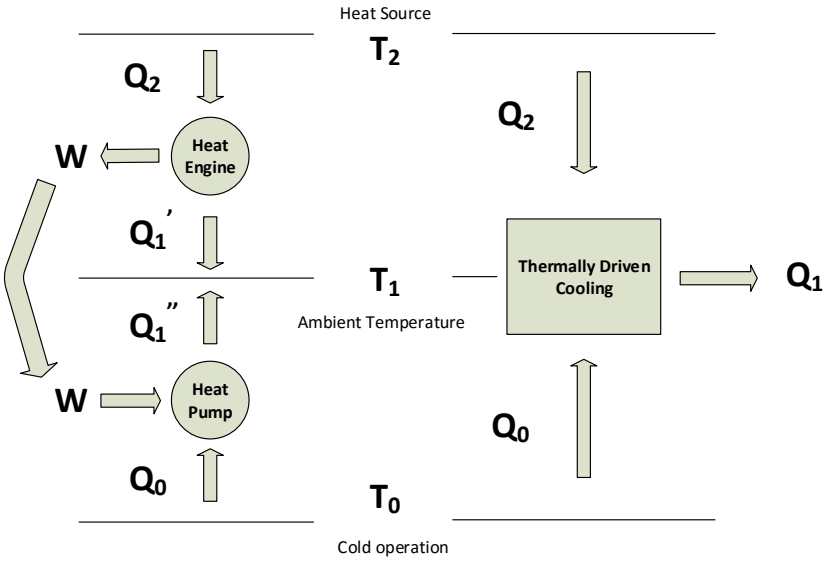

Figure 0-3: Thermally driven cooling scheme.

The heat Q_0 and useful work W can be obtained by the following formula, in ideal conditions (no friction):

$$Q_0 = \frac{T_0}{T_1 - T_0}\, x\, W \tag{2.4}$$

$$W = \frac{T_2 - T_1}{T_2}\, x\, Q_2 \tag{2.5}$$

Consequently, a relationship between the cooling power Q_0 and the driving solar power Q_2 can be obtained. It is defined as the Coefficient of Performance (COP), diving the useful heat in each operation by the driving force (Source: Kühn (2013)).

$$COP_C = \frac{\dot{Q}_0}{\dot{Q}_2} \quad for\ cooling\ operation \tag{2.6}$$

$$COP_h = \frac{\dot{Q}_1}{\dot{Q}_2} = 1 + COP_C \quad for\ heating\ operation \tag{2.7}$$

These coefficients are thermal, as the electrical power needed is usually negligible. It is possible then to define an electrical COP, replacing Q_2 for the electricity consumed in the denominator.

In addition, it is necessary to distinguish between the real COP (provided by the formulae above, with measured heat) and the ideal COP (thermodynamic limit of operation). This ideal COP is impossible to reach, due to several unavoidable losses (such as mechanical friction in machines, etc.). Combining the definition of COP and the Q_0 and W thermodynamically ideal equations, it is possible to obtain as a result the thermodynamic limit of operation (Henning et. Al., 2014):

$$COP_{Carnot} = \frac{1 - \frac{T_1}{T_2}}{\frac{T_1}{T_0} - 1} \tag{2.8}$$

Furthermore, the Process Quality ξ is defined as the ratio of the real COP (often called thermal Energy Efficiency Ratio – EER_{th}) and the thermodynamic limit of the cooling process.

$$\xi = \frac{EER_{th}}{COP_{Carnot}} \tag{2.9}$$

In this work, the EER_{th} will be often called as COP (referred always as the real one, otherwise it will be stated). It is considered a matter of importance to make clear that both refer to the ratio of power over consumed thermal energy by the system. Following the program "Intelligent Energy Europe" with the report of the Austrian Institute of Technology, COP will be used for heating power and EER for cooling power, both having the same definition. Besides, the COP/EER will be always thermal ratios. In case of obtaining electrical COP it will be clarified.

2.4 Principle of Work

2.4.1 Steam Jet Ejector Cooling

A Steam Jet Ejector system consists of three basic subsystems

- Steam Generator
- Cooling Load

- Cooling Machine

The steam generator can be driven by different energy sources. The objective of these studies is to analyze its performance with solar power (usually collectors). The cooling load is represented by the requirements of the building, and driven by the chilled water. The cooling machine is composed basically by the Steam Jet Ejector Chiller (SJEC – Compressor, Evaporator and Condenser) and the Cooling Tower, necessary to keep the condenser's temperature as low as possible. An illustration of the complete system is further presented.

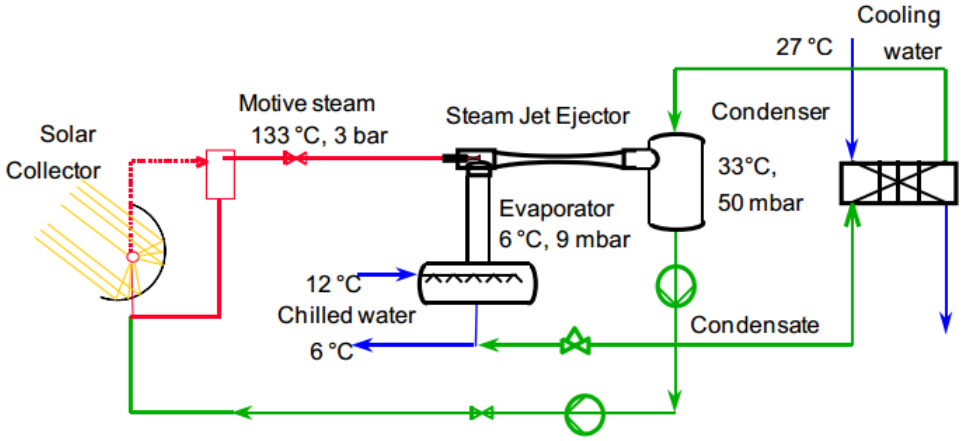

Figure 0-1: Steam Jet Ejector System. Source: Kühn (2013)

The solar heat from the collector is used to produce steam in a steam drum. This later enters the SJE as the Motive Steam at a relative high pressure (0.3 MPa) and temperature (133°C). Following Clemens Pollerberg (et. Al. 2008) description, "it pumps the vaporous refrigerant from the evaporator into the condenser against a higher pressure and reduces the pressure in the evaporator (up to 10 hPa). The pressure reduction causes boiling of the remaining liquid water in the evaporator and generates cold water, which is fed to the convective cooler". The mixture (motive and suction mass flows) flows at supersonic speed and enters the condenser (50 hPa, 33°C). Condensed mixture is cooled at a cooling tower, and after that it flows back to the evaporator and steam drum respectively. A qualitative ph-diagram is presented by Pridasawas (2006) in the following picture:

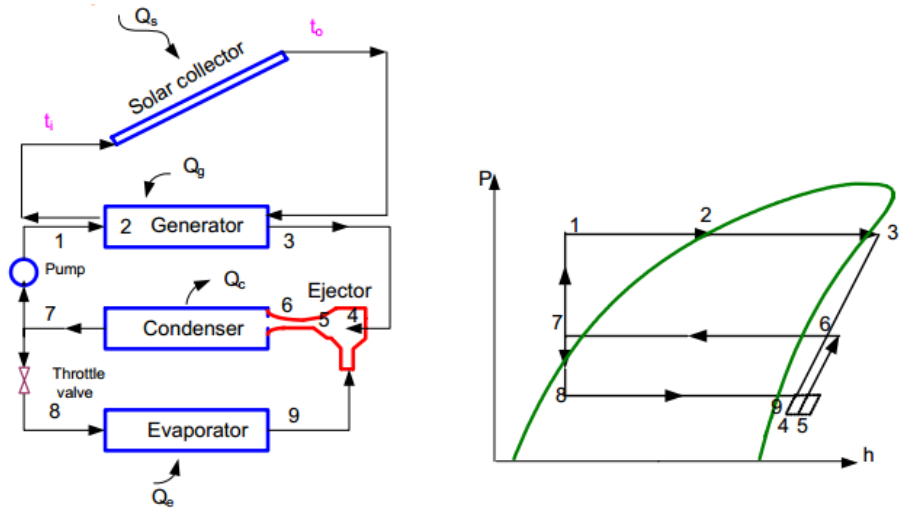

Figure 0-2: SJEC ph diagram. Source: Pridasawas (2006).

To improve the overall performance of the system, multi-stage ejectors were proposed, raising the entrainment of the suction steam. A scheme is thus proposed again by Pridasawas in his work.

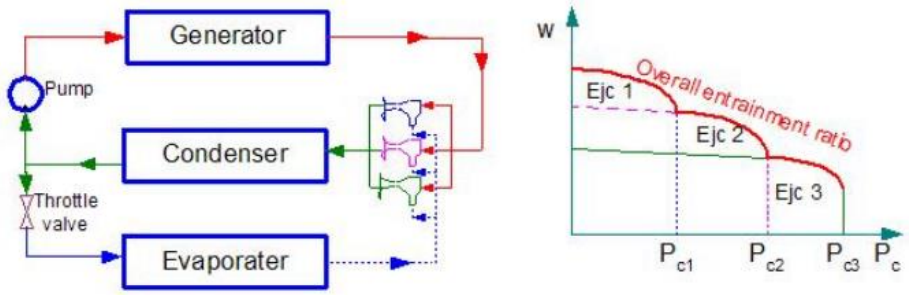

Figure 0-3: Multi-stage SJEC. Source: Pridasawas (2006).

Following the figure 2-11, the COP can be calculated with the in- and outlet enthalpies. As seen before, the COP is the ratio of the cooling power over the generated power (steam drum). Therefore, the COP could be calculated with the following equation.

$$COP = \frac{Q_{cool}}{Q_{gen}} = \frac{m_e\,(h_9 - h_8)}{m_g\,(h_3 - h_1)} \qquad (2.10)$$

Furthermore, some of the advantages listed in several studies are its good partial load behaviour (moderate mean COP with solar power) and the possibility to use water as a refrigerant (manipulated without risks). The necessary temperatures in the steam drum can be easily reached with VTC or PTC, according to Clemens (et. Al. 2008). The EER/COP can be

obtained with the definitions listed above, following the general equations. According to Clemens (2008), these are the main advantages of the SJEC.

- "These results in general indicate that the COP increases with decreasing condenser temperature, which is determined by the source temperature of the cooling medium (…) and so it is important to optimize the condenser design in order to maximize the performance of the system.
- The evaporator temperature has less effects on the COP compared to the condenser temperature and is more dependent on the application and the systems chosen for distribution of the cold.
- When the temperature of the condenser cooling water is low, it permits reducing the motive steam pressure and consequently the motive steam consumption without affecting the system cooling capacity".

2.4.2 Absorption Chiller

There are several absorption pump systems, regarding different refrigerants and absorber materials. In this special opportunity, focus will be made in the Lithium Bromide-water absorber, which is the technology applied for the further comparison. The basic working cycle is depicted in the next figure.

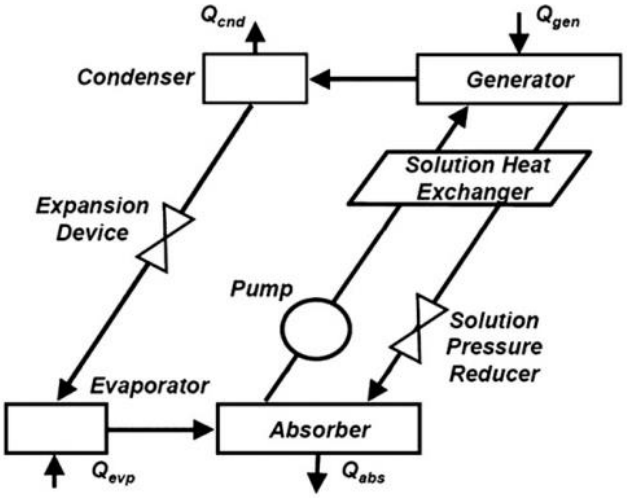

Figure 0-4: Absorption chiller. Source: Deng (et. Al. 2011)

The cycle begins in the evaporator, where heat is extracted (cooling effect) and gained by the refrigerant (water). The water evaporates and flows to the absorber, where it is absorbed by a strong Lithium Bromide (LiBr) solution. This process leads to a heat release due to the absorption, and after that the LiBr solution becomes weak. This weak solution is pumped to the generator to be heated. The heat added desorbs from the solution in vapour form, making it strong again. The water vapour flows to the condenser, where it condenses and releases heat to the ambient. The cycle begins again when the condensed water flows to the evaporator, through an expansion device. The strong solution goes back to the absorber and is ready to work again in the next cycle. The whole system operates below atmospheric pressure, since the water is used as a refrigerant. The next figure shows a pump cycle plotted in a P-T diagram.

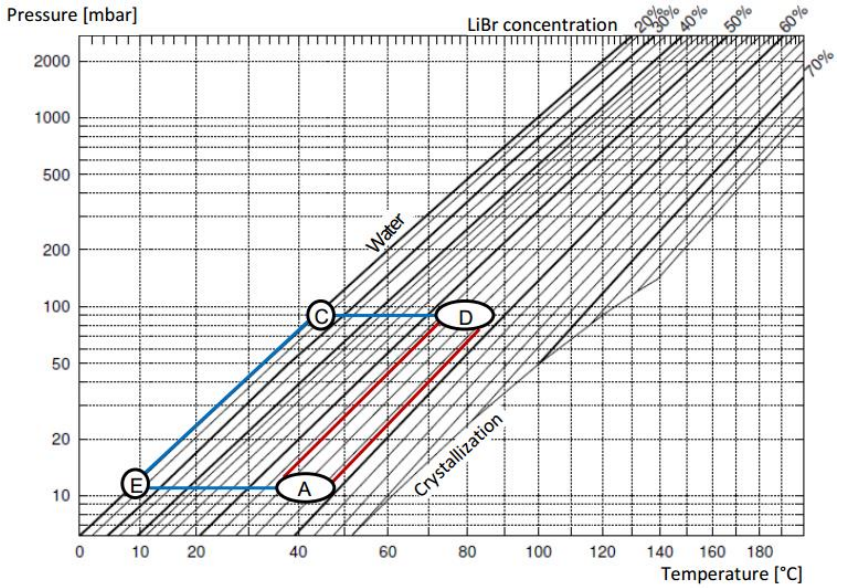

Figure 0-5: Absoprtion chiller PT diagram. Source: Kühn (2013)

The application of this system is obviously limited to 0°C, the freezing point of water. Traditional absorption chillers are powered with steam or hot water, besides utilizing partial or back-up direct fired heating. Another possibility is to drive these chillers with waste heat, improving process efficiencies. Single and double effect chillers are presented in commercial systems nowadays, whilst triple effect chillers are still in development and are a current subject of study. As seen in the SJEC, this absorption chiller can be operated through renewable energy sources, reducing considerably the amount of electricity consumed. Therefore, it is fundamental to know to what extent this can be applied and work reliably in different scenarios.

2.4.3 Solar PV + Compression Chiller

These systems are a combination of a conventional air conditioning device with solar photovoltaic panels. In this case, the electrical power to drive the chiller (mechanical compression) comes from the PV panels instead of the network. The refrigeration cycle that drives the chiller have been previously described. The next figure illustrates a general configuration of these systems.

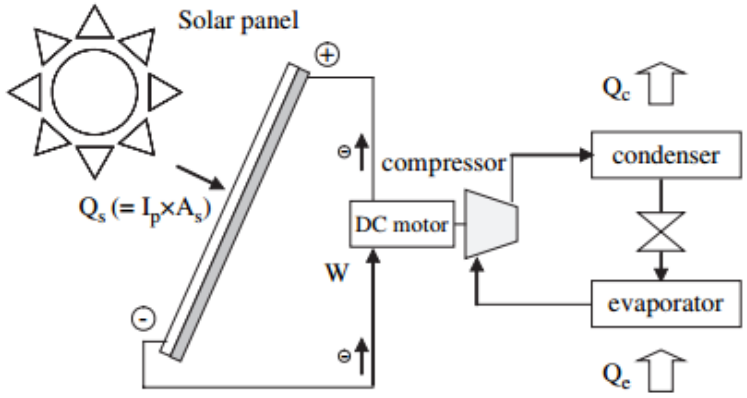

Figure 0-6: Solar PV cooling. Source: Kim, Infante Ferreira (et. Al. 2007).

As a main advantage, compression chillers are a widespread proven technology, and the forthcoming cost degradation of the PV panels in the recent years. Nevertheless, the integration of the panels to the network is still an issue, as it leads to a load mismatch in the grid. In addition to this, there is a high Global Warming Potential (GWP) due to the use of harmful refrigerants.

The efficiency for this system is obtained by combining the single efficiencies of each subsystem (PV + Conventional cooling) and multiplying them. The following formula shows the result:

$$\eta_{tot} = \eta_{PV}\ x\ \varepsilon_{cool} = \frac{W}{G\ x\ A_{PV}}\ x\ \frac{Q_0}{W} \qquad (2.11a)$$

$$\eta_{tot} = \frac{Q_0}{G\ x\ A_{PV}} \qquad (2.11b)$$

The total efficiency is given by the relationship between the cooling output and the solar gains of the PV cell.

2.5 Conclusion

After successfully describing the basics of each cooling system, it is considered important to highlight the main aspects of interest.

The systems that are subject of study are composed by different elements previously described, each of them conforming successive subsystems. Even though is can be hard the make a proper comparison, focus will be made on efficiencies, costs and limits of operation and application of each facility. As a previous statement, following the directives of Dr. Schimdt's lecture (KIT – 2015), investment costs for solar thermal air-conditioning is still at a factor of 1,5 to 2,5 higher than conventional technologies, whereas the operative costs remain between 10% to 40% higher, depending on the size of the facility. Further development is expected in order to make these technologies market-competitive.

To make a final statement, the next figure was obtained from the studies or Dr. Kim and Dr. Infante Ferreira (2007). It presents a good overview of different solar cooling technologies (some of them previously described, whereas some others are not), their efficiencies and COPs and approximate costs related to year 2007.

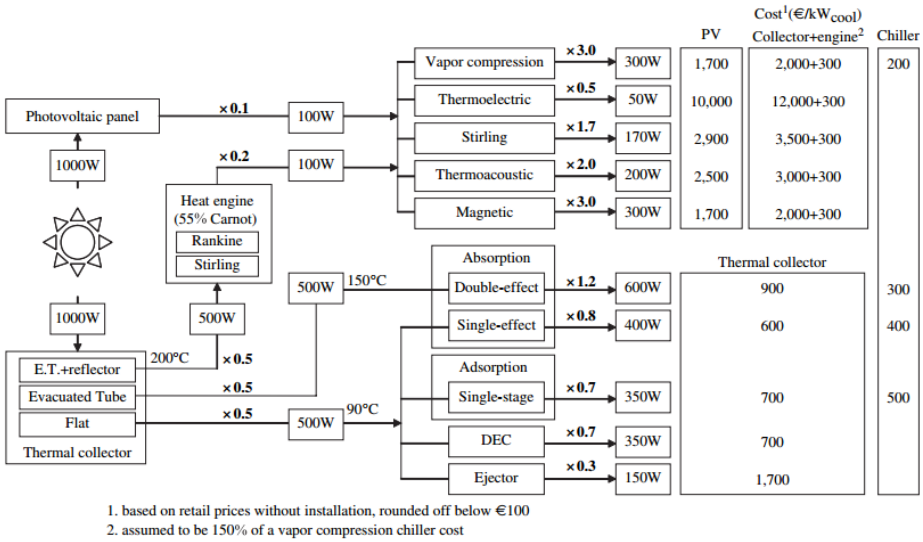

Figure 0-1: Costs overview. Source: Kim, Infante Ferreira (et. Al. 2007).

It was decided to make the comparison between the SJEC present in the Hochschule Karlsruhe and the main technology: double-effect absorption chiller. Other technologies will be considered as well. These comparisons will be developed in the next chapters.

3. Steam Jet Ejector System

3.1 Introduction

In this chapter, the whole analysis of the collected data from the facility in the Hochschule Karlsruhe (HSKA) will be carried out. Firstly, a thorough description of the system is made in order to understand every detail involved. Moreover, a database is created with the measurements of the system during the year 2015. The Key Performance Indicators that will be used in further chapters are introduced. At the end of this section, a complete flow chart of the facility is attached.

3.2 Steam Jet Ejector Facility in the Hochschule Karlsruhe

The SJE system can be divided, as stated in the previous chapter, into three basic subsystems: the solar collectors field, the cooling load (building requirements) and the cooling generation (SJEC and auxiliary components). The description of them will be fulfilled in this section, although the cooling load subsystem is not a subject of study in this work. A summary of this facility is shown in the next figure. The objective of this facility is to provide air-conditioning to the building LB in the Hochschule Karlsruhe. The estimated air-conditioned area is around 3130 m^2.

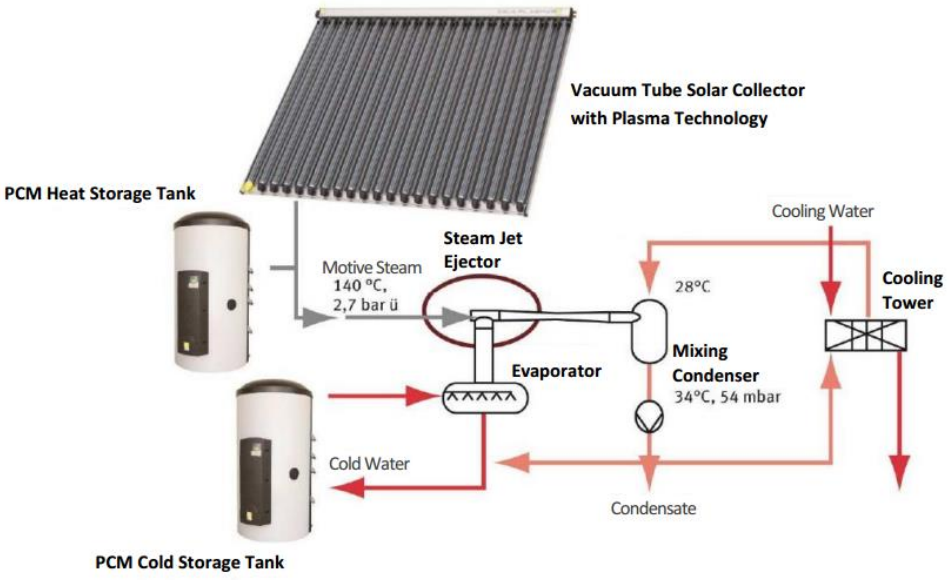

Figure 0-1: SJEC Facility. Source: Short Description ProSolarDSKM (2014)

It is of utmost importance to clarify that this facility is solar autonomous, which means that it does not contain a backup system. This makes the system greener, even though sometimes it might not guarantee every indoor air desired state. Buffers (heat storages) were designed

in order to couple the facility with the cooling demand efficiently. Another consequence of the solar autonomous condition is that the size of the solar collector field is dimensioned to fully cover the heat demands (in Winter, and the heat to cover the ejector demands in Summer), rather than being optimized to the minimum cost.

3.2.1 Solar Collectors subsystem

The solar collectors' subsystem consists basically of:

- Vacuum Tube Collectors
- Steam Drum (steam generation)
- Latent Heat Storage (PCM)
- Water storage and pressure regulation (MAG)

The next figure depicts its basic flow chart. The red arrows represent the path of the water that flows through the collectors.

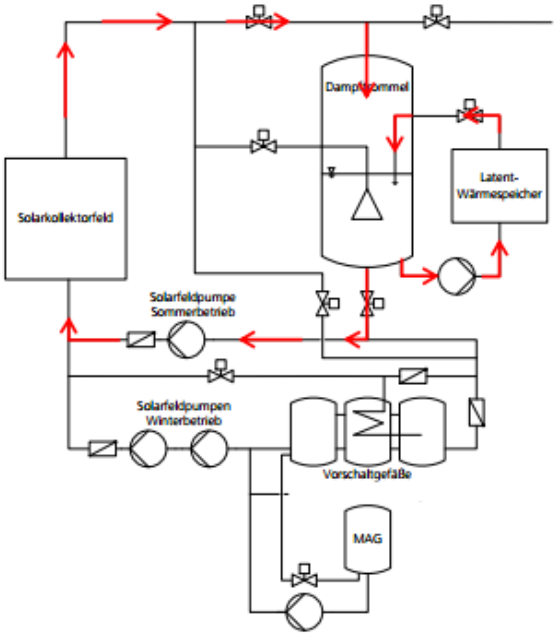

Figure 0-2: Solar collectors' subsystem. Source: Joemann (2014).

Solar radiation is converted to heat by the solar collectors. The storage tank is used as thermal storage when solar radiation is not sufficient. The solar field in the HSKA is performed by VTC with a total of 360 m^2 of surface. These are eight rows of ten collectors, each one with a surface of 4.5 m^2. Therefore, this represents an approximate total of 200 kW in the solar field. The collectors have a south orientation and a slope of 30°. This value depends on the solar

radiation and the temperature difference between the ambient and the collector. The next figure shows these values.

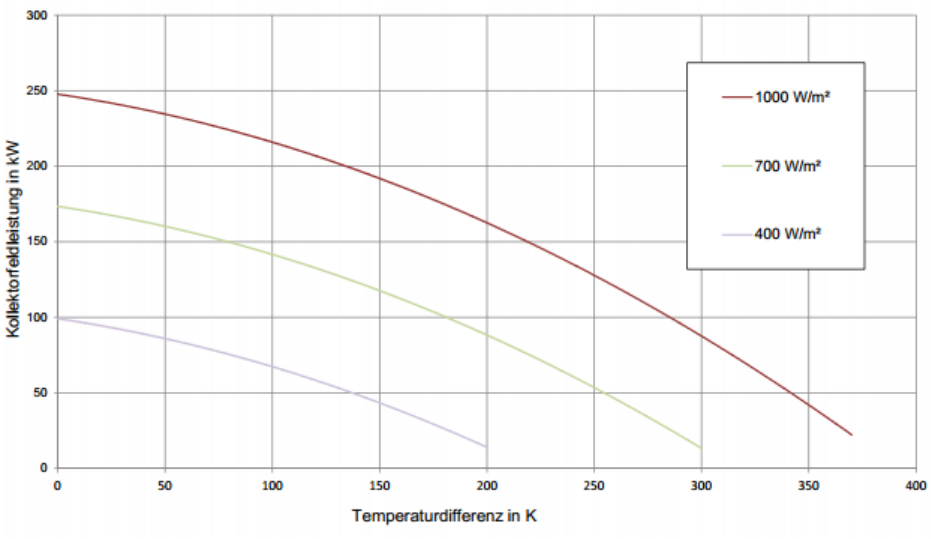

Figure 0-3: Collectors' efficiency. Source: Bauer (2014)

As defined in the subsection 2.2.1, the efficiency of VTC follows the equation (coefficients provided by manufacturer – Ritter Energie- und Umwelttechnik GmbH & Co, certified by TÜV Rheinland):

$$\eta_{VTC} = 0.688 - 0.583\frac{(T_{col} - T_a)}{I} - 0.003\frac{(T_{col} - T_a)^2}{I} \qquad (3.1)$$

The steam drum is fed by the solar collectors in order to produce the motive steam. It has a capacity of 0.4 m^3 and generates steam (maximum mass flow 220 kg/h – at a solar radiation of 500 W/m2 and ΔT = 120 K a mass flow of 140 kg/h was tested) at a temperature of 140 °C (dry saturated or lightly superheated) and a pressure of around 2.7 absolute bar (max. Pressure = 6 bar).

The heat storage is done by phase-change materials (PCM), in this particular case, polyethylene, disposed in rod storage (five modules – 500 kg), in a Lamellae Heat Exchanger. The temperature storage is around 125-132 °C, with a capacity of 50 kWh. The importance of the heat storage relies on the possibility to compensate the cooling demand and the thermal solar energy supply mismatch. This component of the facility is crucial, as without it the possibility to operate with 100% renewable solar energy would not exist.

3.2.2 Cooling generation subsystem

The cooling generation subsystem (Summer operation) consists of the following equipment:

- Steam Jet Ejector
- Evaporator
- Condenser
- Latent cold storage (PCS)
- Cooling tower
- Heat exchanger

The next figure shows the mass flows through the ejector. The red arrows show the motive steam flow, the blue arrows follow the suction mass flow and the orange arrows, the mixture to the condensers. This facility is a 2-step SJEC, with a third ejector (upper part) necessary for eventual discharges.

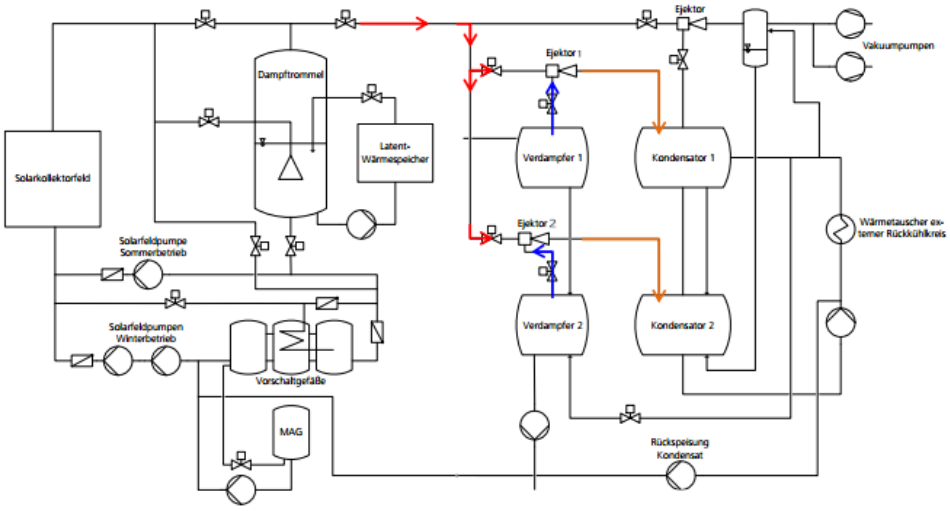

Figure 0-4: Cooling subsystem. Source: Joemann (2014).

The SJEC has a nominal cooling power of 82 kW and an initial tested COP about 0.5.

Evaporator pressures are low (around 12 mbar) as well as temperatures (7-12°C). Condenser pressure (50 mbar) and temperature (inlet max 28°C) depends on mainly the ambient temperature. The water mass flow for the cooling load is around 11 t/h and with a minimum temperature of 6°C (outlet evaporator).

In addition, in order to keep relatively high COPs, the condenser temperature should be as low as possible. That is the main goal of the cooling tower, which cools down the mixture

from the condenser. It carries a mass flow between 20 and 135 m^3/h and holds a maximum outlet temperature (inlet to condenser) of 26°C. It is a wet open cooling tower with a nominal cooling power of 480 KW (when operating from 32°C to 26°C, with an assumed wet bulb temperature of 21°C), and a nominal motor power of 4 kW. The following flow chart illustrates with light blue arrows the circuit of the cooled water (from condenser to cooling tower).

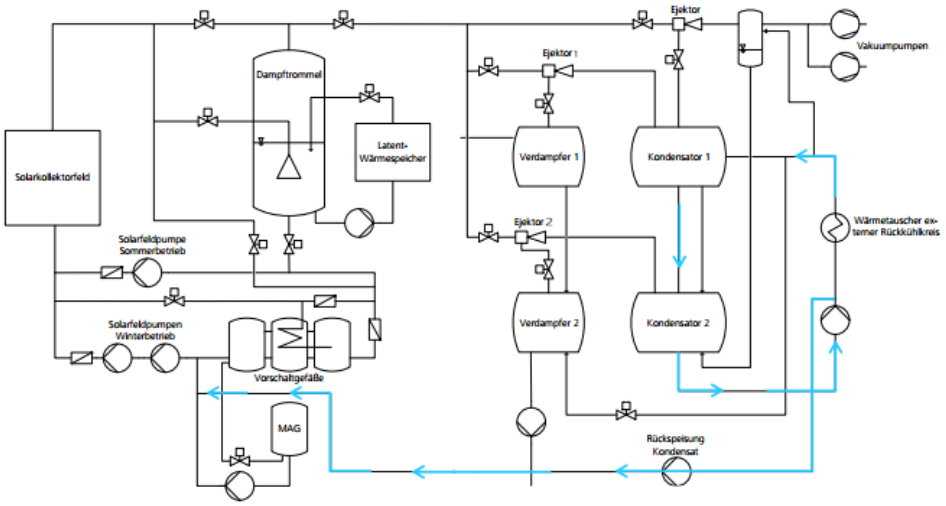

Figure 0-5: Cooled water. Source: Joemann (2014).

Moreover, the facility also works with a cold storage tank, filled with PCM materials (in this case, phase-change slurries). It works with a 30% mixture of paraffin-water. The volume of the tank is 1.5 m^3 and has a storage capacity of around 25 kWh, with working temperatures between 7-12 °C. The cold storage allows the facility to deal with fluctuations in the cooling load.

This connection is showed in the next figure, highlighting with blue arrows the path of the cold water circuit from the evaporator.

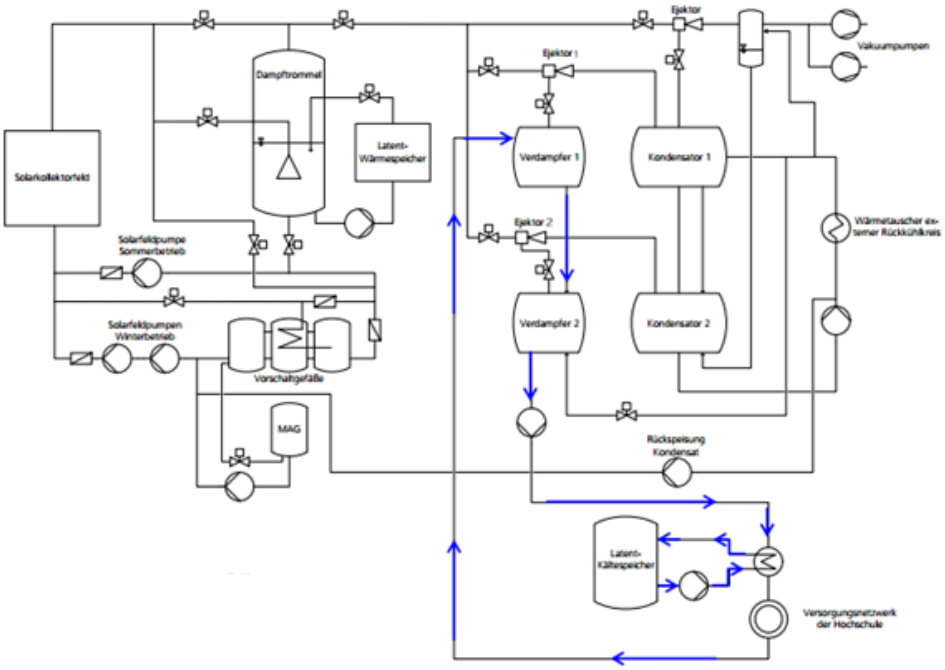

Figure 0-6: Chilled water. Source: Joemann (2014).

The MAG (Membran Ausdehnung Gefäß – Expanding Membrane Vessel in English) is in charge of the pressure regulation in the pipes where the heat/cold exchange between the facility and the building occurs.

3.2.3 Heating generation subsystem

The subsystem for heating generation (Winter operation) is simpler than the previously described for cooling generation. In this case, only the following mentioned equipment take part of the winter operation:

- Vacuum Tube Collectors
- Steam Drum (steam generation)
- Latent Heat Storage (PCM)
- Water storage and pressure regulation (MAG)
- Heat Exchanger

As it can be seen, from the "heating generation subsystem" only the heat exchanger with the building is considered. The steam produced in the steam drum is applied directly for heating. The heating mode of the facility will not be studied in depth in this work, though it is worth mentioning it exists and operated with 100% driving renewable heat.

3.3 Database creation

3.3.1 Objective

The first step of this study was to understand the measured values of the whole facility during certain periods of interest. To make this possible, a database with all the measurements of summer 2015 was created.

The SPS (Speicherprogrammierbare Steuerung – Programmable Logic Controller in English – PLC) software of the facility creates .csv files on a daily basis, measuring 152 variables of different kind. All the files were compiled and processed into a database, to perform several data analysis and to allow the comparison between the facilities. The database is performed with Visual Basic (VBA) in Microsoft Excel 2013.

It is of utmost importance to highlight that the Steam Tables database was performed by Magnus Holmgren – "X Steam Tables v2.6" www.x-eng.com. It was extremely helpful for the development of the database. During the development of this program, the Steam Tables database was not modified from its original content.

3.3.2 Abilities and limitations of the program

In the first place, two VBA Macros were developed to set up the database. The first one takes all the .csv files and creates a unique file, by selecting the folder in which all the text files should be (see figure 3-7). The second one performs some modifications to the text in the unified archive (date and time adjustment, to make possible future filtering, as well as converting text to number format). Both files are in separate Excel workbooks and leave the database ready to be used.

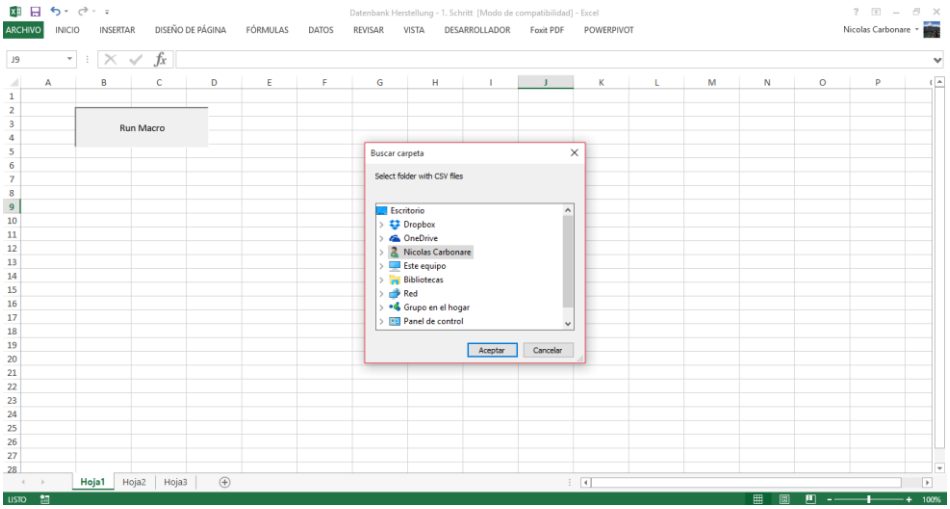

Figure 0-1: Database macro.

In second place, the programming of the analysis software was made. This was thought only to work with the facility of the HsKA. However, it allows to perform different types of analysis. The first step is to introduce date and time filtering. This is a powerful tool, as it makes possible to analyze a whole day, week month or season. Moreover, time windows can be analyzed (i.e. every day from 10 AM to 5 PM during July). Nevertheless, the most important attribute of date and time filtering is the time of response. For example, if the software had worked with a whole seasonal database (assuming five months) to perform every calculation, it would take much more time than it actually does. Five months, with an average of thirty days each, with 150 measurements per minute, makes 32.400.000 cells with data. If someone wants to analyze just one day for twelve hours, it makes it faster to first filter by date and time frame, than to work always with the entire database. One day and twelve hours means 108.000 values against the 32.400.000 of the original database, making the average response time much lower. This should always be the first step of the software: to select the date and time frame in an appropriate way.

Besides, it combines the measured values with calculations performed with them. However, certain values are not measured, but considered important to obtain the performance indicators. These are therefore introduced manually in the “Input” screen. Examples are given in the next figure.

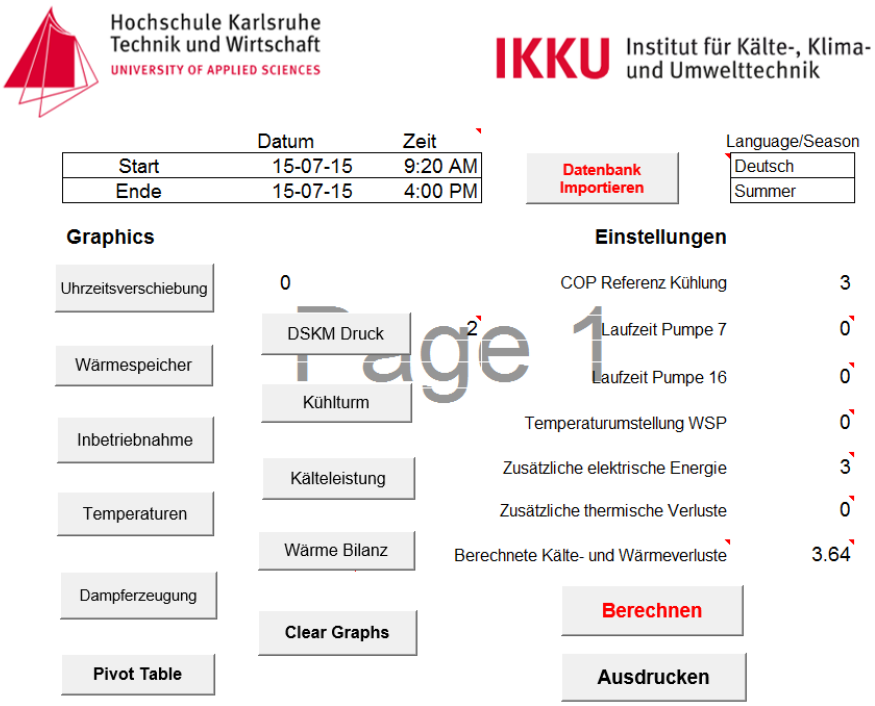

Figure 0-2: Input screen

Graphics play an important role for the analysis of the system's response and performance. The software allows to make some graphical comparisons automatically, selectable in the first screen. Moreover, it also allows to create an automatic Pivot Table with the filtered database

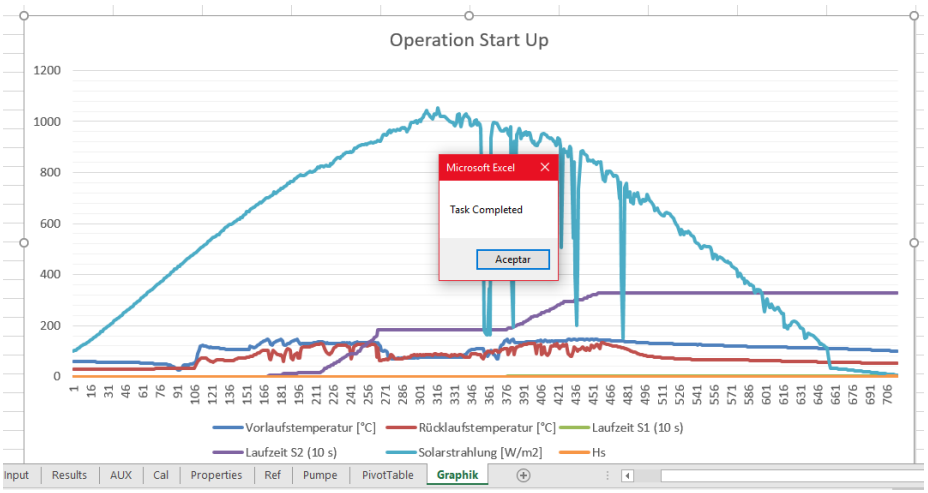

Figure 0-3: Sample graphic output

Finally, the results screen shows the preselected Key Performance Indicators (KPI) for the monitoring and analysis of the facilities' operation. They will be described thoroughly in the next subsections.

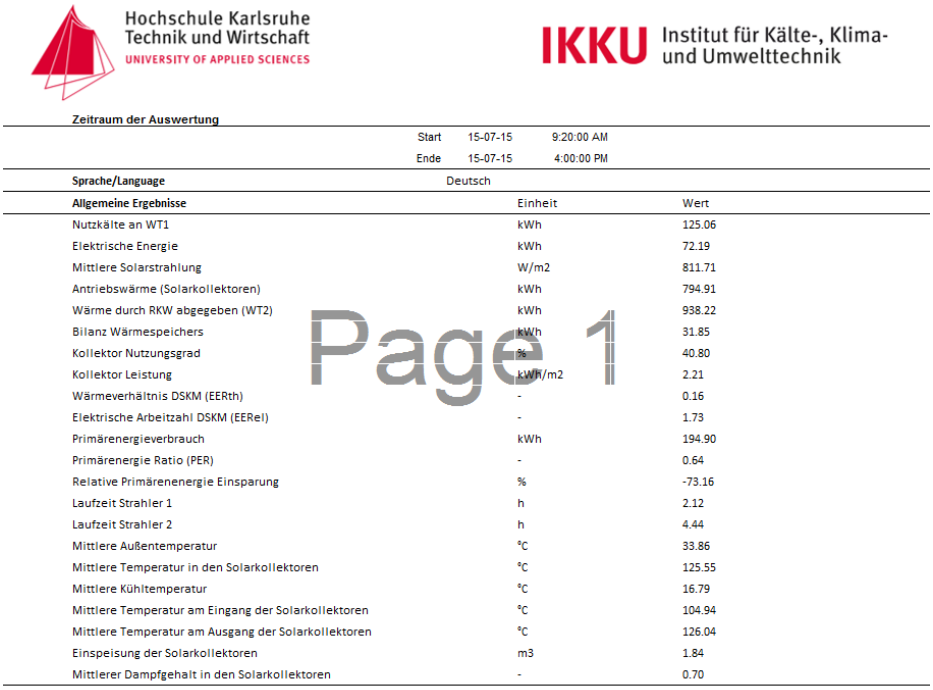

Hochschule Karlsruhe Technik und Wirtschaft
UNIVERSITY OF APPLIED SCIENCES

IKKU Institut für Kälte-, Klima- und Umwelttechnik

Zeitraum der Auswertung

Start	15-07-15	9:20:00 AM
Ende	15-07-15	4:00:00 PM

Sprache/Language	Deutsch	
Allgemeine Ergebnisse	**Einheit**	**Wert**
Nutzkälte an WT1	kWh	125.06
Elektrische Energie	kWh	72.19
Mittlere Solarstrahlung	W/m2	811.71
Antriebswärme (Solarkollektoren)	kWh	794.91
Wärme durch RKW abgegeben (WT2)	kWh	938.22
Bilanz Wärmespeichers	kWh	31.85
Kollektor Nutzungsgrad	%	40.80
Kollektor Leistung	kWh/m2	2.21
Wärmeverhältnis DSKM (EERth)	-	0.16
Elektrische Arbeitzahl DSKM (EERel)	-	1.73
Primärenergieverbrauch	kWh	194.90
Primärenergie Ratio (PER)	-	0.64
Relative Primärenenergie Einsparung	%	-73.16
Laufzeit Strahler 1	h	2.12
Laufzeit Strahler 2	h	4.44
Mittlere Außentemperatur	°C	33.86
Mittlere Temperatur in den Solarkollektoren	°C	125.55
Mittlere Kühltemperatur	°C	16.79
Mittlere Temperatur am Eingang der Solarkollektoren	°C	104.94
Mittlere Temperatur am Ausgang der Solarkollektoren	°C	126.04
Einspeisung der Solarkollektoren	m3	1.84
Mittlerer Dampfgehalt in den Solarkollektoren	-	0.70

Figure 0-4: Results screen output

3.4 Software Calculations

3.4.1 Introduction

To carry the facilities' analysis and comparison out, indicators and ratios of performance should be defined previously. The description of these figures is stated in the following subsection.

3.4.2 Definition and formulae

3.4.2.1 Project Scaling

The definition of parameters of comparison is carefully carried out to perform it in the most realistic and possible way. Any assumptions are made throughout the following examples.

The first item of focus is the project scale. Although it is important to include as many comparison results as possible, the scale provides a reliable contrast for the facilities, i.e., the operative costs of a 10 kW operating solar cooling project cannot be compared with the costs of a 300 kW one. Moreover, not only the output cooling power is considered, but also the driving power, whether it is renewable or not, and its sources. The numerical defined scaling parameters are the following:

$$Nominal\ Cooling\ Power\ [kW] \tag{3.2}$$

$$Relative\ CP = \frac{Collectors´Area\ [m^2]}{Nominal\ Cooling\ Power\ [kW]} \tag{3.3}$$

$$\%RE = \ driving\ power\ covered\ by\ renewable\ energy \tag{3.4}$$

From equation 3.3 can be derived the Collectors' Yield, which is only relative to the Solar Collectors subsystem. This is then defined as the ratio between the Driving Heat from the collectors during a certain time and the useful collectors surface. Its usefulness relies on the real solar gains of the solar collectors, as it differs throughout the different types. The formula for the Collectors' Yield is then:

$$Collectors'\ Yield = \frac{Driving\ Heat\ [kWh]}{Collectors´Area\ [m^2].year} \tag{3.5}$$

This value might be calculated as a total per year, as many other authors perform this in order to develop a comparable standard. The final value will be extrapolated from the summer measurements to the whole year, in order to calculate this value.

3.4.2.2 Solar Collectors' subsystem

In addition to formula 3.5, another indicator for the performance of the solar collectors is the Utilization Factor (UF). This represents the percentage of the total solar heat that is gained by the system. Therefore, the formula is defined as the following:

$$UF = \frac{Driving\ Heat\ [kWh]/1000}{Solar\ Rad\ \left[\frac{W}{m^2}\right] * ColArea\ [m^2] * Hs[h]} \tag{3.6}$$

Although this ratio seems pretty accurate, the values presented will be considered at first instance low. The first possible explanation is that the efficiency of the solar collectors is not considered. Taking a look at equation 3.1, where the efficiency of the Vacuum Tube Collectors is defined, without any thermal losses (only considered optical unavoidable losses, ideal case), the collectors' efficiency is as high as 68.7%. This means that the theoretical threshold of the

useful solar gain is 68.7% percent of the heat irradiated by the Sun, by using this high performance solar system.

3.4.2.3 Performance of the facility (Cooling)

Once scaled, the second step is to contrast the performance of the different facilities. The most common tool is the previously defined energy ratios (see 2.*3 Thermodynamic fundamentals of cooling processes*) and to add the quality of the power source to the analysis.

$$COP_C = \frac{Useful\ Cold\ [kWh]}{Driving\ Energy\ [kWh]} \quad for\ cooling \tag{2.6}$$

$$COP_h = 1 + COP_C \quad for\ heating \tag{2.7}$$

Nevertheless, the Energy Efficiency Ratio (or Coefficient of Performance) can be defined according to the different driving energies. The energy consumption, in order to run the facility, is divided into thermal and electrical energy. This is of utmost importance, as it is one of the key performance ratios of comparison between different facilities.

$$COP_{th} = \frac{Useful\ Cold\ [kWh]}{Driving\ Heat\ [kWh]} \tag{3.7}$$

$$COP_{el} = \frac{Useful\ Cold\ [kWh]}{Electrical\ Energy\ [kWh]} \tag{3.8}$$

The primary energy ratio (PER) is defined as the ratio between the heating or cooling power and the primary energy consumed. This can be separated into renewable primary energy (such as solar energy, for example) and non-renewable primary energy (such as fossil fuels). The importance of this relies on the environmental point of view, as the renewable energy sources are unlimited natural sources, whereas the non-renewable sources may cause different impacts in the Environment. Following the points of assessment defined by Manuel Riepl (2012), the relevant PER value is the non-renewable. The definition of PER is therefore,

$$PER = \frac{Useful\ Cold\ [kWh]}{Primary\ Energy\ Consumption\ [kWh]} \tag{3.9}$$

taking into account the Primary Energy Consumption (PEC) as only from non-renewable sources. Thus, the following step is to perform the calculation of the PEC.

The PEC is calculated considering the different driving energy sources from the facilities that are subject of study. As a preview, will be only considered:

- Solar Energy
- Electrical Energy
- Gas Burner for auxiliary heating (boiler)

As stated before, Solar Energy contributes with no Primary Energy Consumption, as only the non-renewable will be considered. In the case of Electrical Energy, as it is considered secondary energy, it must be taken into account the factor of primary energy conversion (PEF), which means, the primary energy consumed to generate a unit of electrical energy. Following the International Energy Agency (IEA) task 38, the recommended value for the PEF of Electrical Energy is 2.5. For example, to generate 100 kWh of Electrical Energy, 270 kWh of energy from non-renewable sources is invested. For the auxiliary boiler operated with gas, the PEF for gas is 1.1. Nevertheless, in this case the efficiency of the boiler should be considered, as there are some heat losses in the process. Following once more Manuel Riepl's (et. Al. 2012) investigation, the assumed efficiencies are summarized in the next table:

Factor	Assumed Value
$\eta_{\text{Hot Water Boiler}}$	0.90
$\eta_{\text{Steam Boiler}}$	0.85
$\eta_{\text{Gas Burner}}$	0.90

Table 3-1: Primary energy factors. Source: Riepl (et. Al. 2012).

To sum up, combining the formula 3.8 and the table 3-1, the final formula to calculate the Primary Energy Ratio would be the following:

$$PER = \frac{Useful\ Cold\ [kWh]}{EE\ [kWh] *\ PEF_{el} + \sum \frac{HE\ [kWh] * PEF_{ht}}{\eta}} \quad (3.10)$$

With:

- EE = Electrical energy consumption
- HE = Heat energy consumption

The sum of Heat Energies represents the different heat sources, their PEF coefficients and the efficiencies for the energy conversion system.

What is more, it is considered of relevance not only the Primary Energy Ratio, in order to study the real consumption of non-renewable primary energy, but also the potential savings of the facility. To carry this out, it is necessary to establish a standard for conventional heating and cooling equipment, what leads to a comparison between both PER. In conclusion, it is defined the Relative Primary Energy Savings (REPS), which is the percentage (%) of PE that is not consumed by choosing the studied facility instead of a conventional one (by conventional it is understood the most popular and commercially available ones). In this study, the standard is taken as a conventional compression chiller system, with a COP of 2.8 (this can be modified in the software's first screen). Finally, the REPS compared the Primary Energy Consumption of both systems:

$$PEC = EE\ [kWh] * PEF_{el} + \sum \frac{HE\ [kWh] * PEF_{ht}}{\eta} \quad (3.11)$$

$$PEC_{ref} = \frac{Useful\ Cold_{ref}\ [kWh] * PEF_{el}}{COP_{ref}} \quad (3.12)$$

Combining equations 3.11 and 3.12:

$$REPS = \frac{PEC_{ref} - PEC}{PEC_{ref}} \quad (3.13)$$

3.4.2.4 Other Calculations

Other calculations of interest are also performed in the software. These include some temperature mean values (average value), average solar irradiation, water flow through collectors' field, working time from both ejectors and the mean vapor fraction in the field.

It is considered of relevance to mention the fact that the cooling tower is not part of the analysis carried out on this work. The rejected heat of the facility is calculated over the heat exchanger between the condenser circuit and the cooling tower circuit. Additional details will be given in the development of the calculations and in the annexes.

4. Results and Analysis

4.1 Introduction

In this chapter other facilities will be firstly described, which will be contrasted with the HSKA system. Besides, the comparison will be made, carefully choosing the desired parameters and referring to adequate literature. This section will present in detail all the results obtained.

4.2 Analysis of results – Steam jet Ejector

4.2.1 Selection of sample days

The first step was the selection of ten sample days throughout the summer 2015 (first summer of full operation). The next graphic shows the monthly average of the useful cooling power provided by the facility (obtained with Excel pivot tables).

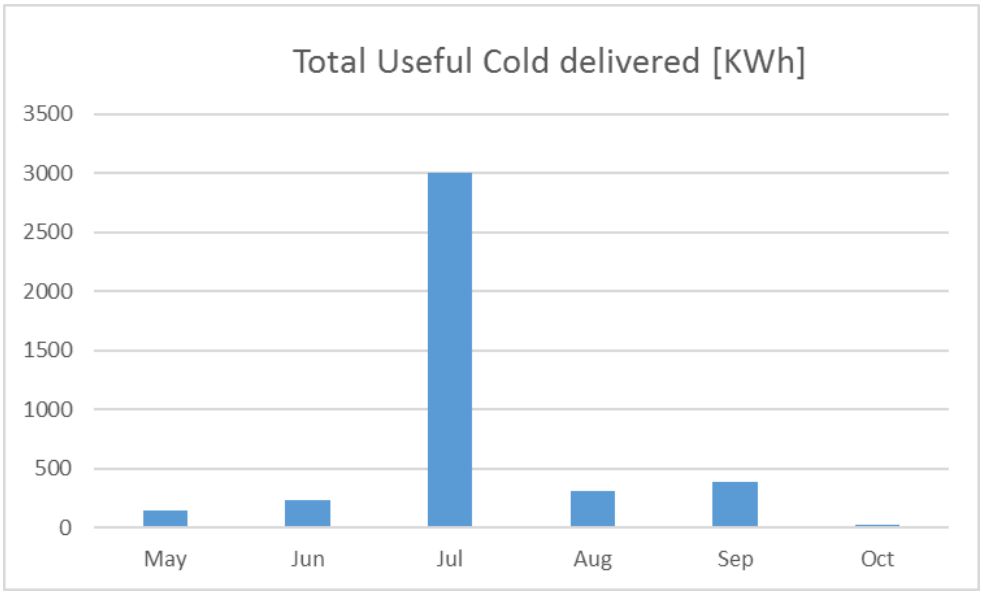

Figure 0-1:Monthly total useful cold (summer 2015)

It can be simply seen that the month of July was the hottest in the year, needing the highest cooling values. However, to decide which days will be taken as example, the concept was to take into account different days with a wide range of ambient conditions (temperature and humidity) and therefore cooling loads (building requirements). The next figures show the daily average of useful cooling power in KW and the selected days highlighted in red. The whole season showed only 25 operational days. Given some sporadic days in which the facility worked for a few minutes, it was considered “operational day” when the total useful cold was above 20 KWh and the ejectors worked at least for an hour. The next figure shows the operational days and the selected example ones.

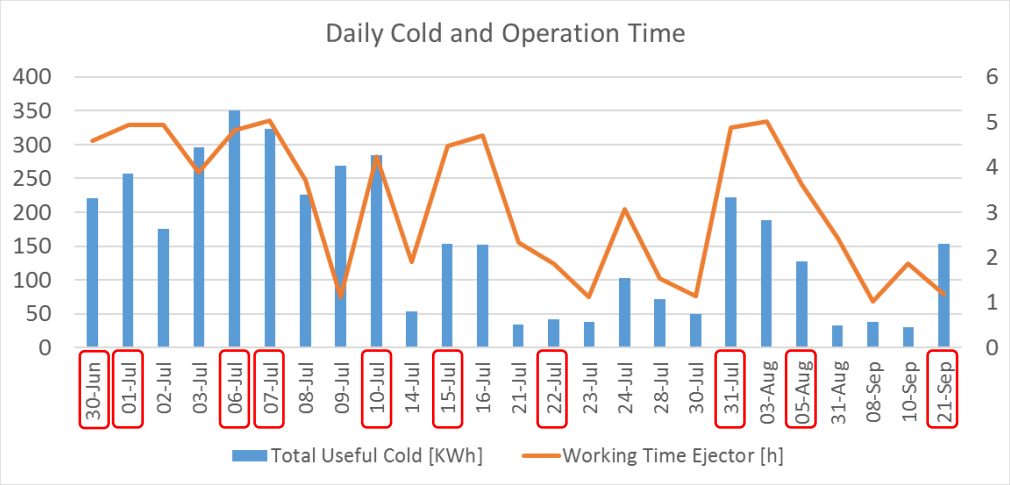

Figure 0-2: Operational days in summer 2015

4.2.2 Working conditions and system limitations

Firstly, it is important to highlight the fact that this is an experimental facility with a prototype cooling system. Therefore, the installation set up and control logic was changed during its duty. And here is the first point of analysis: the effectiveness of the studied installation.

The objective of an air-conditioning system is to provide comfort to the occupants of a certain space in contrast with the uncomfortable weather conditions (specifically, ambient temperature and air moisture). The next figure is the Comfort field according to Leusden & Freymark (1951) and shows the ranges of temperature and humidity that are set as targets for air-conditioning facilities.

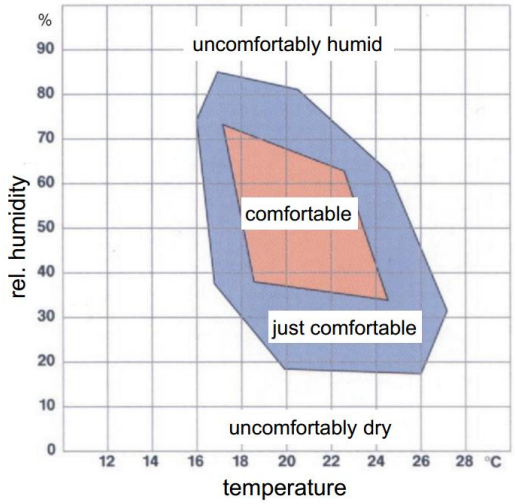

Figure 0-3: Comfort Field. Source: Schmidt (2015).

Besides, in the next figures, the average temperatures and relative humidity are shown for the ambient conditions and the building measured values. This was calculated as an hourly average only in the days where the facility worked.

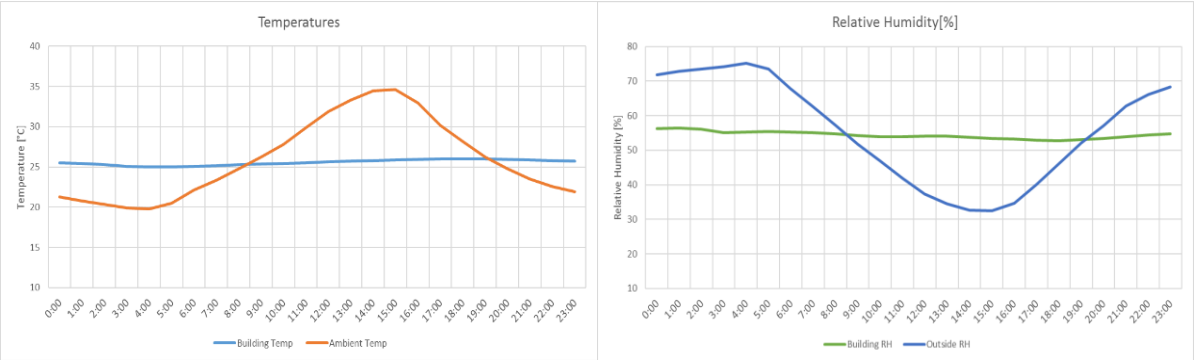

Figure 0-4: Temperature and Relative Humidity.

As it can be seen, the cooling facility provides an almost constant value of temperature (dry bulb – 25.7 °C) and relative humidity (54.7%) to the building, despite the outside oscillating weather conditions. Daily examples of this stability will be shown in the next subsection (4.2.3).

Nevertheless, if the comfort field is considered, the average of the building temperature seems to be higher than the maximum allowed in this zone. The average result of the building temperature and humidity sets the building in the "just-comfortable" zone. The next figure shows a daily average comparison of the building and ambient temperature, focusing in the daylight timeframe, where the temperatures reach values high enough to require air-conditioning.

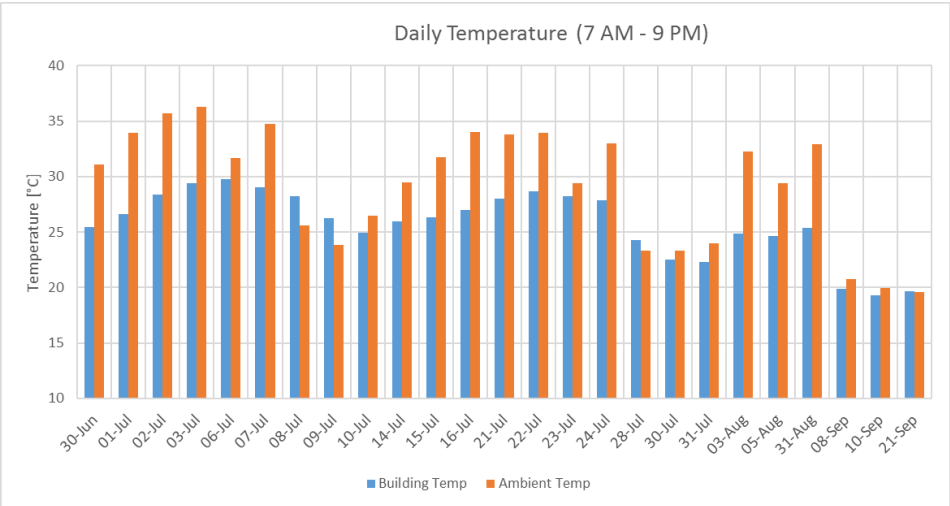

Figure 0-5: Daily temperature in the service days.

From this graphic it can be easily identified that, in the days where the average ambient temperature is above 30°C, there are some difficulties for the facility to reach the desired building temperature. On eight of the thirteen days, in which the average ambient temperature is above 30°C, there is at least an hour-long peak above 40°C. The next image shows an hourly average temperature of the hottest days of the period and the building temperature results.

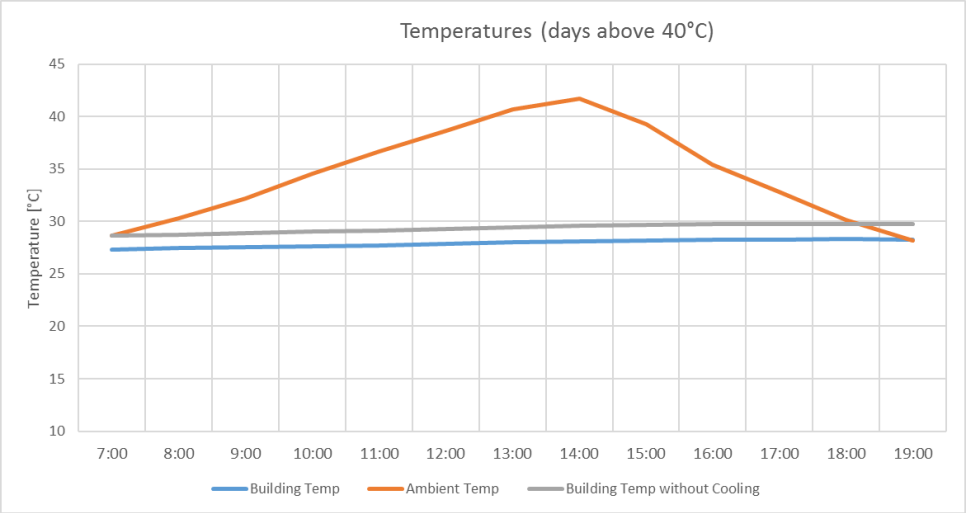

Figure 0-6: Temperature in the hottest days.

The building average temperature in these days (eight) and for the specified timeframe reaches 27.9°C, which is about 2°C higher than the average value of the period. Nevertheless, there are five days in which the facility did not work and the ambient temperature also reached 40°C. On those days, the average building temperature registered is as high as 29.4°C, showing that the facility contributed at least by improving the comfort conditions, even though the result is not optimal. In the next subsections, focus will be made on the operation of the steam jet ejector chiller in order to identify the causes of these non-desired temperatures on the days the installation worked.

What is more, it is also crucial to identify the operative boundaries of the facility. From the measurements in Summer 2015, the limits of operation are:

	Building Temp. (Ambient T) [°C]
Maximum	29.67 (44.68)
Minimum	19.66 (24.59)

Table 4-1: Limits of operation

The maximum was measured on 06.07.2015 and the minimum on 21.09.2015.

As a further recommendation, it would be necessary to identify the reasons of having only 25 working days in the whole season.

4.2.3 SJEC Operation and Cooling Power

4.2.3.1 Condenser and evaporator

In order to achieve the desired temperatures in the building, the chilled water must be cold enough to provide the air-conditioning. As seen in chapter 3, the cooling process takes place in the evaporator. However, to make this possible, the condenser also plays an important role, as its temperature should be as low as possible (Pollerberg et. Al. 2007). The next table summarizes the observed values for the example days.

Date	Hs Operation	Building T [°C]	Evaporator T [°C]	Ambient T [°C]	Condenser T [°C]
30.06.15	5.5	25.18	19.54	34.91	25.66
01.07.15	6	26.25	18.44	35.35	26.74
06.07.15	7.5	29.53	17.92	33.3	23.22
07.07.15	6	28.93	21.3	36.81	27.58
10.07.15	7	24.85	17.24	28.38	21.76
15.07.15	3.5	26.17	21.18	30.96	27.03
22.07.15	3.5	28.41	27.16	36.7	30.38
31.07.15	5.5	22.19	15.15	25.53	22.44
05.08.15	2.5	24.53	20.77	35.39	29.29
21.09.15	1.5	19.46	26.32	25.43	23.06

Table 4-2: Different Temperatures.

The day 06.07.2015 shows an odd value, as the condenser and evaporator temperatures seem to be in a very good average, but the building temperature is not cooled down as it would be desired. One possibility could be the presence of very high heat loads in the building during these particular day. Also the measurement obtained for the day 21.09.2015 will not be trusted, but in this case is the evaporator temperature which shows a strange high value, although the building temperature seems really low for this chilled water value.

To continue with the example, three days on the table 4-2 will be taken and explained in full detail in the next subsections. As claimed before, the performance of the facility, in those days which the average temperature is below 30°C, shows good results. Focus will therefore be made in the following days:

- **30.06.2015** – High ambient temperature and good response
- **22.07.2015** – Highest condenser temperature and poor response
- **07.07.2015** – Highest ambient temperature and poor response

The day 05.08.2015 also shows a very high ambient temperature and excellent facility response. Nevertheless, the facility only worked for 2.5 h, making the measurements of the

day 30.06.2015 more enrichening and trustworthy (5.5 h working hours). The next figures show the temperatures for the selected days.

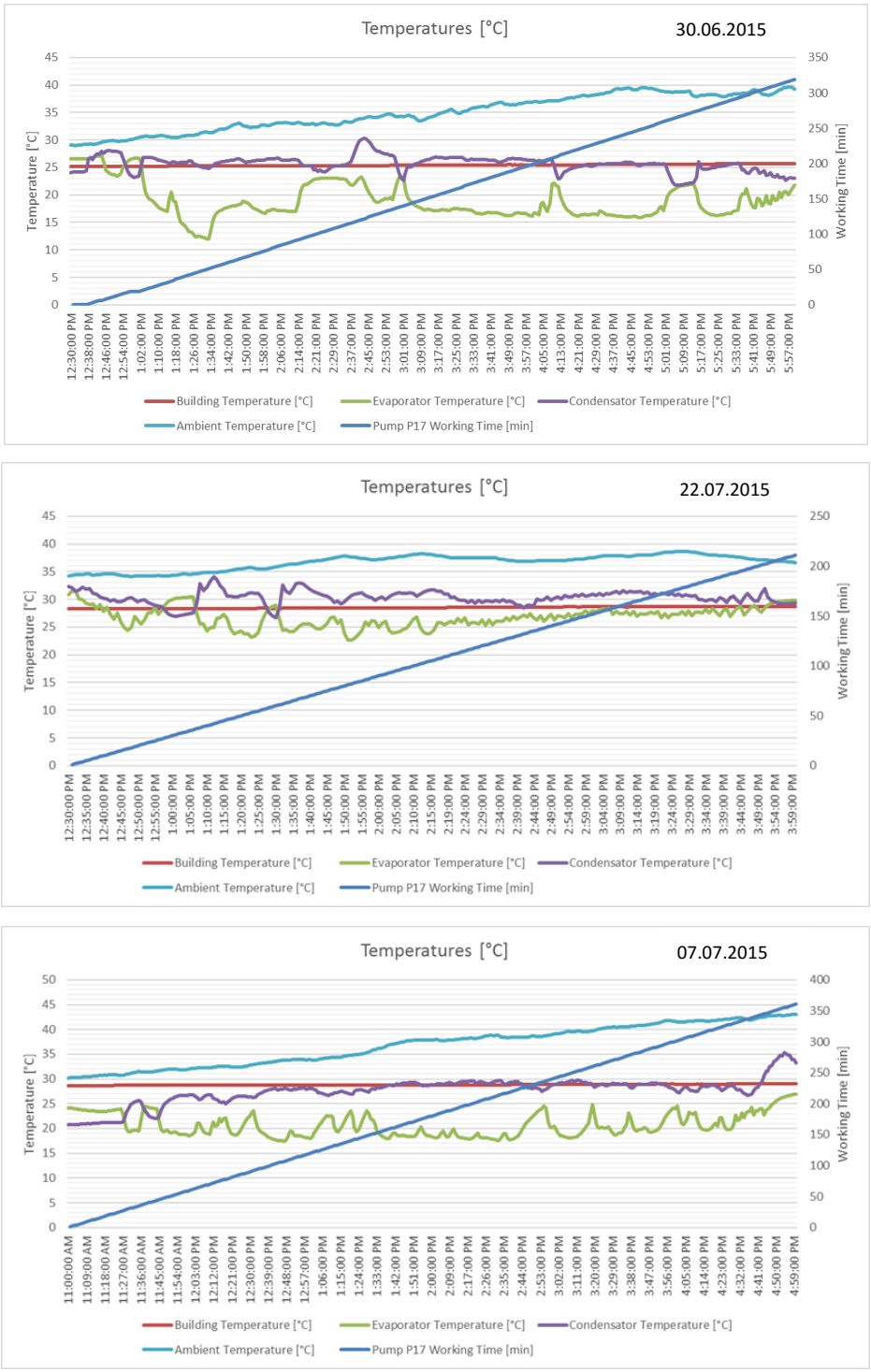

Figure 0-7: Different temperatures in sample days

As it can be seen, in these selected timeframes the ambient temperature is almost always above 30 °C. The evaporator temperature is relatively high (as it was designed to be under 12

°C), especially on 22.07. On 30.06 the evaporator reaches at about 1:30 PM the instantaneous value of 12 °C. Since it is the variable of main interest, focus on this temperature is made.

As described in chapter 3, the evaporator temperature depends on its pressure (suction pressure - should be around 12 mbar), which depends on the motive steam and the condenser temperature/pressure. The motive steam is provided by the solar collectors' system, while the condenser temperature depends on the cooling tower. As stated, a high evaporator temperature can be caused by not enough motive steam (mass flow/pressure) or a very high condenser temperature/pressure.

- 30.06.15 presents an acceptable condenser temperature, therefore a low enough evaporator temperature and, finally, a good cooling performance.
- 22.07.15 presents a very high condenser temperature.
- 07.07.15 shows like 30.06 a high condenser and evaporator temperature (although lower than 30.06) and a poor performance (high building temperature). A maximum ambient temperature of 43°C is reached.

The performance of the steam jet ejector and the obtained pressures on the system will be further discussed in the next subsection.

4.2.3.2 Ejector operation

The next figures show the ejectors operation graphic and the pressures involved.

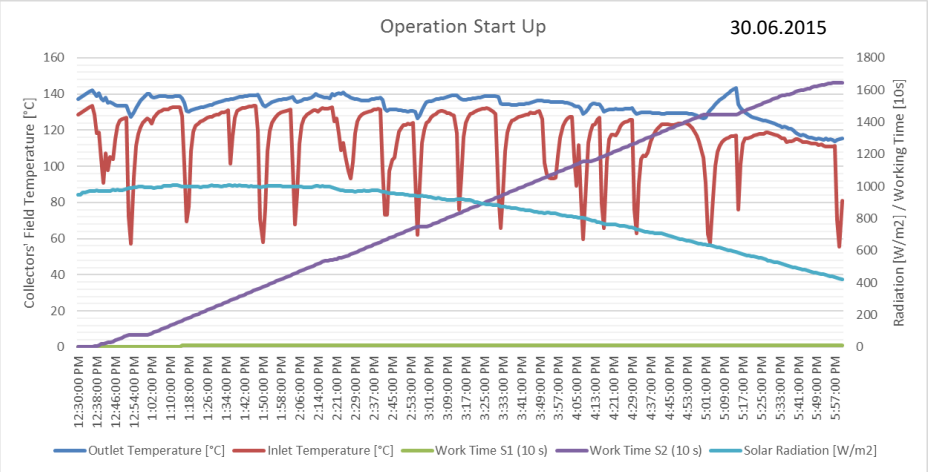

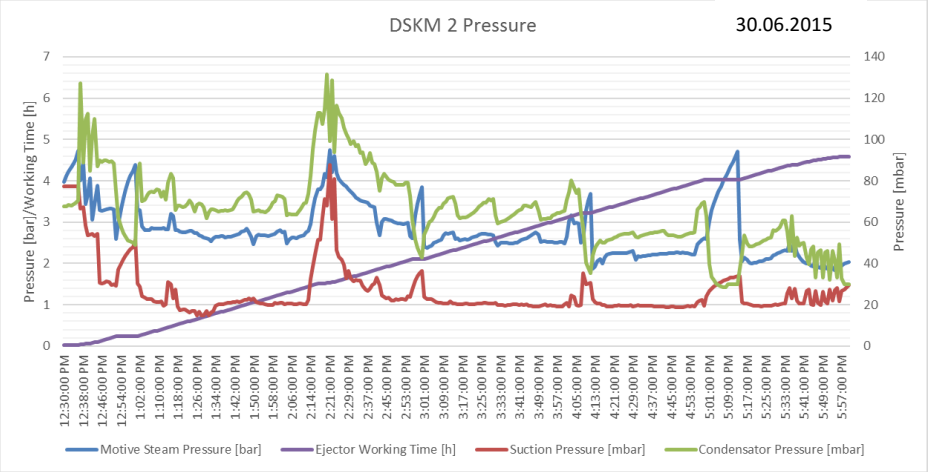

Figure 0-8: SJEC Operation on 30.06.2015

At 30.06.2015 it can be seen that the evaporator shows a running pressure about 20 mbar (by peak load 16 mbar). Even though it is not the desired pressure, it is low enough to produce an effective cooling power. Condenser pressure stays around 60 mbar (lower in the afternoon) and motive steam between 2 and 3 bar.

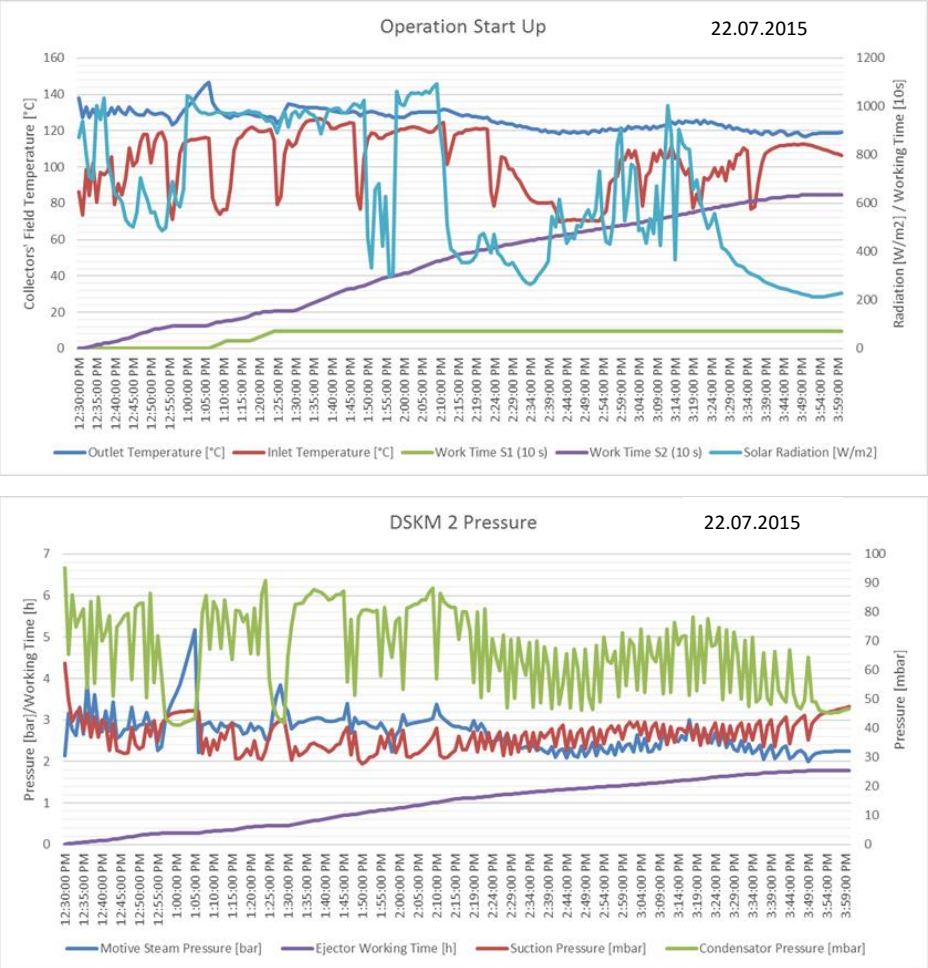

Figure 0-9: SJEC Operation on 22.07.2015

On 22.07 it can be seen that the evaporator pressure is high (around 40 mbar), causing an insufficient cooling power. Motive steam shows a pressure about 3 bar and condenser also stays at a high pressure (60-80 mbar). What is more, there is a strong oscillation in the pressure values. In the operation start-up graphic it can be seen that the solar radiation was not constant (probably a cloudy day), and the temperatures in the solar collectors' field also show difficulties, translated into problems to generate the motive steam. The combination of an intermittent steam generation and very high ambient temperature and humidity (affecting cooling tower's service) are probably the main reasons of this insufficient performance.

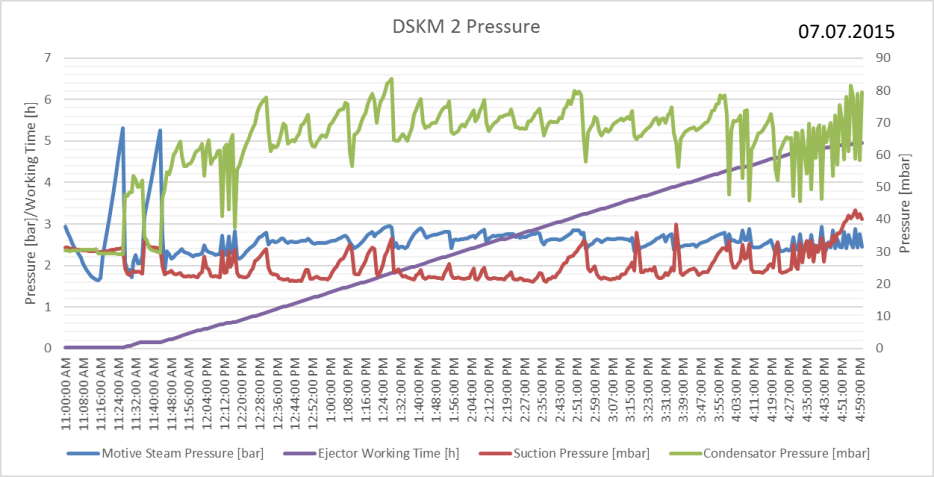

Figure 0-10: SJEC Operation on 07.07.2015

The operation start-up graphic of 07.07.2015 looks similar to the shown on 30.06.2015, and can be seen in the annex. It is important to make clear that the solar radiation on this day was constant and the solar collector's field worked under normal conditions. Here it is seen again that the motive steam pressure is around 2.5 and 3 bar. Evaporator and condenser pressures seem a bit lower than on 22.07, although not low enough to produce a reasonable performance of the cooling facility (Evaporator 20-30 mbar / Condenser 60-75 mbar).

In this three picked days the motive steam seems in the designed range of pressure and temperature. However, it can turn out to be insufficient due to the high condenser pressures presented (as explained in the chapter 3). In the next subsection, a closer look to the heat rejection circuit will be taken, as it is crucial to keep the condenser temperature (and pressure) as low as possible.

4.2.3.3 Heat rejection

The next figures show the heat rejected (cooling tower) instantaneous power and the ambient and condenser temperatures.

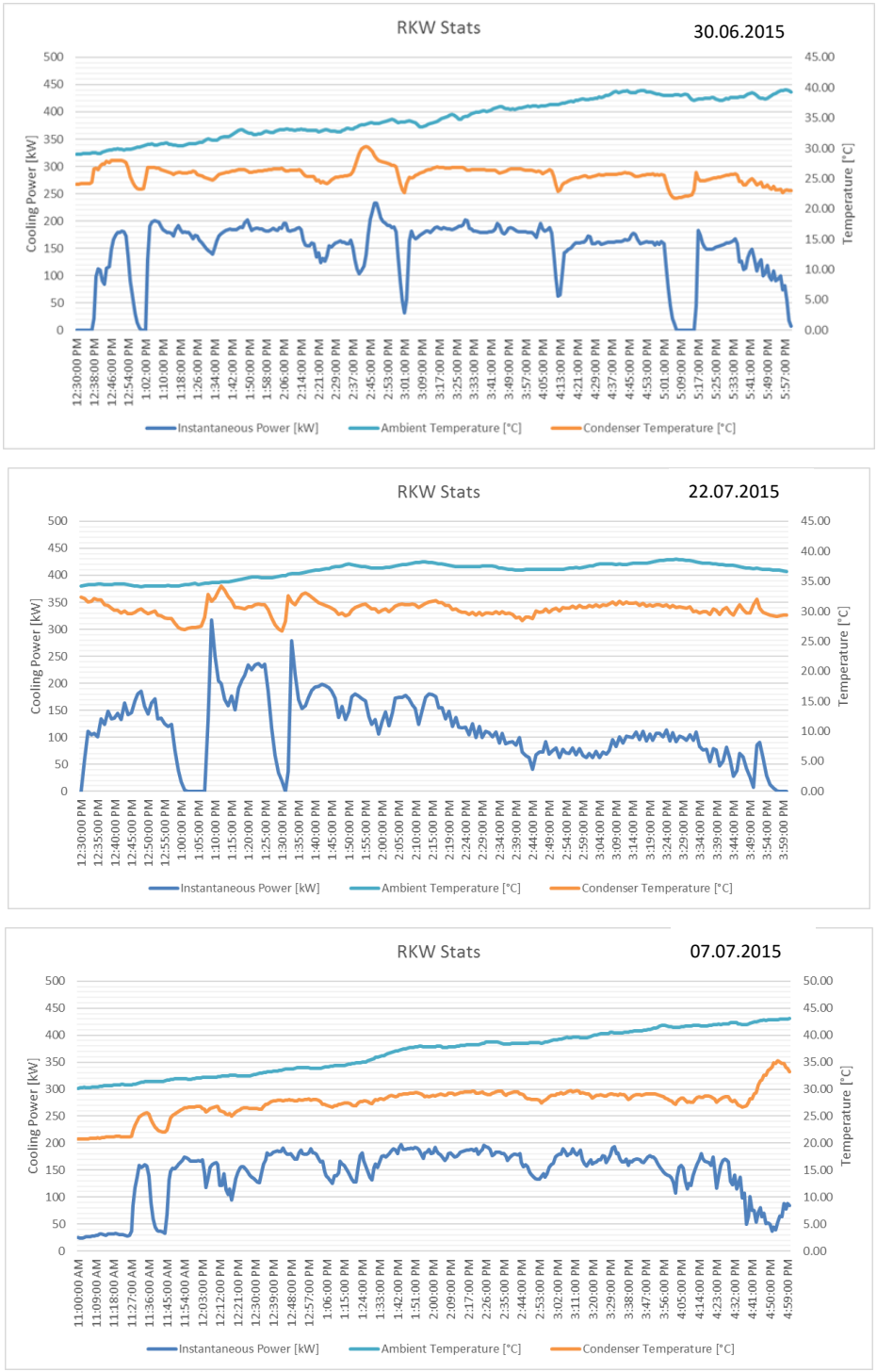

Figure 0-11: Heat Rejected and Temperatures

The designed nominal power of the cooling tower is 480 KW but taking into account a cooling from 32 to 26°C. In the hottest days this is not possible, due to higher ambient temperatures. It can be seen that on 30.06.2015 the power stays around 200 KW with some oscillations,

cooling the condenser down to an average of 25 °C. On 07.07.215 the cooling power is around the same values; however, the high ambient temperature causes a higher condenser one, even though the ΔT is almost the same. On 22.07 there is a power peak of about 300 KW; nevertheless, the cooling power stays around 170 KW for the first two hours and about 100 KW for the rest of it. This lower value is reflected in the value of the condenser temperature (about 30°C), which is probably the cause why the motive steam is not enough to produce an acceptable performance. A possible following step could be the study of the cooling tower in itself to provide low enough condenser temperatures in very high ambient ones.

4.2.3.4 Cooling power

The cooling generation process has already been discussed in the previous subsections. In this case the cooling power of the facility will be discussed. The next table shows the operation cooling values for the taken days.

Date	Hs Operation	Building T [°C]	Ambient T [°C]	Mean C. Power [KW]
30.06.15	5.5	25.18	34.91	39.79
01.07.15	6	26.25	35.35	42.96
06.07.15	7.5	29.53	33.3	45.58
07.07.15	6	28.93	36.81	42.98
10.07.15	7	24.85	28.38	39.58
15.07.15	3.5	26.17	30.96	33.77
22.07.15	3.5	28.41	36.7	19.13
31.07.15	5.5	22.19	25.53	38.37
05.08.15	2.5	24.53	35.39	22.40
21.09.15	1.5	19.46	25.43	60.96

Table 4-3: Cooling power

The next figures show the cooling power and the respective mentioned temperatures. The nominal cooling power of the SJEC facility was set in 82 KW. In connection with the previous analysis, it is expected a stable and high cooling power for 30.06.2015 and 07.07.2015, with the last one suffering some more oscillations due to the high condenser temperature. The 22.07.2015 is expected to have strong oscillations due to the radiation variations and, therefore, the motive steam variations.

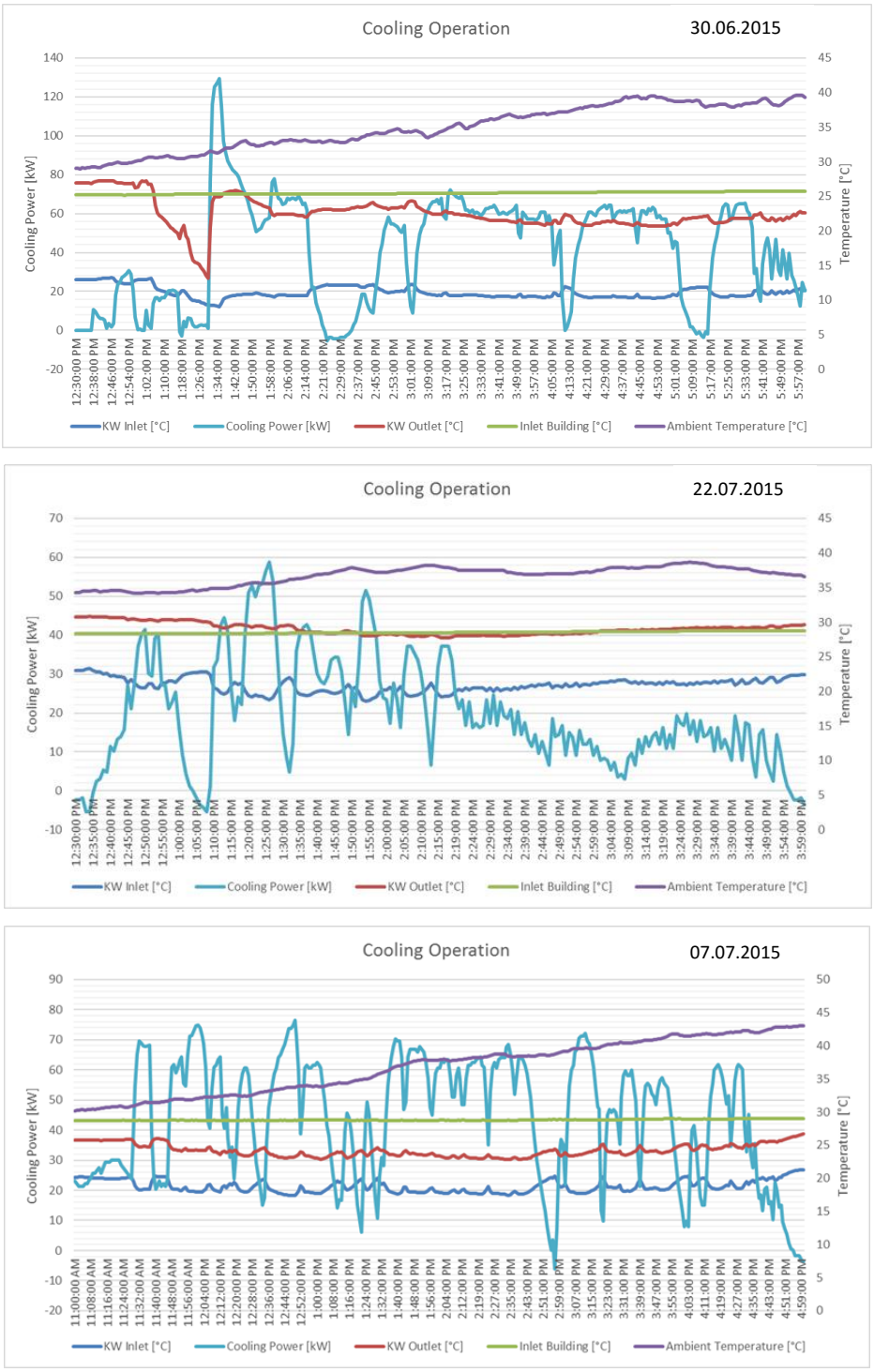

Figure 0-12: Cooling Operation

The results show the expected values. 30.06.2015 is stable between 60 and 70 KW, 22.07.2015 show better cooling values in the first two hours (20-40 KW) than in the final ones (cooling values under 20 KW) and 07.07.2015 presents oscillations with better results than the last mentioned day (40-70 KW).

The monitoring of the 2015 cooling season showed that the steam jet ejector chiller worked reliable in the days where ambient temperature was under 32°C, and the desired air-

conditioning of the building LB was given. The building temperature was kept around 25°C over most of these days. The average cooling capacity of the system laid between 40 KW and 60 KW (average of almost 33 KW), which is below the nominal capacity of 82 KW of the SJEC chiller. This part-load operation caused by the low cooling capacity on the building side has a negative impact on the thermal Coefficient of Performance (COPth) as well as on the electrical COPel of the system. It must be taken into account that in the hottest days (above 32°C average) the cooling performance was poor and the desired building temperature could not be delivered.

A 82 KW chiller can ideally yield a maximum of 1968 KWh of cooling energy per day, assuming incessant operation. The number of operation hours in a solar cooling system, however, can be limited by the heat source. A 5.5-hours long operation (like 30.06.2015 for example) would ideally still yield 450 KWh of cooling energy. The 2015 season shows daily cooling energies between 0 and 350 kWh, with an average of 150 KWh per working day.

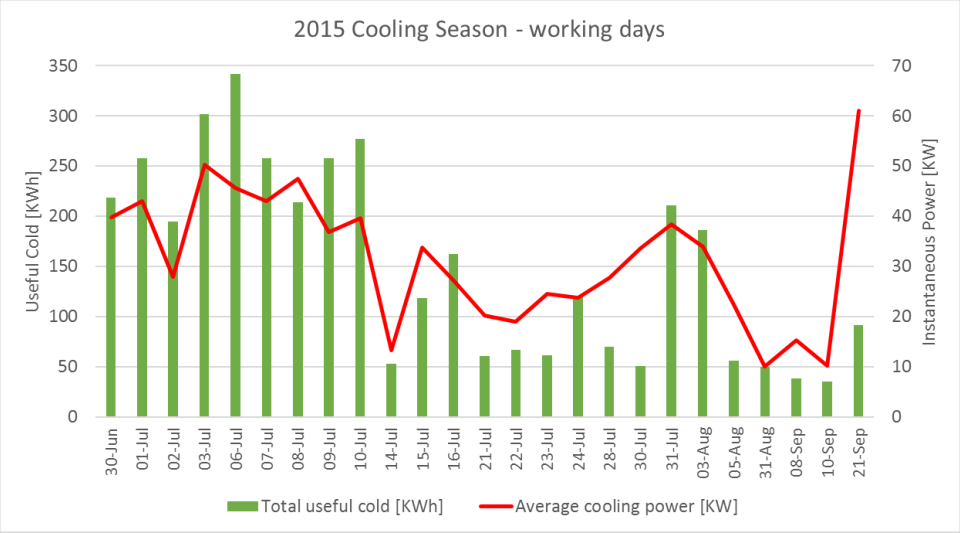

Figure 0-13: Seasonal performance 2015

There were in total around 130 hours of operation (part-load), translated into 44 equivalent full operation hours. This behavior should be in the future further studied to provide better cooling results.

4.2.4 Solar collectors' field

It is assumed that the motive heat is calculated only in the timeframe of the cooling operation. This means that, whenever there is solar radiation, there might be as well flowing water through the collectors, taking heat from the solar radiation. However, this heat is only turned into the warm up of the facility and heat losses, which is not at interest of this study. The

inflow and outflow pipes are standard DN50. The next table summarizes the relevant figures for the solar collectors' circuit.

Date	Hs Op.	Motive Heat [KWh]	Coll' ΔT [°C]	Inlet Flow [m3]	Radiation [W/m2]	Coll' Ut. Factor
30.06.15	5.5	566.36	17.23	1.49	838.48	34.58%
01.07.15	6	686.57	23.25	1.76	880.71	35.80%
06.07.15	7.5	656.07	31.83	2.09	845.54	28.43%
07.07.15	6	632.18	18.94	1.78	818.09	35.78%
10.07.15	7	720.52	28.04	2.53	848.5	33.70%
15.07.15	3.5	475.93	23.38	0.98	910.23	41.50%
22.07.15	3.5	347.16	22.83	0.78	637.52	43.22%
31.07.15	5.5	639.29	20.2	1.44	841.42	38.34%
05.08.15	2.5	259.36	18.05	0.64	723.55	39.82%
21.09.15	1.5	173.67	16.79	0.56	800.3	40.18%

Table 4-4: Solar collectors' field data

Although three example days have been followed through the work, for this subsection, the days 30.06.2015 and 07.07.2015 will be replaced only by the day 06.07.2015, as it shows a low utilization factor. Moreover, the results of the days 07.07.2015 and 30.06.2015 turn to be similar, as showed the previous graphics. The propagation of errors of the following calculations throw a result of 2.44%, as it can be seen further in subsection 4.5.4.

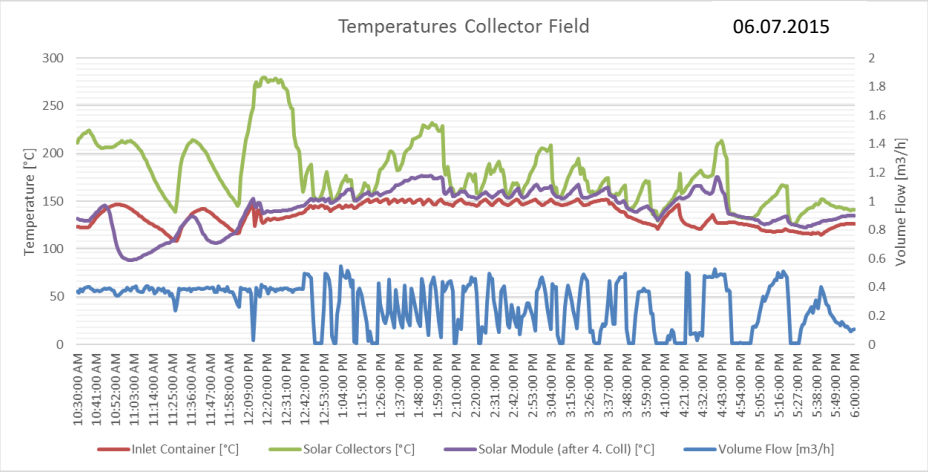

Figure 0-14:Collectors' data on 06.07.2015

As it can be seen from the graphic, the pump P14 allows an inlet flow of 0.45 m^3/h. This value is considerably high, as this water flow cannot be completely evaporated in the solar collectors. On this day, the evaporation rate was lower than 80%. This was also identified by Frau Bauer in the Ritter Solar GmbH final report about the installation and mounting of the facility. Following Frau Bauer's calculations to obtain the performance of the collectors, the heat is calculated by an enthalpy difference of water. On this day, about 75% of the water was turned into vapor. The pressure in solar collectors is assumed to be an average between

the immediate pressure before inlet (PIRC-W-11-1) and the pressure inside the steam drum (PIRC-B1-1). The summary of the figures on 06.07.2015 are:

- 7.5 h operation – 2.09 m^3 inflow
- Evaporation temperature = 146.91°C – h_{evap} = 2123.2 KJ/Kg
- Tout = 178.91°C – Tin = 113.91°C
- 656.07 KWh motive steam – 25.55 KWh storaged heat
- Total heat gained = 998.38 KWh
- Radiation = 845.54 W/m2 (2.3 MWh) → losses = 13.87%

Collectors' losses can be estimated by 4% of the daily solar radiation. Additional losses may occur in pipes, heat storage, and possible pressure losses. The next figure and calculations are the same, corresponding to 22.07.15.

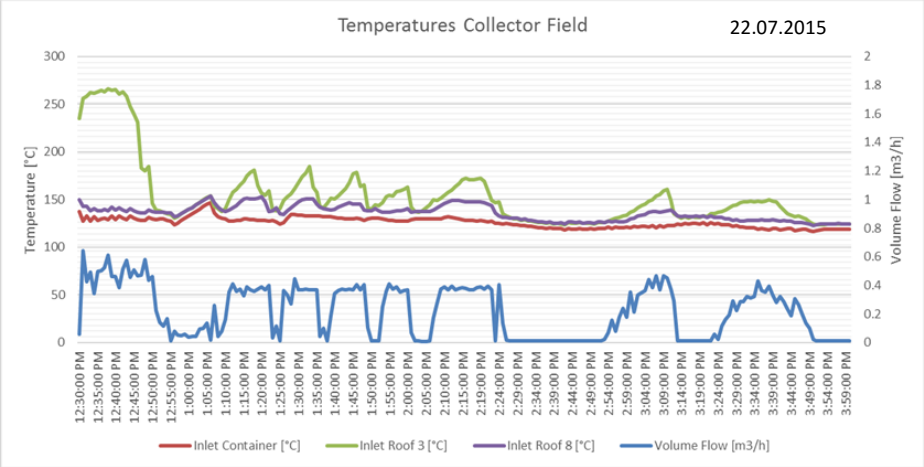

Figure 0-15: Collectors' data on 22.07.2015

- 3.5 h operation – 0.78 m^3 inflow
- Evaporation temperature = 135.85°C – h_{evap} = 2156.6 KJ/Kg
- Tout = 153.46 °C – Tin = 99.17°C
- 346.77 KWh motive steam – 19.46 KWh storaged heat
- Total heat gained = 459.30 KWh
- Radiation = 637.52 W/m2 (0.8 MWh) → losses = 11.59%

The next figure summarizes the collectors' performance for the 2015 season.

Figure 0-16: Collectors' performance

There is an evident relationship between the solar radiation and the collectors' yield. Utilization factor stayed between 30% and 40% most of the days. In order to obtain the yearly collectors' yield, the winter heat gains are also considered in the next graphic.

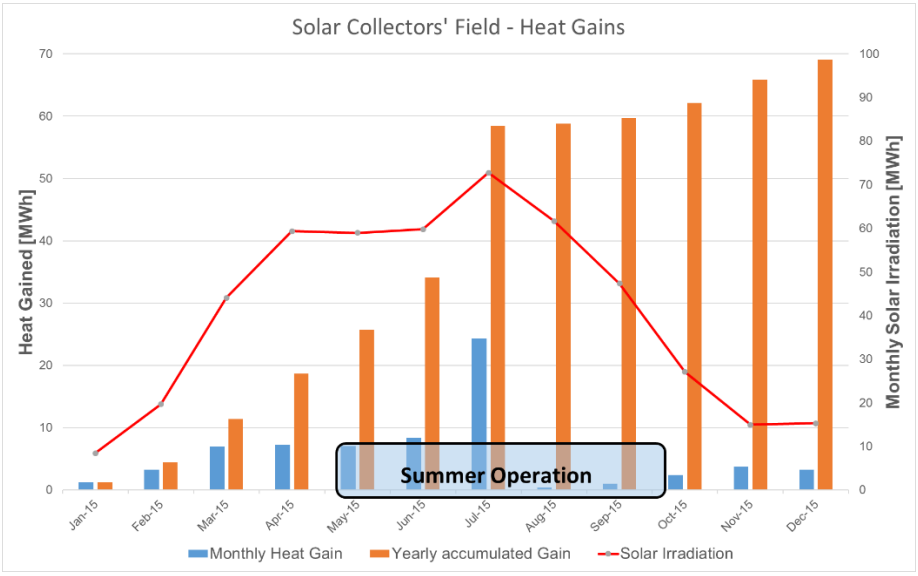

Figure 0-17: Yearly Heat Gains – 2015

As a surprising result, August and September 2015 barely contribute to the yearly heat gained. It results fundamental to make clear that this is not due to breakdown in the operation or technical problems on the collectors' field, but to the absence of cooling power in most of these days in these two months. The fact of an absence of operation contributes to lower considerably the annual collectors' yield.

As seen on equation 3.5, the annual collectors' yield is calculated further. This is a key indicator to evaluate the performance of the solar collectors and to make it comparable with other facilities.

$$Collectors'\ Yield = \frac{Driving\ Heat\ [kWh]}{Collectors´Area\ [m^2].\ year} = 192\frac{KWh}{m^2 a} \qquad (3.5)$$

4.2.5 Heat storage

The heat storage plays an important role in the support of the motive steam, to smooth the oscillations of the solar collectors' performance. It results of utmost importance to state that, since there were some errors found on the measurements of the heat storage, the temperatures values were daily adjusted in order to obtain a clear charging- and discharging phase. Depending on the ambient temperature, it can happen that the discharging phase does not finish at 0 KWh and there is heat stored (either positive or negative, depending on the sign of the difference).

The next figures show the performance of the heat storage on two of the three previously analyzed days.

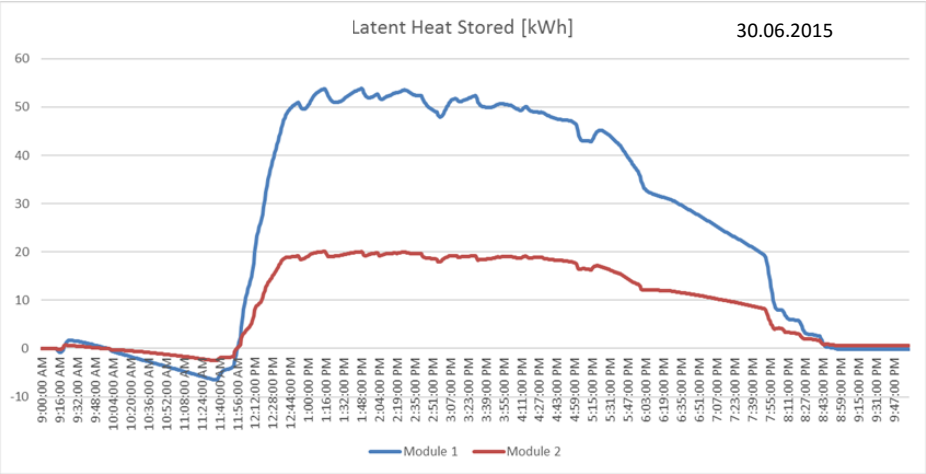

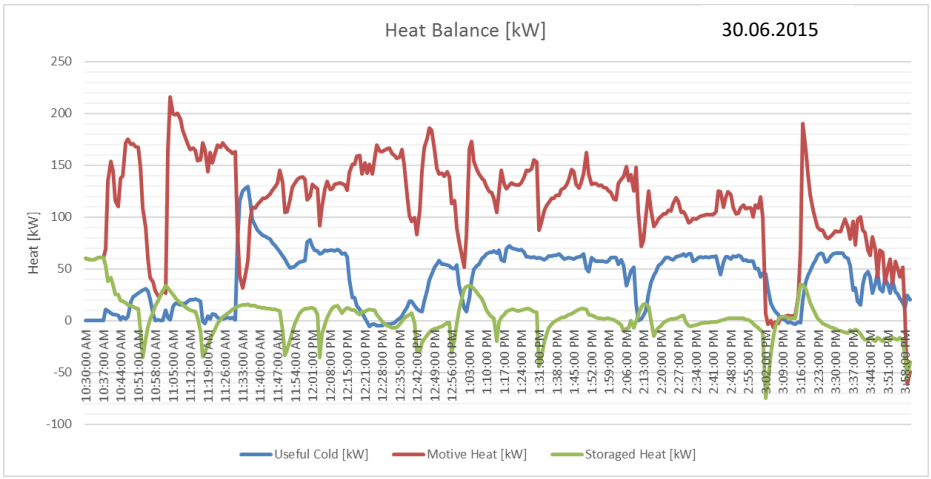

Figure 0-18: Heat storage on 30.06.2015.

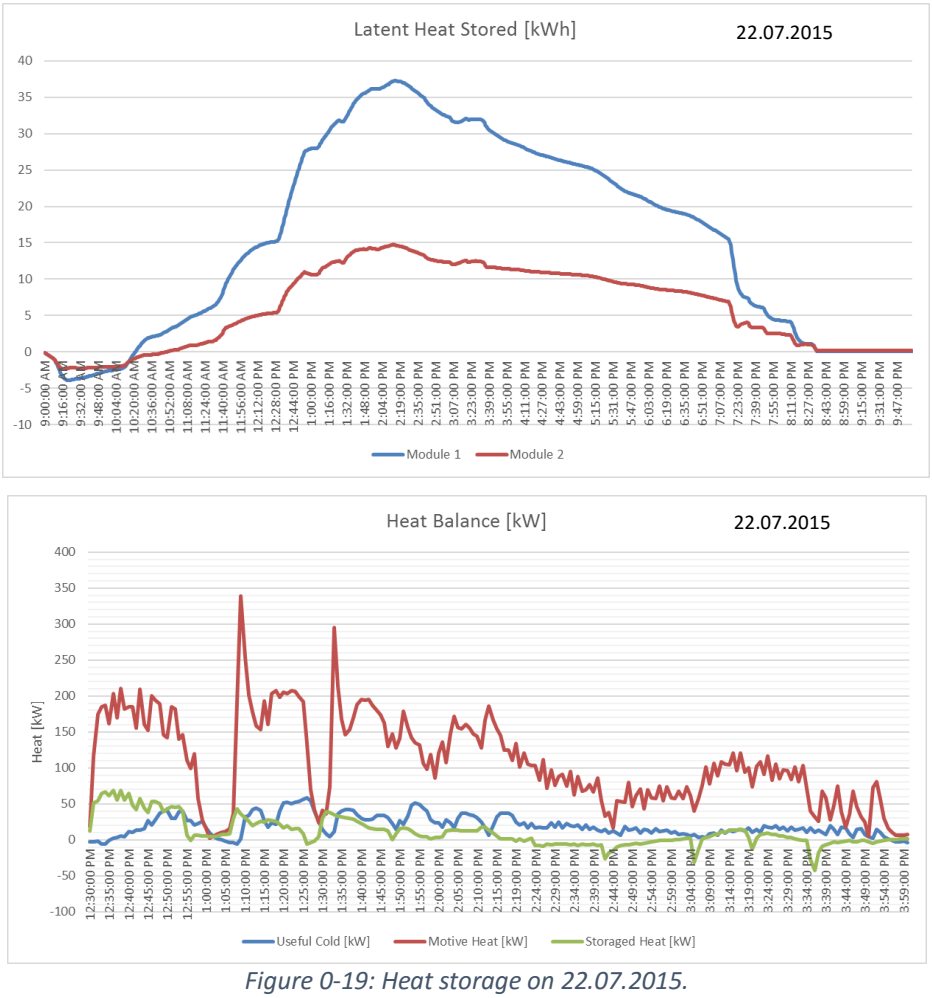

Figure 0-19: Heat storage on 22.07.2015.

A total gap of 70 KWh was stored on the first example, while on the second the value of 55 KWh was reached. Different profiles appear on both examples. While the first day remarks a quick heat accumulation (70 KWh in less than one hour), the second shows smoother phases (55 KWh accumulated in three hours). It can be said that, during the steep charging slope on the first day, there was a high radiation value and the chiller was still not working at that time,

so it can be assumed that most of the heat provided by the solar field was delivered to the warm up of the facility and the heat storage. On the second day, since intermittent solar radiation values were identified, it is expected that the phases result smoother, as the team generated is also lower than in the first example.

To summarize, it can be said that the heat storage presented a good performance, as it helps to support the operation of the cooling facility.

4.2.6 Electrical consumption

In this subsection the electrical energy consumption of the facility is analyzed, as it results crucial for the indicators showing the final performance. As this is a 100% renewable energy driven chiller, the electrical consumption results key when it comes to the analysis of the primary energy consumption and the potential savings of the installation. A total of 1.23 MWh were consumed during the 25 working days. The next figures show a distribution of this consumption taken from the different sources during the 2015 summer operation.

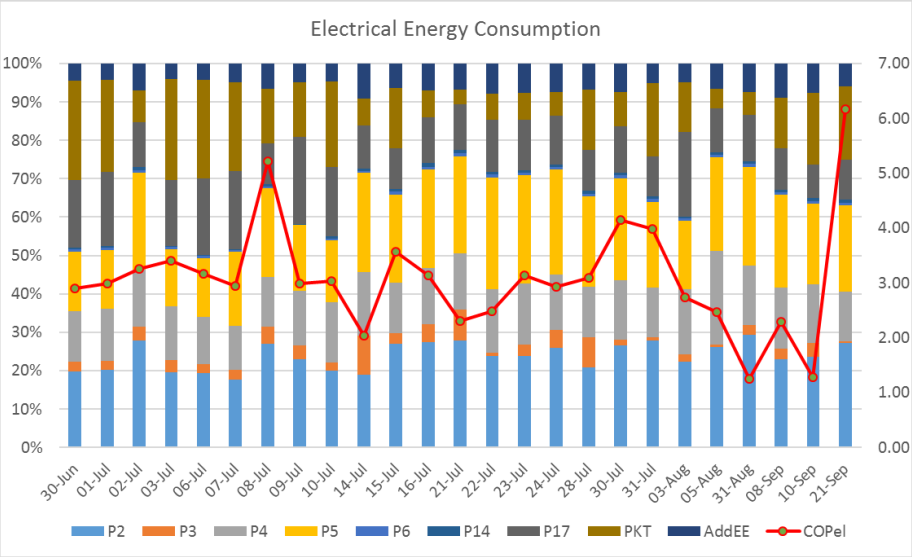

Figure 0-20: Electrical energy relative consumption and COPel

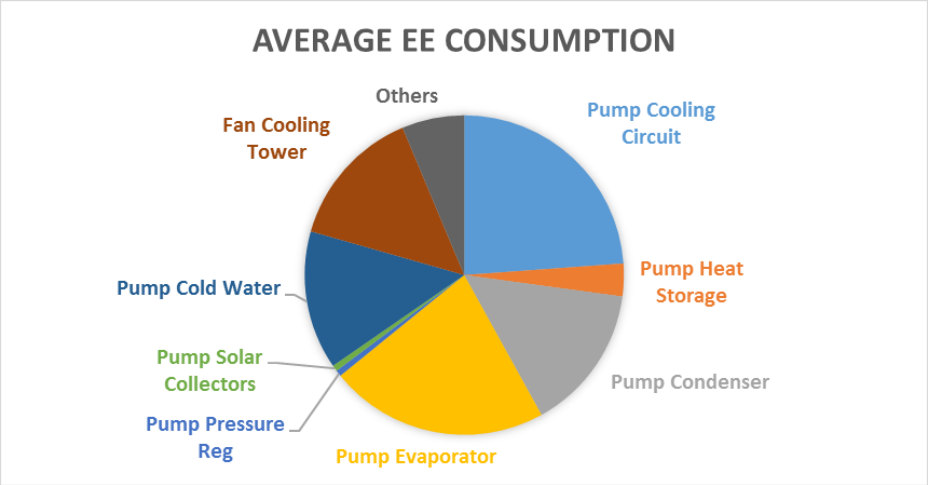

Figure 0-21: Average electrical energy relative consumption

It can be seen that the main sources of consumption are related to the chiller operation and heat rejection circuits. When combined, the fan of the cooling tower and the pump of this circuit represent the main electricity consumption of the facility (38%). Along with condenser, evaporator and cold water pumps, they represent the 89% of the total consumption.

In first place, taking a deeper look at the cooling circuit and its pumps, they represent together about 50% of the total electrical consumption over the 2015 summer season. As it has been already discussed, the control of this pumps results crucial for the electrical energy consumption. As the speed of the pumps result as a key attribute, it is of utmost importance to provide an efficient part-load control of the cooling operation, in order to optimize the consumption of the facility and, therefore, a better result in the primary energy consumption of the facility.

Regarding the cooling circuit, Prof. Hans-Martin Henning (2014) stated in his work that, for the primary energy analysis of a cooling facility, the COPel of the cooling tower results critical, as it is a big influence on the primary energy consumption. He proposes that this value should always be above 20. The calculation of this COPel is analogous to the proposed in equation 3.8, but taking the rejected heat [KWh] and the electrical energy consumption of this circuit [KWh]. The next figure shows the daily results of these calculations.

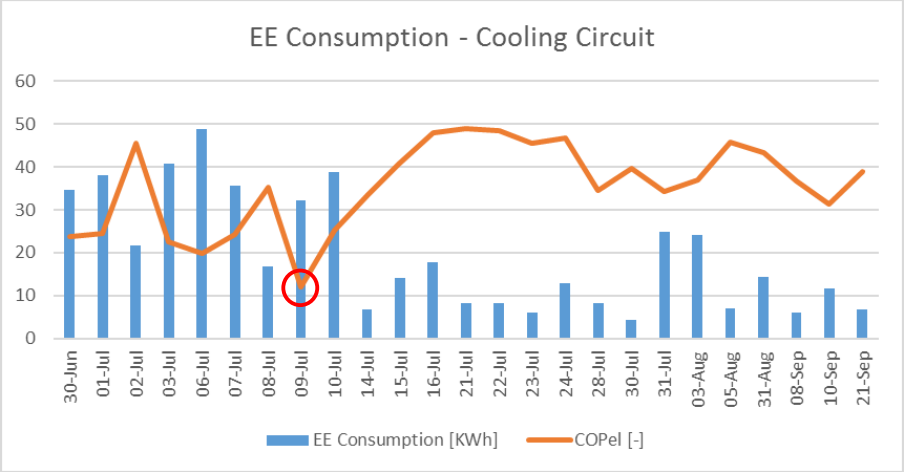

Figure 0-22: Cooling circuit EE consumption

The average of the COPel is 35.46, above the proposed value of 20. It was found only one operation day below (09.07.2015). What can be identified, is that this day presents an unusual COPth value (1.98, highest of the season), caused by a very high cooling power (about 260 KWh) in a cloudy (average radiation below 400 W/m2) and fairly warm day (temperature does not reach 30°C). Which is also not coherent is the fact that there are seven hours of cooling service and just 1.4 hours of accumulated working time for the ejectors. As a low motive heat is presented, also a low heat rejection is given, explaining the poor result of the cooling circuit's COPel.

The stand-by operation consumes an electrical power of 0.6 KW, as measured. Its influence on the PE consumption will be further analyzed in the summary of results.

4.2.7 Costs overview

This subsection presents a global summary of the installation costs. They will not be furthered detailed, as they are not the objective of this work. They are distributed as follows:

- Solar collectors + Installation € 65,300
- Heat Storage € 21,750
- Installation costs (piping, etc) € 10,500
- SJEC € 50,000
- Cooling Tower € 10,000

The next figure represents the percentage of influence of each cost on the facility. Planning costs are not represented, as it was performed by the IKKU Team in the Hochschule Karlsruhe.

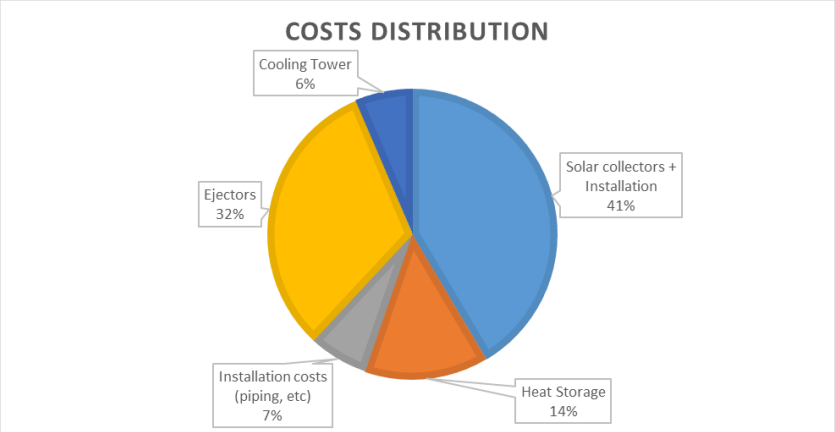

Figure 0-23: Costs distribution of the facility

4.2.8 Key Performance Indicators

4.2.8.1 Achieved thermal COP under operation

In the next table a summary of the main indicators per day can be seen.

Date	Hs Op.	COPth	COPel	PER	Ambient T [°C]	Condenser T [°C]	Mean C. Power [KW]
30.06.15	5.5	0.38	2.90	1.16	34.91	25.66	39.79
01.07.15	6	0.38	2.99	1.20	35.35	26.74	42.96
06.07.15	7.5	0.53	3.16	1.26	33.30	23.22	45.58
07.07.15	6	0.41	2.94	1.18	36.81	27.58	42.98
10.07.15	7	0.38	3.03	1.21	28.38	21.76	39.58
15.07.15	3.5	0.25	3.57	1.43	30.96	27.03	33.77
22.07.15	3.5	0.19	2.49	0.99	36.67	30.38	19.13
31.07.15	5.5	0.33	3.99	1.60	25.53	22.44	38.37
05.08.15	2.5	0.22	2.47	0.99	35.39	29.29	22.40
21.09.15	1.5	0.53	6.16	2.46	25.43	23.06	60.96

Table 4-5: Summary of KPIs

In the presentation of the facility it was stated that the thermal COP was tested above 0.5. In the 2015 summer season only a few days reached the 0.5 initial value. In the next figures the relationship between the COP and other variables will be shown. The picked days are 30.06.2015 and 22.07.2015, following the provided examples in the previous subsections. The first graphic shows how condenser temperature can influence the COP and motive steam pressure. The second one shows the COP affected by the evaporator and condenser temperatures.

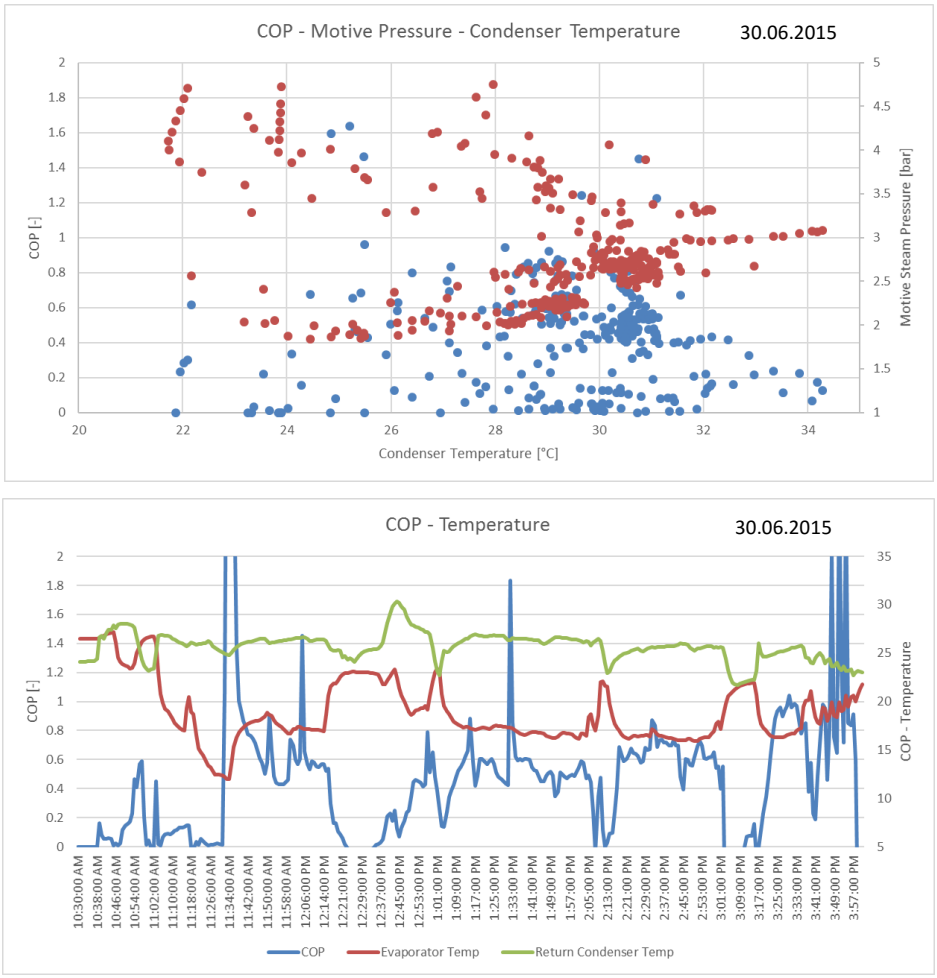

Figure 0-24: COP Figures on 30.06.2015

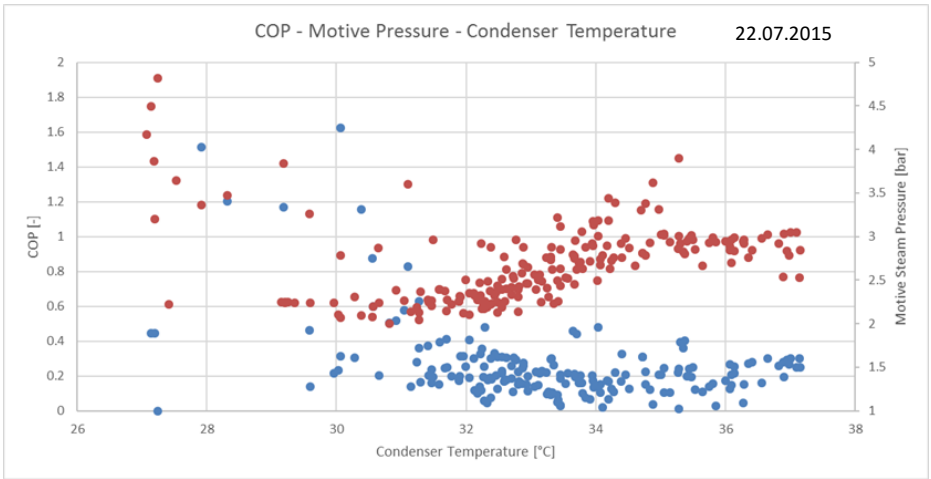

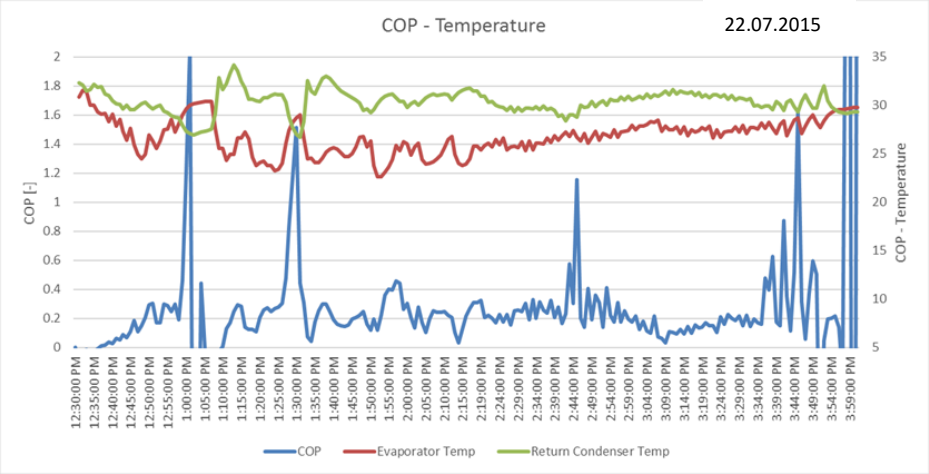

Figure 0-25: COP Figures on 22.07.2015

As it can be seen on the first graphics, a higher condenser temperature requires a higher motive steam pressure (slope of the red dots). Regarding the COP, on 30.06.2015 it can be seen that the condenser temperature is lower than on 22.07.2015, and the COP is higher. Both examples show a slight negative slope on the blue dots, which mean that as the condenser temperature increases, the COP decreases with it. Both results were expected, as it was mentioned in the literature previously analyzed.

On the second graphics there is the instantaneous thermal COP related to both evaporator and condenser temperatures. It can be easily distinguished that the figures on 30.06.2015 show lower evaporator temperatures than on 22.07.2015, which is translated into a higher cooling power and, therefore, a higher COPth value. On both images it can be logically determined that:

- Lower Evaporator Temperature → Higher Cooling Power → Higher COPth
- Lower Condenser Temperature → Lower Motive Steam → Higher COPth
- Higher Motive Steam Pressure → Higher COPth
- Lower Condenser Pressure → Lower Motive Steam required → Higer COPth

4.2.8.2 Summary of results – seasonal values

The next figure shows the cooling load [KW] per hour of service. The average cooling power was around 32 KW, totalizing 130 working hours in 25 days and 43.8 equivalent full load hours.

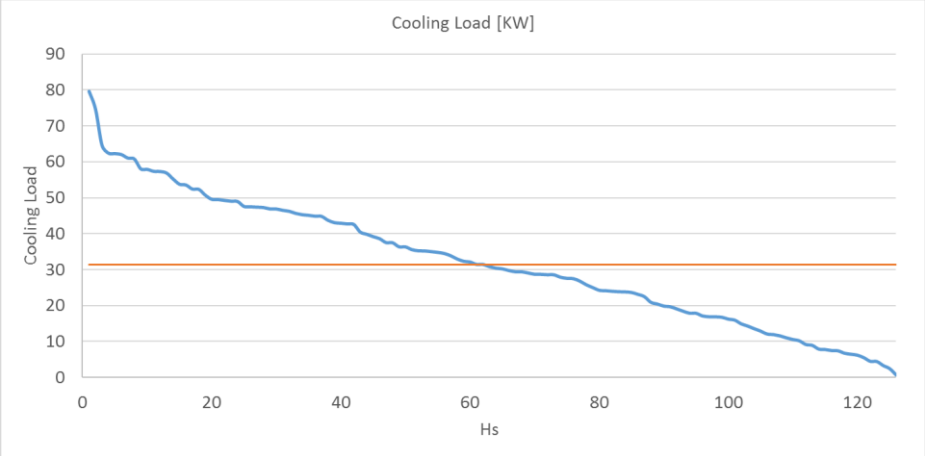

Figure 0-26: Cooling Load in KW

The next figure shows the evolution of the thermal and electrical COP per working day. Averages are also shown.

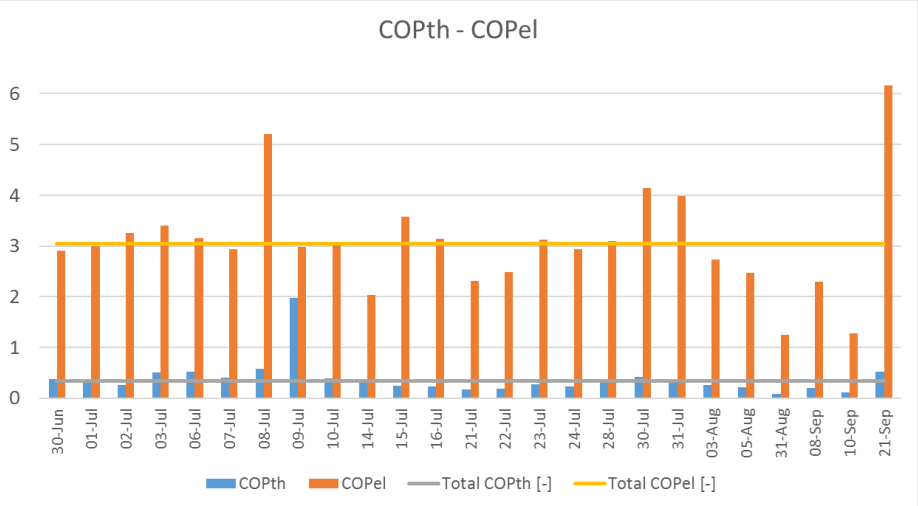

Figure 0-27: COPth and COPel

The next graphic shows the primary energy ratio (PER) of the facility. As stated before, it is directly related to the electrical energy consumption and, therefore, follows the trend of the electrical COP in the previous figure. To calculate the reference PER, and following the suggested in the IEA Task 38a, a COP of 2.8 was estimated for a conventional compression chiller, and the primary energy factor (PEF) for electricity was elected as 2.5.

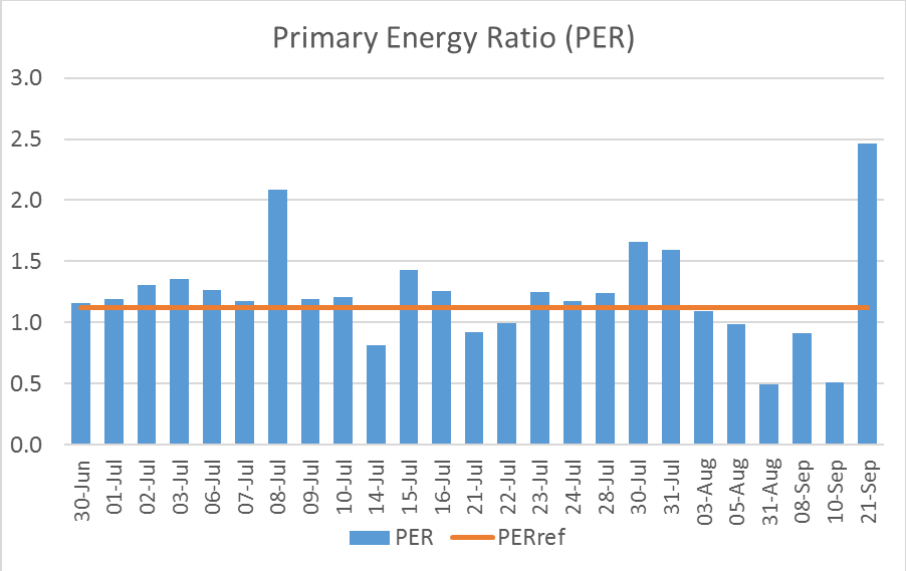

Figure 0-28: Primary Energy Ratio (PER)

The following tables summarize the calculated values for the whole 2015 summer season. Besides, the **COPel** considering stand-by mode (from 04.05.2015 to 07.10.2015) totalizes **1.62**. Therefore, the **PER** considering stand-by mode is as low as **0.65**, totalizing negative energy savings of -38%.

Summary summer 2015 (04.05.15-07.10.15)	
Working days	25
Average operation [Hs]	4.56
Total useful cold [KWh]	3951.2
Average cooling power [KW]	34.66
Total motive heat [KWh]	11129.3
Average ambient temperature [°C]	30.8
Average building temperature [°C]	25.3
Total electrical consumption [KWh]	1226.7
Solar radiation [W/m2]	761.7
Total COPth [-]	0.36
Total COPel [-]	3.22
Total PER [-]	1.29
PER savings [%]	19.5
Total rejected heat [KWh]	14794.6
Collectors' yield [KWh/m2*day]	30.91
Collectors' utilization factor [%]	36%

	COPth/el	PER	Building Temp. (Ambient T) [°C]	Coll. Factor [%]
Maximum	1.98/6.16	2.48	29.67 (44.68)	53.3%
Minimum	0.09/1.24	0.50	19.66 (24.59)	13.3%

Table 4-6: 2015 seasonal results

4.3 Steam Jet Ejector vs. Absorption chiller

4.3.1 Absorption Chiller Facility in ZAE Bayern – Basic description

The importance of this facility, that makes it extremely useful for comparison, is the scale. While most of the carried-out investigations in Europe are focused in small scale facilities (under 20 KW cooling power), the ZAE Bayern developed a 90 KW cooling facility, with a single/double stage absorption chiller driven by a combination of solar thermal collectors and gas. The installation is mounted in Arnstorf in the firma Lindner AG.

The next figure shows the system layout in cooling mode. The analysis will only cover this mode, as this work focuses on the summer operation (cooling mode) of the facilities.

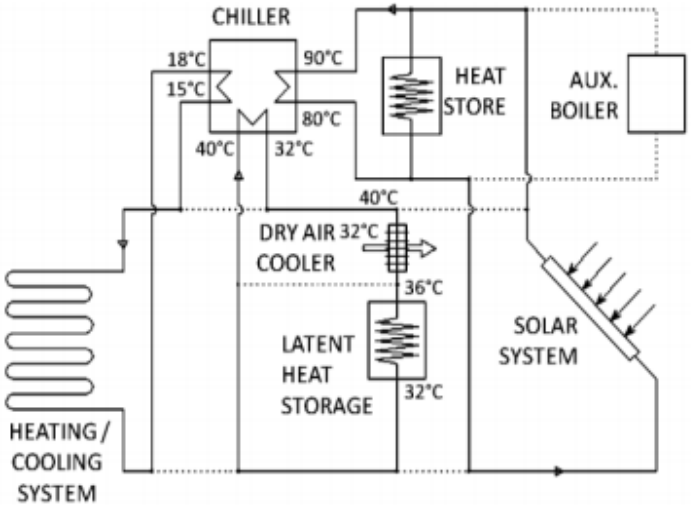

Figure 0-1: ABS system layout. Source: Riepl (et. Al. 2012)

The main differences between the facilities are:

- Absorption chiller single/double effect instead of SJEC
- Flat plate collectors instead of vacuum tube
- Dry cooling tower with heat storage instead of wet open
- Auxiliary gas burner as heat back up

The next table summarizes the characteristics of the facility. It is important to remark that the objective of this prototype was to reach a solar fraction of 60%. This is a key difference between this and the HsKA approach, as the intention was to drive the steam jet ejector with 100% solar energy. The producer of the chiller is the firma Thermax, and it is driven with hot water (about 90°C).

Data of the Installation	Arnstorf	Karlsruhe
Air-conditioned Area	3500 m2	3130 m2
Cooling/Heating power	90/160 KW	82/200
Chiller type	Absorption Single/Double effect, Li/Br	Steam Jet Ejector
Solar collector area (effective)	264 m2	360 m2
Collector type	Flat Plate	Vacuum Tube
Cooling Tower	Dry	Wet open
Heat Storage	2 x 1.5 m3	500 kg PE
Cold Storage	None	1.5 m3
Sensible water heat storage	17 m3	None
Heat backup	Integrated gas burner	None

Table 4-7: System characteristics - compared. Source: Riepl (et. Al. 2012)

The absorption chiller (ABS) can be operated in single or double effect mode. The single effect mode is driven by solar energy plus a hot water boiler (90°C) as back up. The double effect mode is driven by the solar energy plus a steam boiler (160°C), as the double effect requires more motive heat. The double/single effect is driven by a gas burner, in which the exhaust gases are recirculated to drive the single effect in parallel with the double effect, leading to theoretical lower primary energy consumptions. On these studies, it was concluded that the mixing of solar energy and fossil fuels lead to poorer performances; this means that, when the solar energy is not enough to drive the system, the collectors field is turned off and the facility is driven entirely with fossil fuels (in this case, natural gas). Results will be analyzed for the three operative modes of the facility.

As said before, the heating mode of the facility will not be analyzed, as it is not the objective of this work. Even though there are existent differences between this facility and the studied in the HsKA, both models are comparable and a comparison of their results and experiences can be fruitful looking forward to future prototypes.

4.3.2 Comparison of daily working conditions

The studies performed on the ZAE facility in Arnstorf were carried out during summer 2011. Before making any comments, it is very important to clarify that the Primary Energy Ratio (PER) defined in the ZAE Bayern's work is the inverse as the one defined in this work. Therefore, all the PER obtained should be converted in order to be comparable.

Due to similarities of the ambient conditions, the days 13.09.2011 for the ABS and the 31.07.2015 for the SJEC were selected for the comparison.

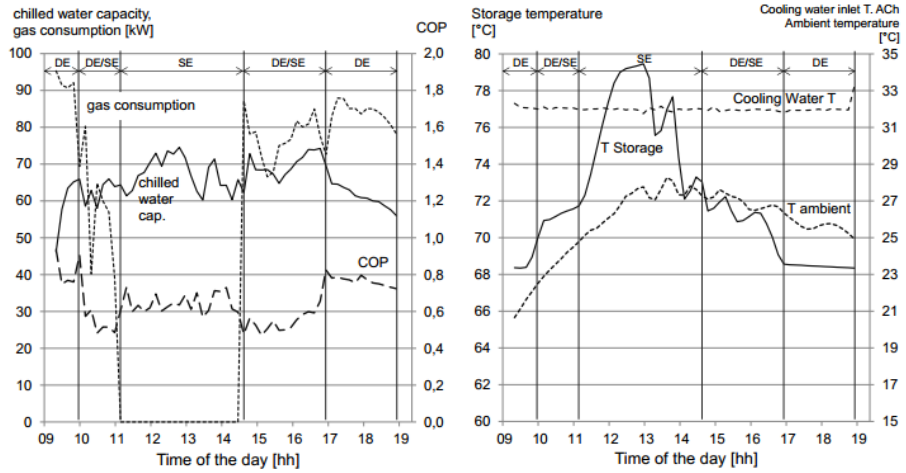

Figure 0-2: ABS facility – operation 13.09.2011. Source: Riepl (et. Al. 2012)

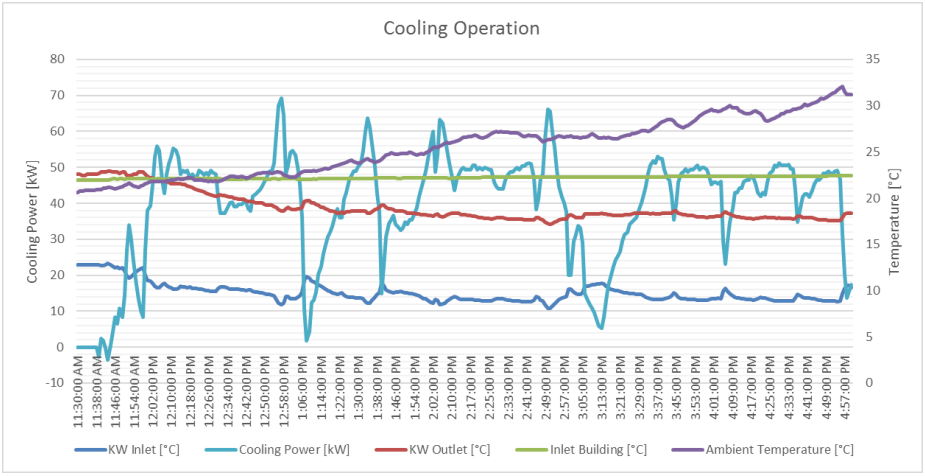

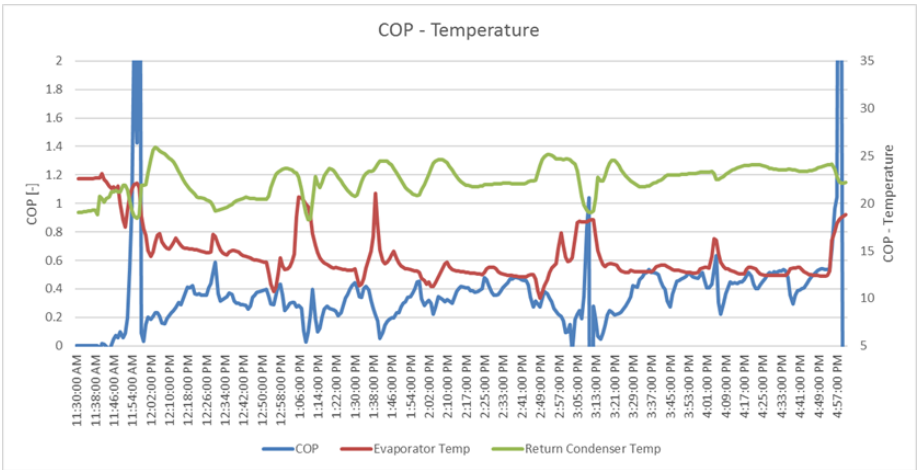

Figure 0-3: SJEC facility – operation 31.07.2015

In the figures 4-31 the operation conditions of the selected day (13.09.2011) are represented. Even though different days are represented for both facilities, some conditions are similar. Peak ambient temperatures are 28 and 30°C (somehow lower by the ABS example day) and

long operation times were identified (above 6 h). Cooling power seems more stable for the absorption chiller (seven hours long between 60 and 70 KW), although the steam jet ejector chiller also presented an acceptable performance, as it can be seen from its power (40-70 KW) and the building temperature (22-23 °C). Return condenser temperature (cooling water by figure 4-31) stayed under 25°C for the SJEC, and around 32 °C for the ABS. This main difference relies on the fact that cooling towers are very different in each facility (wet for SJEC, dry for ABS). Nevertheless, both seem to be cool enough to provide a reliable operation on these days. Taking a look at the COPth, the ABS presented higher results (stable between 0.5 and 0.8) in comparison with the SJEC (stable between 0.2 and 0.6). The lowest COP in the ABS facility is achieved by DE/SE operation (combined solar and gas). When the operation is presented in SE (only solar power), COPth stays between 0.6 and 0.7. It is worth mentioning that this operation can only be reached in partial load, as the solar fraction achieved by the facility reaches 54%. This shows an overall excellent performance of the ABS facility, when operating in single-effect mode, only driven with renewable solar energy.

The next tables summarize the operational results for both example days (SE operation).

Cumulated daily values	**DAY1 - 13.09.2011**
a) Cooling energy **total**/SE/DESE/DE [kWh] | [% of total]	**650**/230/235/185 | 100/35/36/28
Cooling energy **DESE**: from solar/**gas** [kWh] | [% o.t.]	121/114 | 18/**18**
b) Gas consumption **total**/SE/**DESE**/DE [kWh] | [% o.t.]	**513**/0/249/264 | 100/0/**48**/52
c) Electrical COP total[1]/SE/DESE/DE [kWh cool/kWh el]	**10,5**/12,4/11,4/12,9
[1]total = including all stand-by current (night&day)	
d) $PER_{Cooling}$ **total**/SE/DESE/DE [kWh PE/kWh cool.]	**1,12**/0,21/1,39/1,77 →
$PER_{Cooling}$ DESE: from solar/**gas**	0,23/**2,64**
e) Solar irradiation[2]: total / solar heat gained [kWh]	1742/588
[2]Irradiation on collector area	
f) Solar fraction of cooling demand: **total**/SE/DESE [%]	**54**/35/19
g) PE equivalent electrical compression chiller system EER	**2,32**
Mean values of the day	
g) Ambient temperature: 24h/time of chiller operation [°C]	20,8/25,6
h) Cooling water inlet temperature absorption chiller [°C]	**31,9**
i) Chilled water capacity: total/SE/DESE/SE [kW]	64,8/67,2/67,3/59,2
j) COP_{ACh}: total/SE/DESE/DE	0,63/0,63/0,54/0,71
k) Mean solution temperature: HTG SE/DESE/DE [°C]	---/106,3/95,8
l) Mean solution temperature: LTG SE/DESE/DE [°C]	69,8/69,2/62,3
m) Mean solution temperature absorber: SE/DESE/DE [°C]	39,2/40,9/38,5

Table 4-8: ABS Daily results – 13.09.2011. Source: Riepl (et. Al. 2012)

➔ Inverted PER values = 0.89/**4.76**/0.72/0.56

Overall Results	Unit	Value
Useful Cold at WT1	kWh	211.01
Electric Energy	kWh	53.49
Mean Solar Radiation	W/m2	841.82
Driving Heat (Solar Collectors)	kWh	651.85
Heat rejected through RKW (WT2)	kWh	852.44
Balance of Storaged Heat	kWh	37.69
Collectors' Utilization Factor	%	39.11
Collectors' Yield	kWh/m2	1.81
Thermal Energy Efficiency Ratio SJE (EERth)	-	0.32
Electric Energy Efficiency Ratio SJE (EERel)	-	3.94
Primary Energy Consumption	kWh	133.72
Primary Energy Ratio (PER)	-	1.58
Relative Primary Energy Savings	%	29.02

Table 4-9: SJEC Daily results – 31.07.2015

➔ Total Electrical COP (incl. Stand-by) = **3.09** / PER = 1.23

The results can then be compared. The ABS delivered three times bigger cooling energy (as it operated almost twice the time and the air-conditioned surface is 10% bigger). While SJEC covered that with 100% solar energy, the fraction for ABS reached 54%. The thermal COP was almost double in the ABS facility. However, this indicator is not that representative for the SJEC facility, as it is driven only with solar thermal energy. Electrical COP was above average for the SJEC, although half of the presented by ABS. The IEA Task 38 proposed an objective of COPel = 10. None of them reached it, though ABS was close enough. What is more, the PER of the SJEC facility is bigger. This means that even though the SJEC shows a worse performance, at least it contributed to a saving in primary energy (about 16%), while the ABS shows a negative PE saving of -16%. A logic cause for this operational result is the utilization of gas as a back-up motive heat for the ABS facility.

Taking just a look at the single-effect operation mode for the ABS facility, the position changes. With an average cooling power of 67 KW, and more cold delivered (230 against 211 KWh), the performance numbers are much better. Electrical COP reached values above 12, and the PER (converted) is of 4.76, allowing much higher PE savings than the SJEC facility. Thermal COP is also in ABS about double the SJEC. It would be an interest comparison to test two facilities of these kind in the same day with same weather conditions. The issue of the utilization of gas back-up makes the ABS facility more reliable than DKSM, in terms of reaching the desired temperature in the air-conditioned building.

4.3.3 Comparison of results and KPIs

The results obtained in the analysis of the facility are in this subsection presented. The next table was taken from a paper published by Manuel Riepl (et. Al. 2012).

Cumulated values	**Cooling period 2011 (02.09.-08.10.2011)**
a) Cooling energy **total**/SE/DESE/DE [kWh] | [% of total]	**12035**/5466/2645/3964 | **100**/45/22/33
Cooling energy **DESE**: from solar/**gas** [kWh] | [% o.t.]	1701/944 | 14/**8**
b) Gas consumption **total**/SE/**DESE**/DE [kWh] | [% o.t.]	**8157**/0/2285/5232 | 100/0/**28**/64
c) $COP_{Chiller}$: **total**/SE/DESE/DE [1]	**0,68**/0,63/0,55/0,83
[1]Weighted by the specific cooling energy amount	
c) Electrical COP total[2]/SE/DESE/DE [kWh cool/kWh el]	**8,7**/12,1/12,3/12,5
[2]total = including all stand-by current (night&day)	
d) $PER_{Cooling}$ **total**/SE/DESE/DE [kWh PE/kWh cool.]	**1,04**/0,23/1,13/1,66
$PER_{Cooling}$ DESE: from solar/**gas**	0,21/**1,79**
e) Solar irradiation[3]: total / solar heat gained [kWh] | used [%]	46937/12755 | 27
[3]Irradiation on collector area	
f) Solar fraction of cooling demand: **total**/SE/DESE [%]	**54**/45/9
g) PE equivalent electrical compression chiller system EER	**2,49**
h) Operational hours chiller **total**/SE/DESE/DE [h] | [% o.t.]	**186**/82/36/69 | 44/19/37
i) Full load hours (90 kW) [h]	**134**

Table 4-10: ABS Seasonal results. Source: Riepl (et. Al. 2012)

➔ Inverted PER = 0.96/4.35/0.88/0.60

Comparing the table 4-10 with the seasonal results of the SJEC (tables 4-7), a much better performance from the ABS can be easily recognized. All the key performance indicators lead to this conclusion. However, both facilities provided seasonal negative primary energy savings, which is a key point to consider the future of solar cooling with the current technology. The only part that shows a better performance for the SJEC is the solar collectors system, with a higher utilization factor. Nevertheless, this was highly expectable, as the VTC are nowadays one of the top collectors available in the market.

The difference on the amount of cold energy delivered relies on the fact that there were more operational days for the ABS facility in the 2011 season than for the SJEC in the year 2015. Causes for this are not only the fact the SJEC was turned off on weekends, but also the register of failures during the SJEC 2015 operation and possible differences in the control strategy of the facility (different targeted building temperatures, for example).

The next figures will show daily summaries of different values, comparable from ABS to SJEC facilities.

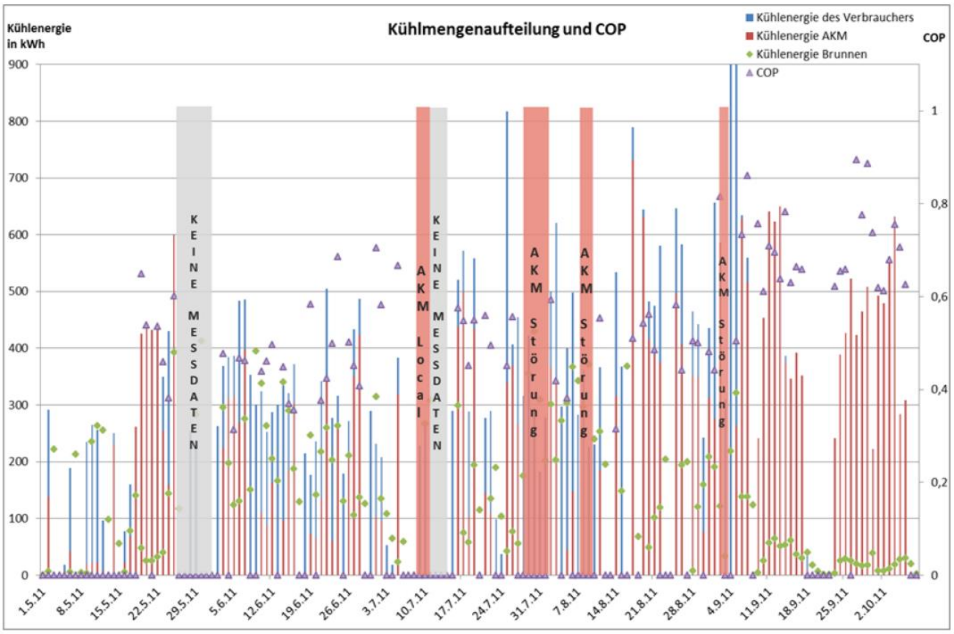

Figure 0-4: Cold energy and COP in 2011. Source: Helm (et. Al. 2013)

The season length was almost the same for the two facilities. However, first significant working day for SJEC was 30.06.2015, whereas for ABS was 02.05.2011. Long operating hours show better thermal performances in the ABS facility.

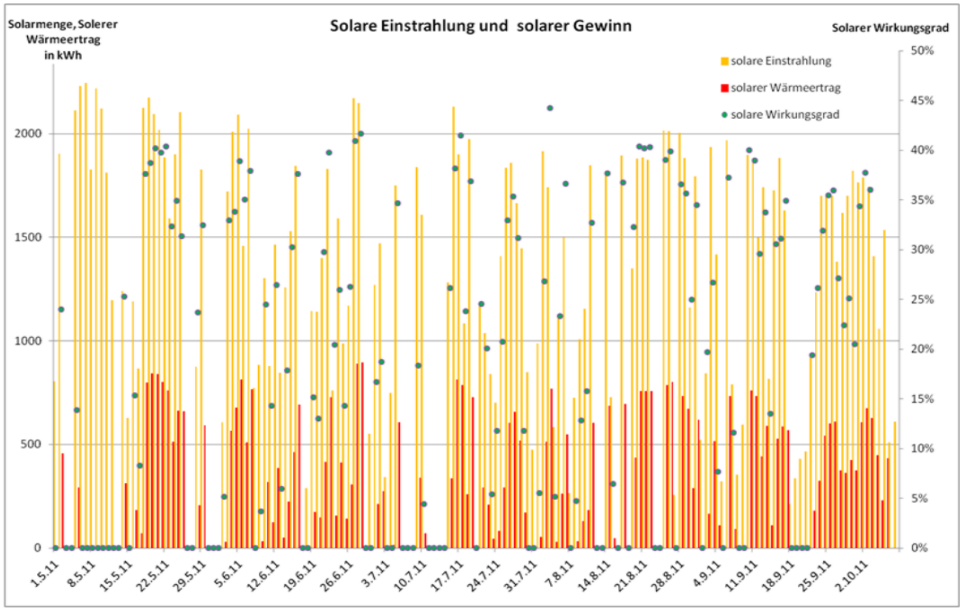

Figure 0-5: Solar radiation and motive heat in 2011. Source: Helm (et. Al. 2013)

As noticed on table 4-10, the solar collectors field of ABS shows a poorer performance than the SJEC. Yet it would be interest to analyze the potential solar collectors' efficiency of the SJEC facility, when it worked more days than it actually did on the 2015 season.

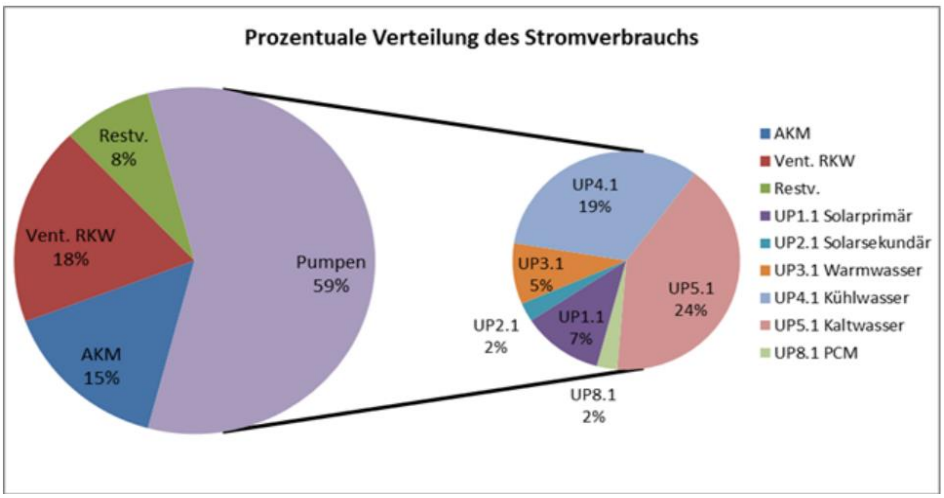

Figure 0-6: Percentage distribution of electricity consumption in 2011. Source: Helm (et. Al. 2013)

A key point of comparison, where relies the primary energy consumption, is the electrical energy. It can be seen that the total consumption of pumps represented for ABS 59%, whereas in SJEC it took the 79%. The highest electrical consumption peaks in both cases for the chilled water and cooling circuit pumps, both between 20 and 24% of the total. The chiller operation consumed for ABS 44%, while it arouses around 51% for the SJEC.

The cooling tower fan consumed 18% for ABS, while it occupied 14% for SJEC. In total, the cooling circuit represents 37% for the ABS facility and 38% for the SJEC, with similar results. All in all, it can be seen that the operational mode of both facilities was in partial load conditions. A good control of this is necessary to avoid excessive electrical consumption, lowering the efficiencies and primary energy ratios of the solar cooling facilities.

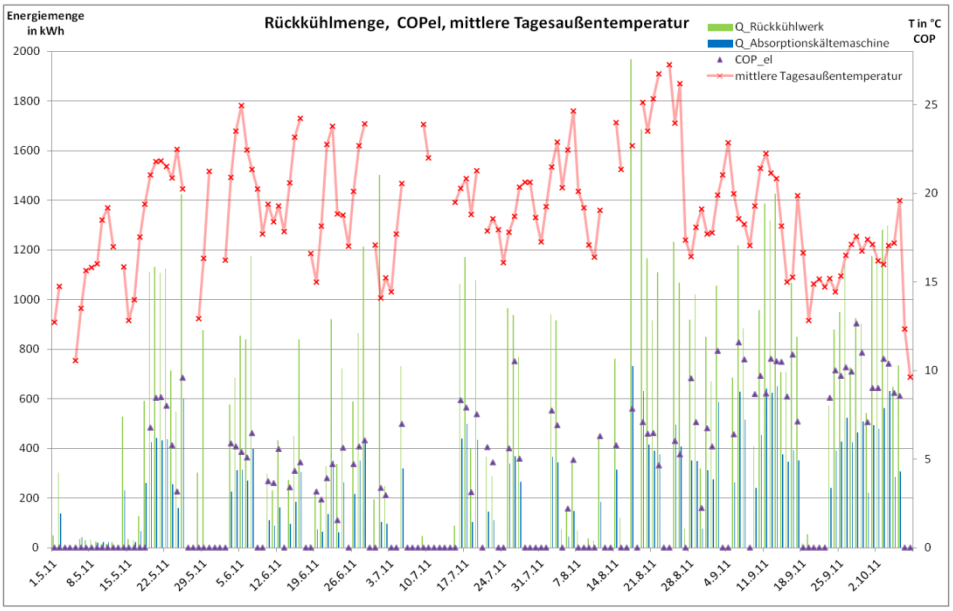

Figure 0-7: Cooling tower and ambient temperature in 2011. Source: Helm (et. Al. 2013)

The last figure 4-35 shows the heat rejected through cooling tower to the ambient and the outside temperature for the ABS facility in the 2011 summer season. Long operating hours allow to raise considerably the electrical COP, as it not only increases the feed-in cold, but also lowers the influence of stand-by operation.

In addition, it results fundamental to highlight that only on three days under operation the daily average temperature was above 25°C. For the SJEC were registered instantaneous temperatures of almost 45°C and daily averages above 30°C. The low ambient temperatures allow the ABS facility to perform considerably well with a dry cooling tower. Besides, the necessity of a high pressure motive steam for the SJEC highlights the task of the cooling tower, as a lower condenser temperature allows the machine to operate with less motive heat (pressure). In conclusion, the cooling tower in the SJEC facility needs to achieve maximum temperature differences of 20 K, which are not considered in the ABS heat rejection circuit (as it operates with low temperature heat sources). Although in the consulted papers there is no data about building temperature, it is assumed that the desired temperature was achieved, as it is stated that the amount of delivered cold was enough to claim a good ABS performance. This is another difference with the SJEC, which could not achieve the desired values in the hottest days (above 35°C). However, as stated before, there is no record of the performance of the ABS in such ambient conditions in order to make a proper comparison.

As another conclusion, the absorption facility made possible the development of a very reliable system with a high solar energy fraction (around 60%). As stated before, it would be interesting to analyze a new development of absorption chillers with high solar fractions and to analyze the primary energy consumption on these cases and on hot weathers, although it can be assumed that the developed chilling capacity of the ABS facility could also perform well in single-effect mode (100% renewable energy) with acceptable chilled water temperatures.

4.4 Steam Jet Ejector vs. Other facilities

4.4.1 Scaling of the project

As defined in the subsection 3.4.2.1, the project must be scaled to make comparable the comparison figures. Taking the equations 3.2, 3.3, 3.4 and 3.5, the figures for the Steam Jet Ejector Facility are:

$$Nominal\ Cooling\ Power\ [kW] = 82\ KW \tag{3.2}$$

$$Relative\ CP = \frac{Collectors´Area\ [m^2]}{Nominal\ Cooling\ Power\ [kW]} = 4.88\frac{m^2}{KW} \tag{3.3}$$

$$\%RE = \ driving\ heat\ covered\ by\ renewable\ energy = 100\% \tag{3.4}$$

$$Collectors'\ Yield = \frac{Driving\ Heat\ [kWh]}{Collectors´Area\ [m^2].year} = \ 192\frac{KWh}{m^2a} \tag{3.5}$$

The next figure compares the relationship of collectors' area and cooling power from the steam jet ejector facility with the rest of the observed installations.

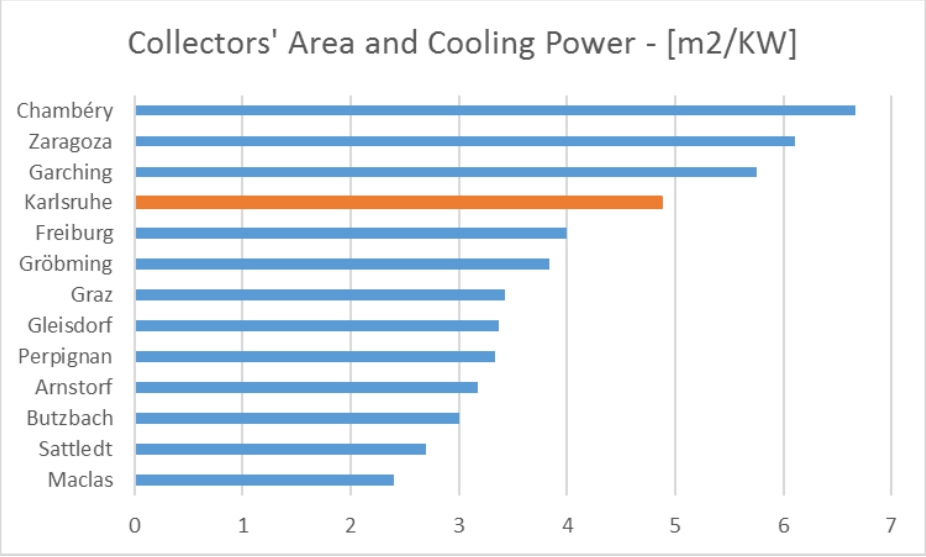

Figure 0-1: Comparison of facilities. Source: IEA Task 38a (2010)

4.4.2 Results comparison

In this subsection, the results of the analysis for the SJEC facility will be compared with figures provided from the IEA Task 38a, in order to relate its performance to other similar facilities. The following table provides a summary of the installations considered.

Year	City	Nom CP [KW]	Coll. Area [m2]	Chiller	AC area [m2]	Storage	Heat Rejection	Aux heater type (KW)	m2/KW
2009	Maclas	10	24	Absorption	210	Heat - Cold	Dry	Chiller (aux cold - 3 KW)	2.4
2007	Sattledt	15	40.5	Absorption	150	Heat - Cold	Wet open	Gas Boiler (9 KW)	2.7
2009	Butzbach	20	60	Absorption	335	Heat - Cold	Wet open	Gas Boiler (28 KW)	3.0
2011	Arnstorf	90	286	Absorption	3500	Heat - Cold	Dry	Gas Boiler (90 KW)	3.2
2009	Perpignan	7.5	25	Adsorption	180	Heat - Cold	Dry	Chiller (aux cold)	3.3
2010	Gleisdorf	19	64	Absorption	1000	Heat	Wet open	3xCHP + Gas boiler (69 KW)	3.4
2009/10	Graz	17.5	60	Absorption	435	Heat - Cold	Hybrid	District Heat	3.4
2009/10	Gröbming	12	46	Absorption	700	Heat	Wet open	Biomass (150 KW)	3.8
2009/10	Freiburg	5.5	22	Adsorption	42	Heat	Dry	Heat network - aux. chiller	4.0
2015	Karlsruhe	82	400	Steam Ejector	3130	Heat - Cold	Wet open	None	4.9
2009	Garching	10	57.5	Absorption	400	Heat	Dry + latent storage	Pellet boiler	5.8
2008	Zaragoza	4.5	27.5	Absorption	215	Heat	Dry + Geothermal	Yes (not used)	6.1
2009/10	Chambéry	4.5	30	Absorption	21	Heat - Cold	Geothermal field	Electric heater + backup	6.7

Table 4-11: Facilities' summary - CP = Cooling Power. Source: IEA Task 38a (2010)

Most of the facilities of the comparison are small scale (under 20 KW cooling power) and with absorption chiller units, with back-up heaters. More details over the facilities can be found on the report of IEA Task 38a (2010). The next figure shows the COPth. The red line is the value achieved by the facility in the HSKA.

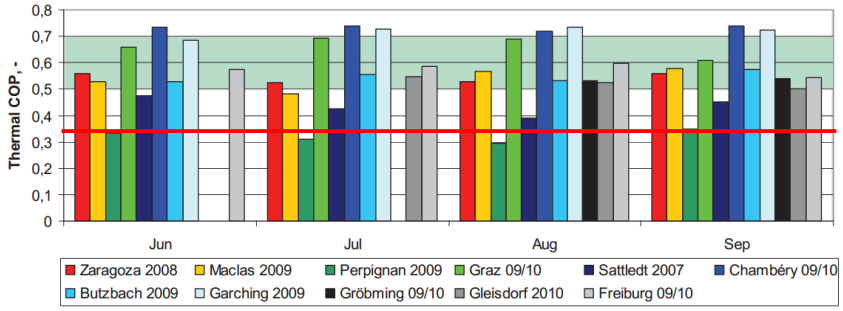

Figure 0-2: Thermal COP. Source: IEA Task 38a (2010)

Only one of the twelve compared facilities achieved a lower COPth, showing that this value could be improved. The next graphic shows the comparison of COPel. It is important to mention that the COPel is calculated without stand-by operation consumption.

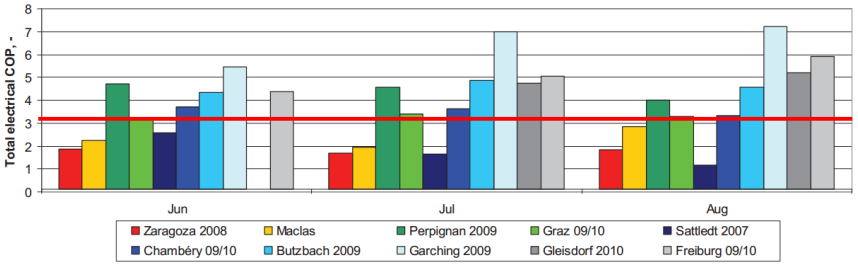

Figure 0-3: Electrical COP. Source: IEA Task 38a (2010)

On the contrary, the COPel under operation shows fairly good results in comparison with other facilities. As the electrical consumption in a 100% renewable energy installation is the only source of primary energy consumption, this indicator results of key importance.

The Primary Energy Savings are obtained comparing the PE consumption of the studied facility with a reference one. As a reference installation, a 2.8 COP compression chiller was selected,

and back-ups were provided with different facilities (IEA Task 38a (2010), pages 50-53). It is important to mention that the PR savings, as well as the COPel already seen, were calculated only under operational mode (not considering stand-by consumption). What is more, the facilities' savings are calculated throughout a year, including the PE savings added by winter operation (except Maclas and Zaragoza, which did not count with heating systems). The results show that the position of the operational savings of the SJEC facility is within the average of the analyzed facilities, showing at least positive savings.

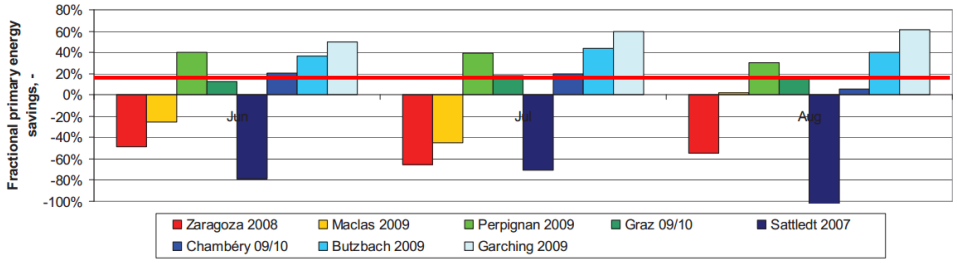

Figure 0-4: Primary Energy Savings. Source: IEA Task 38a (2010)

The next figure shows the collector field performance in the different facilities. It is important to highlight that five out of six facilities present flat plate collectors, in comparison with the HSKA facility, which is equipped with vacuum tube collectors.

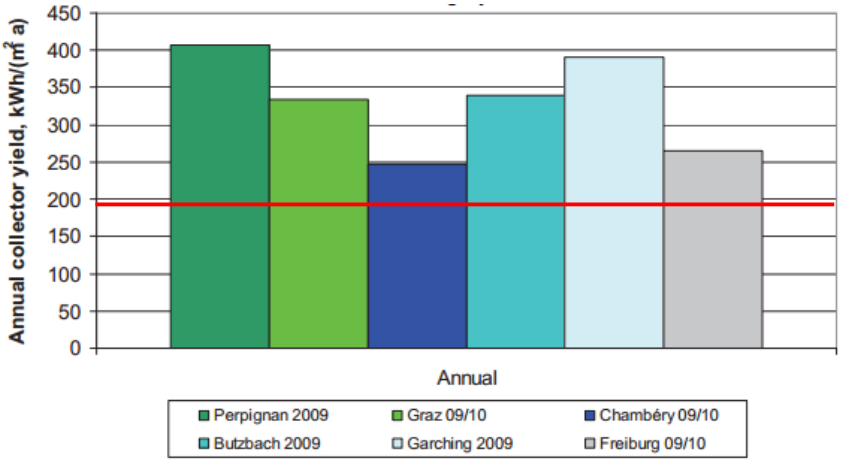

Figure 0-5: Collector Yield. Source: IEA Task 38a (2010)

Even though the value of the SJEC facility is the only one under 200 KWh/m^{2}a, there are two key points that explain this result. One is the already identified inefficient control strategy in the solar collectors, as the water flow seems very high to evaporate it totally, already identified in the report by Bauer (2014). The second one relies on the fact that, as only 25 of 152 total days of summer showed significant cooling operation (above 20 KWh delivered), the facility is on the other days turned off. This means that, especially in the months of August

and September 2015, the heat gains are very low, as the facility was not working (see figure 4-17). Besides, there is no operation of the facility on weekends, lowering also the collectors' yield on winter period. It can be then considered, that the collectors field in the SJEC facility operated approximately nine months out of twelve. If an extrapolation of this values is done, the collectors' yield would reach a value of 256 KWh/m^{2}a. However, this quick calculation does not take into account that the summer period shows significant solar radiation values, allowing higher heat gains.

Following the collectors' field performance, the next figure compares the main indicators of the SJEC facility with the one in Butzbach (Fraunhofer ISE). Even though this facility presents only 60 m^2 aperture area (360 m^2 for HSKA), the comparison is possible as both present vacuum tube collectors. On the left side, the Butzbach results are presented, whereas in the right side, the SJEC facility is drawn.

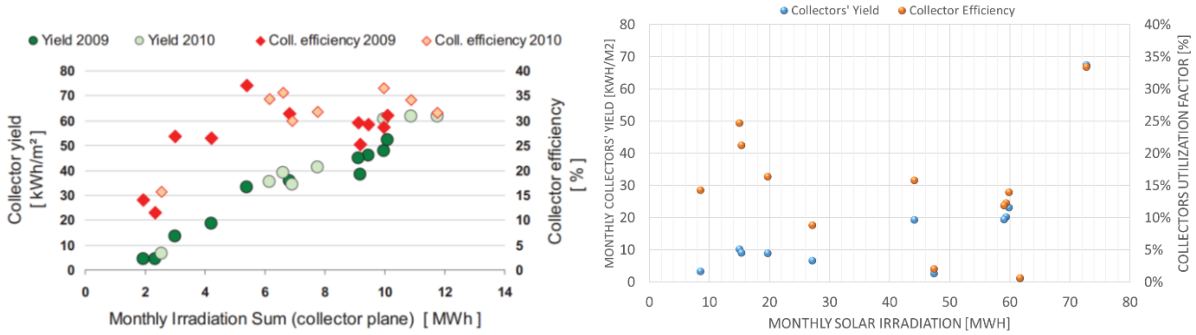

Figure 0-6: Collectors' Performance. Source: IEA Task 38a (2010)

In order to back up what was stated above, the reason why the SJEC facility presents such low collector yields (nine months under 20 KWh/m^2) is the low amount of operative days. This also is an influence in the value of the collectors' utilization factor, as only three months are above 20%, which is a relative low value. Conclusions about will be further described.

4.5 Treatment of errors in the SJE Facility

4.5.1 Introduction

The propagation of error calculations is performed following the steps of the Engineering Statistics Handbook from the National Institute of Standards and Technology (NIST) from the United States of America. In this work it was mainly applied to the heat storage and its unbalance between the loading and unloading phases.

The main equation to propagate the errors is presented as follows. It was selected, as the errors are random and independent of each other. The general equation "q" is firstly defined. Then the error of "q", depending on its variables, is calculated.

$$q = f(x, y, \dots, w)$$

$$\delta q = \sqrt{\left(\frac{\partial q}{\partial x}\delta x\right)^2 + \left(\frac{\partial q}{\partial y}\delta y\right)^2 + \cdots + \left(\frac{\partial q}{\partial w}\delta w\right)^2} \qquad (4.1)$$

The errors are mainly considered by the measurement tolerance of the sensors. Each one will be described in this subsection. It is also crucial to state that there are several measurement errors registered by the SPS Software. In order to perform calculations properly, the database was cleaned of errors and some decision rules to avoid them were defined. These will also be explained in this chapter.

4.5.2 Heat Storage

In the case of the heat storage, the following assumptions were made:

- Water is liquid, as taken from the bottom of steam drum
- Density remains almost constant at 950 Kg/m^3
- Constant Cp remains almost constant at 4.22 KJ/Kg
- Average daily values for volume flow and temperature are taken

Since the heat stored is calculated by an enthalpy difference of the inflow and outflow water through the storage, the following equation applies for the instantaneous power.

$$\dot{Q}[kW] = \frac{\rho \,.\, \dot{V}.\, C_p \,.\, (T_{in} - T_{out})}{3600} \qquad (4.2)$$

There are three variables that can present error measurements due to sensor tolerance:

- Tin and Tout ➔ $\delta T = 0.9\ K$ (absolute error)
- Volume flow ➔ $\varepsilon\dot{V} = 0.3\ \%$ (relative error) ➔ $\delta\dot{V} = 0.003\,.\dot{V}$ (absolute error)

Therefore, the error of the instantaneous power is:

$$\delta Q = \sqrt{\left(\frac{\partial Q}{\partial V}.\delta V\right)^2 + \left(\frac{\partial Q}{\partial Tin}.\delta Tin\right)^2 + \left(\frac{\partial Q}{\partial Tout}.\delta Tout\right)^2} \qquad (4.3)$$

Deriving equation 4.2 it results

$$\frac{\partial \dot{Q}}{\partial \dot{V}} = \frac{\rho.\ C_p\,.\,(T_{in}\ -\ T_{out}\,)}{3600} \qquad (4.4)$$

$$\left|\frac{\partial \dot{Q}}{\partial Tin}\right| = \left|\frac{\partial \dot{Q}}{\partial Tout}\right| = \frac{\rho.\dot{V}\ C_p}{3600} \qquad (4.5)$$

As an example, the day 15.07.15 from 7:27 AM to 7:01 PM (timeframe in which the heat storage worked) is taken to calculate the errors propagation. The volume flow is measured by FIR-W-7-2 (and duplicated, since FIR-W-7-1 is stuck in -14.22 m^3/h, which means is not working properly), the inlet and outlet temperatures for module 1 are TIRC-W-7-1 and TIRC-W-8-7 respectively; for module 2, they are TIRC-W-7-2 and TIRC-W-8-6. The collected data is:

- Volume Flow through both pipes = 3.916 m^3/h
- Tin1 = 109.63 °C = 382.78 K ; Tout1 = 108.99 °C = 382.14 K
- Tin2 = 110.20 °C = 383.35 K ; Tout2 = 109.71 °C = 382.86 K

$$\frac{\partial Q}{\partial V}.\delta V = 0.0083\ KW\ ;\ \frac{\partial Q}{\partial Tin}.\delta Tin = \frac{\partial Q}{\partial Tout}.\delta Tout = 3.93\ KW$$

$$\therefore \quad \delta Q_{M1} = \delta Q_{M2} = 5.55\ KW$$

From the calculations it can be clearly derived that the temperature tolerance of the sensors plays an important role in the heat stored. The next graphic shows for the module 1 in the selected time frame the instantaneous power of heat storage.

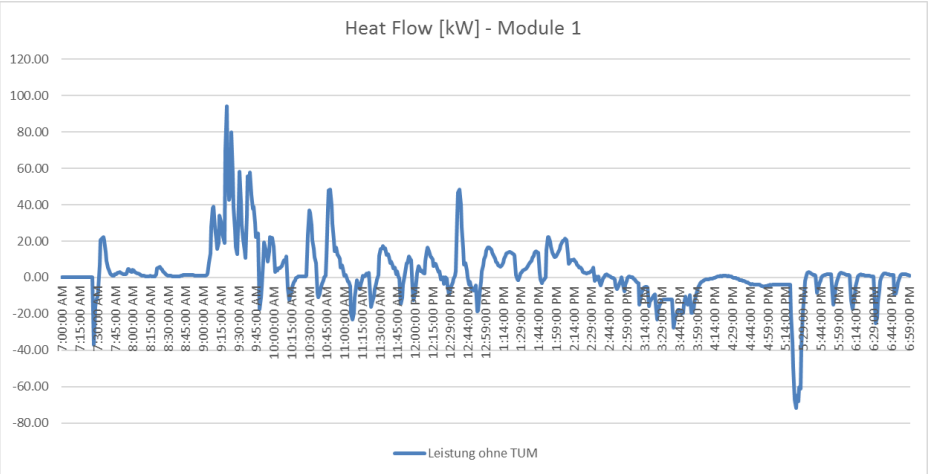

Figure 0-1: Heat Flow in module 1 of Heat Storage

As it can be seen, besides the peaks at 9:20 AM and 5:20 PM, the heat flow rarely is greater than +/- 40 KW. This means that, as a relative error, the error calculation of the heat flux is above 25%. However, this study is not considering the accumulation of errors. The errors are repeated every minute since the measurements are taken within this time distance. In the next figure, an integration of the heat flow is performed, obtained the curve for the accumulated energy in the heat storage (in KWh). In this case, it is also drawn an optimistic and pessimistic case, in which the temperature error tolerance of the sensors is taken to the extreme case (+/- 0.9 K for every measurement). The results can be seen in the next figure.

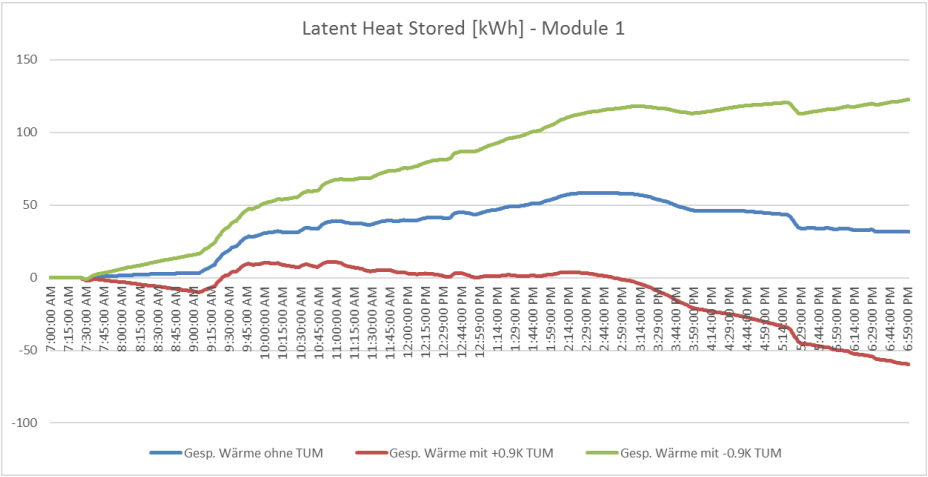

Figure 0-2: Heat stored in module 1.

The blue line represents the direct integration of the curve in the previous figure. The green line represents the extreme case in which the inlet temperature is raised by +0.9K and the

outlet temperature is subtracted by -0.9 K (maximum heat stored). The other case is drawn by the red curve, in which the minimum heat is stored (or even released, as it can be seen). In this case, the inlet temperature is reduced by -0.9K and the outlet temperature is increased by +0.9 K. Even though the energy accumulated is dependent on the previous value, this graphic shows that the heat stored at the end of the day can vary from 120 to – 60 KWh. It is accepted in this work that different temperature shifts (according to each day) will be made in order to reach a final value of 0 KWh stored at the end of the day. It is acquainted that errors through this process are committed and accepted. The calibration of sensors was performed to ensure the proper measurement. The results are presented in the next subsection.

4.5.3 Sensor Calibration – Heat Storage

The calibrated sensors are TIRC-W-7-1 and TIRC-W-8-7, which are respectively inlet and outlet from the Heat Storage module 1. The complete procedure is presented in the Annex III. The next figure represents the trendlines of the measured points.

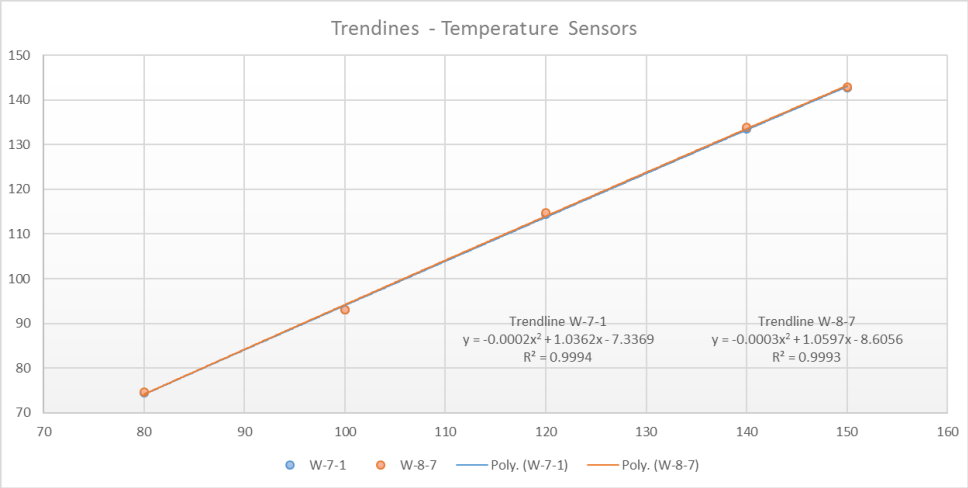

Figure 0-3: Trendline for temperature sensors

As it can be easily seen, both curves respond to very similar equations, with a very high R^2 value. In addition, a distance of almost 6/7 degrees under the exact set value is observable for each measurement.

This drives to a crucial conclusion, which is that both sensors provide almost the same response to the same temperature shift. Since these are used for the thermal storage (needed ΔT), it can be derived that, even though the sensors are not properly calibrated, they provide enough evidence that they are in a fairly correct range. Due to the noticeable deviation of 6/7 degrees for each measurement, it is assumed that the applied temperature shift of 0.9K is

acceptable. This deviation is provided by the thermometers' manufacturer and is necessary to obtain coherent charging and discharging phases. Therefore, the example days will be provided with a manual temperature shift of +/- 0.9K to reach a balance between the charging and discharging phases.

4.5.4 Motive Heat

As performed on subsection 4.5.2, the error calculation for the motive heat absorbed by the solar collectors was calculated. The motive heat is calculated in this case with the following equation:

$$\dot{Q}[kW] = \frac{\rho_{vap}.\ \dot{V}.\ C_{p,vap}\ .T_{out}\ - \rho_{liq}.\ \dot{V}.\ C_{p,liq}\ .\ T_{in}}{3600} \qquad (4.6)$$

Therefore, the error of the instantaneous power is, as before:

$$\delta Q = \sqrt{\left(\frac{\partial Q}{\partial V}.\delta V\right)^2 + \left(\frac{\partial Q}{\partial Tin}.\delta Tin\right)^2 + \left(\frac{\partial Q}{\partial Tout}.\delta Tout\right)^2} \qquad (4.7)$$

Taking as the example day from subsection 4.2.4 the 06.07.15, the relative error obtained for the motive heat is 2.44%. The mathematical development is the same as employed on subsection 4.5.2.

4.5.5 Measurement Errors

Throughout the performing of the database and calculations, several system failures were encountered. These not only created difficulties at the time of the analysis, but also forced the software to be error-proof. Some examples will be listed in this section.

The volume flow sensor FIR-W-7-1, which conducts the water through the Module 1 of the Heat Storage, is found often stuck at some random values (usually 0.003472 or -14.22). As it can be proven in other reference days, the values of this and FIR-W-7-2 (module 2) should be almost the same, nearly rounding the value of 4 m^3/h. Besides, the pump P3 is feeding both pipes with these sensors, and has a nominal volume flow of 12 m^3/h. As a rule of decision, when the sensor number 1 is between the values of 0.5 and 6 m^3/h is considered to be operating properly. Otherwise, the stored value is considered wrong and for the calculations, the value of FIR-W-7-2 is copied.

Another frequent problem with the heat storage is precisely the value of speed % of the pump P3. Sometimes this value is stuck to zero, while the volume flow sensors indicate there is water flowing through the pipes. Since there are no registered errors in FIR-W-7-2, a crossed check through this sensor and the pump is made. Whenever the pump shows no speed and there is water flowing through the pipes, the speed is calculated through the first law of affinity of Fluid Machinery. This states that the relationship between volume flow in the pump and speed is linear:

$$\frac{\dot{V}_2}{\dot{V}_1} = \frac{n_2}{n_1} \cdot \left(\frac{D_2}{D_1}\right)^3 ; D\ remains\ constant \qquad (4.8)$$

It is important to state that the nominal volume flow of the pump is 12 m3/h. For example, if FIR-W-7-1 is stuck at a negative value, FIR-W-7-2 shows 4 m^3/h and the speed of pump 3 is 0%, the following corrections are made:

- FIR-W-7-1 = -14.22 m^3/h → FIR-W-7-1 = FIR-W-7-2 = 4 m^3/h
- Speed P3 = 100 . (12/8) = 66.66 % speed

What is more, the value of the pressure sensor PIRC-W-6-2 is several times stuck around 2 bar relative. As this sensor results key in the calculation of the heat stored, it will be replaced by the value of the outflow of the heat storage, sensor PIR-W-8-1. As this values are not supposed to be very different, and the density and constant Cp values do not vary significantly with pressure, this approximation does not provide a big influence in the value of the heat stored, which proved to be a very sensible calculation.

Sensor PIRC-B6-1 is also sometimes stuck at the value of -18.96 bar relative. As it also integrates the steam drum - heat storage circuit, it is replaced for the value of the pressure sensor PIR-W-8-1.

Furthermore, another issue happened with the temperature sensors in the collector field. On the 21.09.15 errors were registered in the sensor TFeld 3_6, recording a stuck temperature of 3276.7 for three hours. As it is physically impossible to register this temperatures, all sensors are proofed to be under 300°C. Whenever a sensor gets over this value, it takes the average value of other sensors in its same place (for example, TFeld 3_6 copies the value of TFeld 3_5, which should be in theory almost the same). This measurement error was frequently found during the months of September and October 2015.

5. General Conclusion

Regarding the operational performance, the cold delivered during the operation days seemed enough when the instantaneous ambient temperature stayed below very high temperatures (below 35°C). The next graphics show summaries of daily and hourly temperature averages.

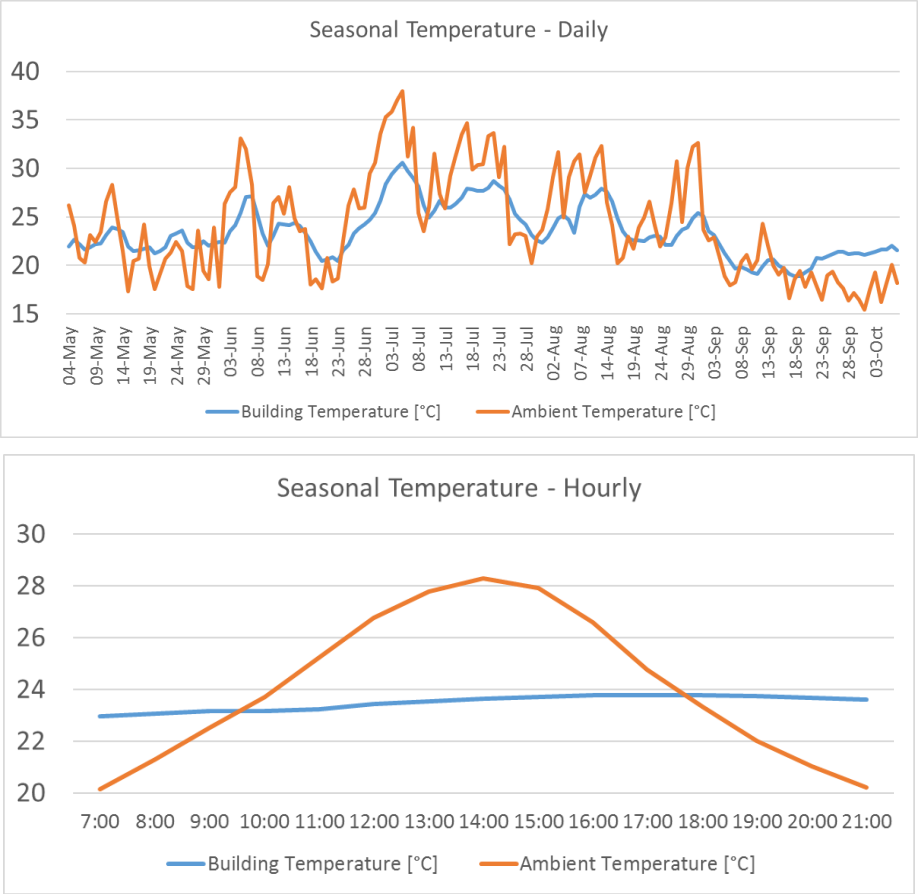

Figure 0-1: Temperatures summer season 2015

As a recommendation, it should be analyzed the non-operational days, in order to identify the reasons why it did not provide a successful cooling power.

For the days above 35°C, there was not enough power. It should be technical and economically studied the possibility of having a backup chiller for those days (as long as the amount of hot days allow this, and the investment costs). What is more, it should be decided if the fulfilling of 100% comfort conditions is economically feasible under further investments (cold backup).

Regarding the technical performance of the facility, the thermal COP showed lower values than the initially obtained. As a main cause it could be identified that long operational hours could not be achieved (in comparison with the ABS facility), and it is on these days that the

best thermal efficiency was seen. Focusing on the electrical consumption, the research goal of 10 for the COPel was not even close obtained. 50 % of the electricity is consumed by the driving chiller pumps and almost additional 40% on the cooling tower circuit. It was identified that most of the time the facility did not work under nominal power. This part load control should be specifically optimized in order to avoid too much electrical consumption on pumps. For future investments, it should be taken into account the possibility of having high efficiency pumps for the above mentioned cases. Moreover, the possibility of shutting down completely the facility on weekends should be considered, to reduce the stand-by electrical consumption.

Furthermore, taking a closer look at the collectors' field, the first measure is the regulation of the fed-in water volume flow. The current value of 0.45 m^3/h seems too high, and can possibly not be completely evaporated, lowering the collectors' yield and the obtainable motive steam pressure. Huge optimization opportunities arise for the collectors' circuit. However, collectors' yield during operational days show a good performance, even in partly cloudy days.

Part of the low available cooling power on the hottest days was due to a high condenser temperature. This means that the cooling tower power was not enough to provide the necessary cooled water. A separate static analysis of the cooling tower could be recommended in order to improve this performance.

Focusing on the heat storage, an acceptable deviation of +/- 0.9 K was accepted due to the temperature sensors performance. This has a huge variability of the results presented (ΔT always below 2°C). However, the results of the heat and cold storage tanks are successful, as they provided the support it was expected from them.

Regarding the overall costs, the solar collectors represent the most expensive investment. It would be interesting to analyze a similar cooling facility driven with another cheaper heat source (such as waste heat) and to calculate its economic feasibility.

To sum up, the results of the operation of the Steam Jet Ejector (SJEC) facility seem to be positive with a huge optimization potential and improvement opportunities. It is a positive experience as it furthers to the development of new technological efficient solutions that contribute to energy consumption reductions and to protect the environment by reducing the emission of CO2 to the atmosphere.

Annex I: Weather conditions in Karlsruhe

In this Annex a brief introduction of average figures of the Weather of Karlsruhe. The main idea is to show to which conditions the facility was designed.

The first graphic shows the daily high and low temperatures (daily average – not considering hourly development) throughout a year for Karlsruhe. It is clear that the hottest period is during summer, between the end of May and the beginning of August. This timeframe is where the solar cooling facility is required (summer operation from 4th May to 5th October in 2015, covering all possible hot days).

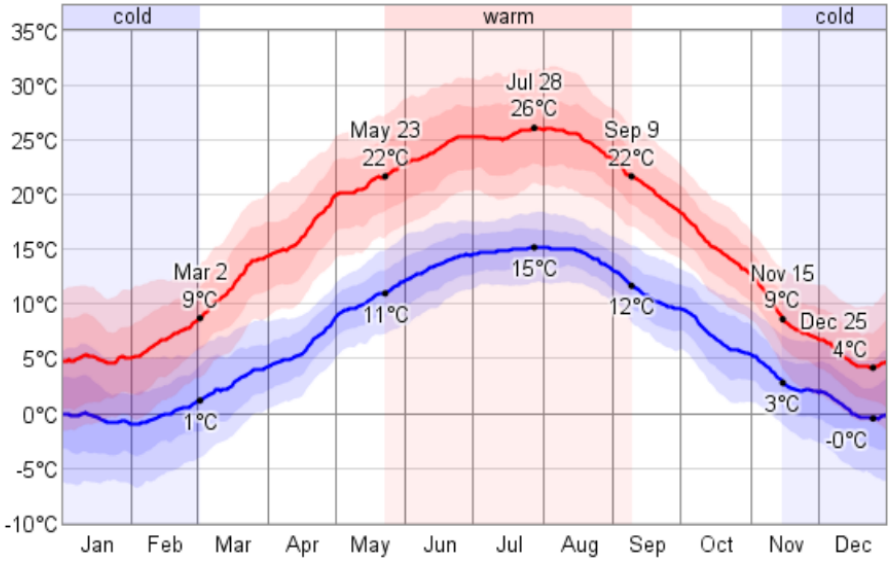

The daily average low (blue) and high (red) temperature with percentile bands (inner band from 25th to 75th percentile, outer band from 10th to 90th percentile).

Figure AI-1: High and low temperatures

Due to the fact that the facility is designed to work with 100% renewable energy (solar collectors) the timeframe of solar radiation is considered a variable of utmost importance, especially on the hottest days, when the cooling load is high. The following figure shows the sunrise and sunset time for a complete year (2012).

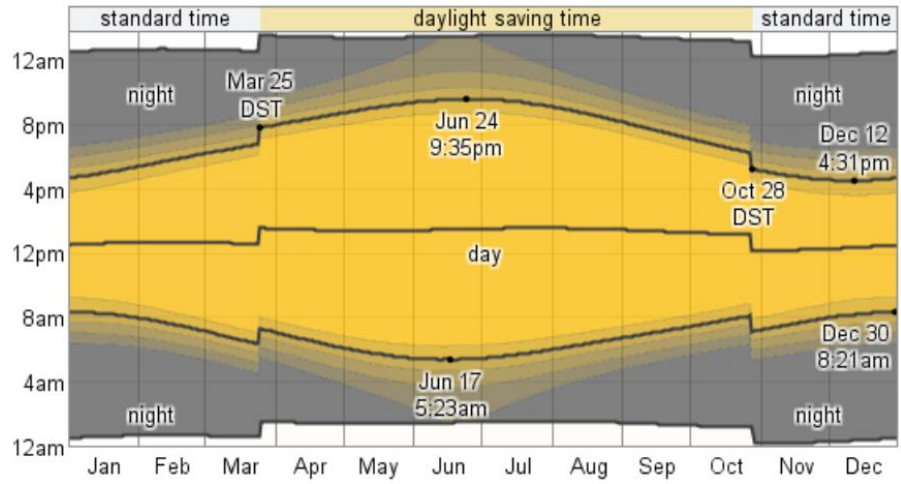

Figure AI-2: Available daylight

Moreover, another factor that strongly influences the available solar radiation on collectors' surface is the cloud cover. The next figure shows the daily average throughout a year:

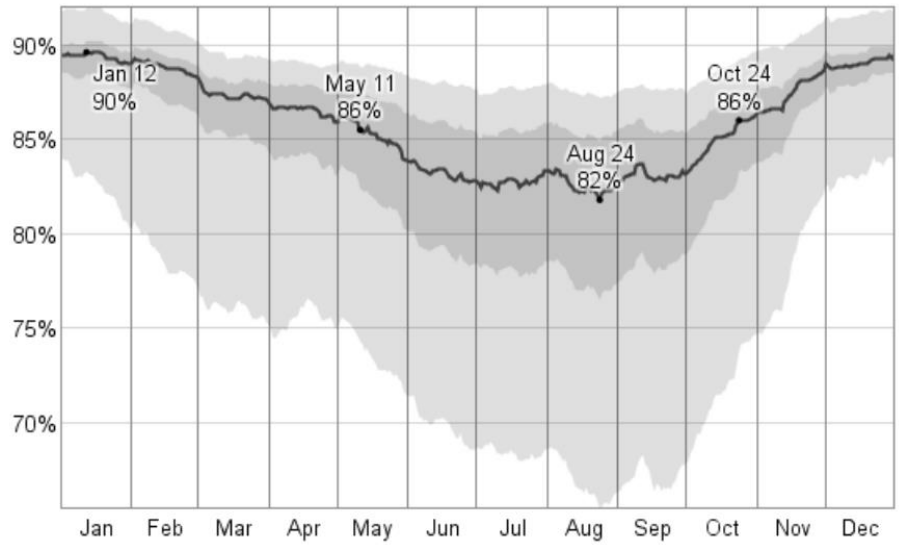

Figure AI-3: Median Cloud Cover

As the heat should be rejected to the atmosphere, Weather conditions play an important role also for heat rejection through the cooling tower. The selected method is a wet cooling tower, so that the Wet Bulb Temperature of the atmospheric air is the cooling limit. In order to determine it, not only the outside temperature but also the relative humidity is taken into account. Here the daily averages are shown.

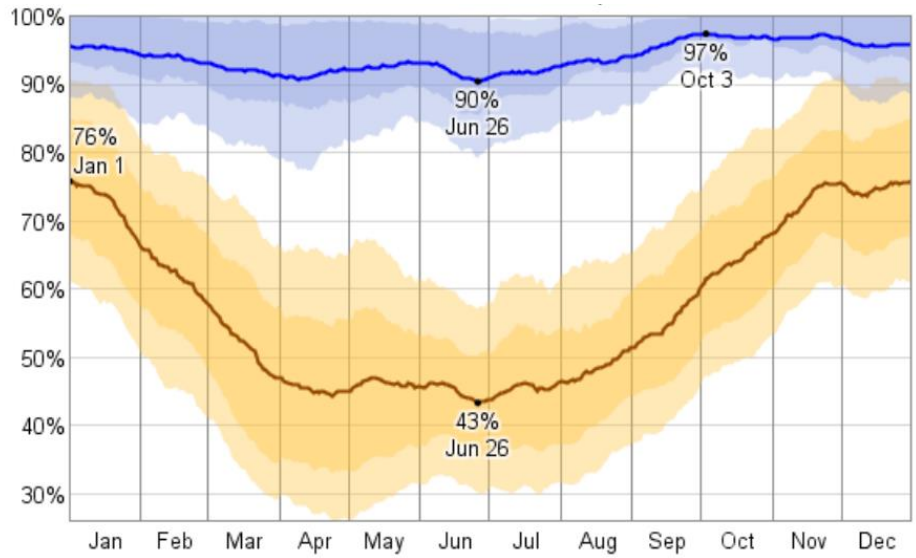

Figure AI-4: Relative Humidity

The last variable considered of importance is the wind speed, as it usually plays a role for the relative humidity and the feel like outside conditions. The daily average velocities are shown in the next figure.

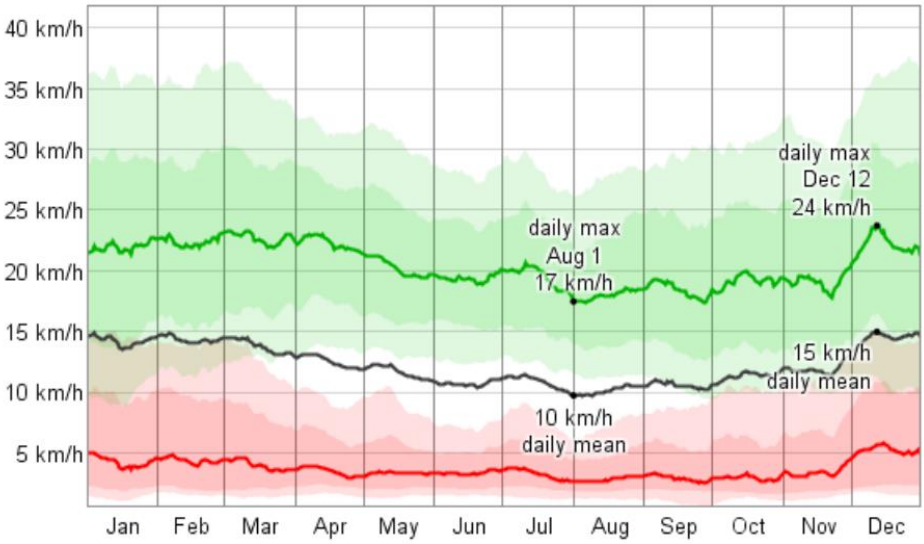

Figure AI-5: Wind Speed

Annex II: Further calculations – Detailed description

In this annex the calculations performed by the software and auxiliary spreadsheets will be developed.

II.1 – Software calculations

The software developed performs calculations within a time and date range given by the user. The programming was made in Visual Basic (VBA) as explained in the corresponding chapter of the thesis. This annex will cover all the calculations performed that were not explained during the thesis.

II.1.1 – Cold and Heat Storage

As stated in chapter 3, both heat and cold storage are developed as latent heat storage due to the high energy stored and released during the phase change of the selected material. The first step is therefore to calculate the capacity of the mentioned storage.

To calculate the capacity of both storages, an enthalpy balance of the flowing water was carried out.

- Constant Cp and Density are assumed constant, since there is no change of state. Values of 998 Kg/m^3 and 4,182 KJ/(Kg K) are taken.
- For heat storage, the pressure at the inlet has several measurement errors, but should be similar as the outlet pressure in the theory. So it was decided that the outlet pressure will be applied in both sides. Volume flow is given by FIR-W-7-1 (modules 1-2-3) and FIR-W-7-2 (modules 4-5).
- For cold storage, the heat exchanger WT4 represents the charging and discharging phases. The independent circuit is not taken into account. The volume flow is given by FIR-KW-1-1.
- Tank losses are calculated through auxiliary spreadsheet and added manually.
- Peak temperatures were defined through maximum and minimum values for the 2015 summer measurements. Cold Storage (Outlet – TIR-KW-2-1; Inlet – TIR-KW-1-1) from 6°C to 15°C and Heat Storage (Outlet 1-2-3 – TIRC-W-8-7; Inlet 1-2-3 – TIRC-W-7-1; Outlet 4-5 TIRC-W-8-6; Inlet 4-5 – TIRC-W-7-2; Pressure PIR-W-8-1) from 60°C to 150°C.

The equation that defines the heat capacity is the following:

$$Q\ [KWh] = \frac{m\left(C_p.\Delta T + \ h_{vap,sol}\right)}{3600} \qquad \text{(AII.1)}$$

With the properties stated in the annex, **the calculated capacities are 50 KWh for the Heat Storage and 25 KWh for the Cold Storage**. The charging and discharging phases are obtained with a calculation of the instantaneous heat flow [KW] per minute, and performing an integration of the curve obtained (adding the values, obtaining the final value in KWh). This can be observed in the presented graphics throughout the work.

II.1.2 – Pumps and Jet Ejector

The pumps and jet ejector play obviously a major role in the facility. Both are grouped in this subsection because of their measurement variable. Ejectors 1 and 2 and pump 6 are measured as working time in seconds. Pumps 7 and 16 are added manually also by working time in seconds. Then it is simple to calculate the hours of service of these devices. The rest of the measured pumps (2, 3, 4, 5, 14 and 17) are measured through percentage of nominal speed. It is considered that, when the pump is running above 20% is turned on, counting the working time in minutes.

What is important for the pumps is to distinguish between the hydraulic and electric power. Hydraulic power is necessary to calculate the energy provided to the circuit. Electric energy is necessary to measure the electrical energy consumption of the facility and to elaborate the correspondent KPIs (this will be treated in the next subsection). According to the definition in the book "Fluid Mechanics" from Frank M. White (2009), the formula to obtain the hydraulic power is

$$P_{hyd}[KWh] = \frac{\rho\ g\ \dot{Q}\ H}{3600} \qquad \text{(AII.2)}$$

with all the variables in SI Units. As main assumption, the density of water remains constant and the volume flow is obtained through the law of affinity of turbomachinery (D = constant)

$$\frac{\dot{V}_2}{\dot{V}_1} = \frac{n_2}{n_1} \cdot \left(\frac{D_2}{D_1}\right)^3 \qquad \text{(AII.3)}$$

The pumps' data was obtained through catalogues and manufacturer information. A summary of these is shown in the next table.

Pumpe	Hersteller	Typ	S in Watt (Motor)	P in Watt (Pumpe)	cos phi mit	Nenndrehzahl Motor in 1/min	Q m^3/h	Förderhöhe	Hyd Leistung [KW]
P2	Grundfos	MG100LC2-28FF215-H3	3688.23	**3000**	0.85	2910	15.80	14	0.6
P3	Grundfos	CRIE10-03 X-FGJ-I-F-HQQE	2353.86	**2200**	0.90	3501	12.10	30	1.0
P4	Grundfos	CRN90-3 M-F-G-E	3666.41	**3000**	0.74	1445	45.00	16	1.9
P5	Grundfos	CRN32-3 MB-F-G-E	2724.34	**2200**	0.74	1445	16.00	12.6	0.5
P14	Grundfos	CRN1-19 X-FGJ-G-E-HQQE	206.08	**250**	0.70	1410	12.10	20	0.6
P17	Grundfos	MG100LC2-28FF215-H3	3688.23	**3000**	0.85	2910	15.00	30	1.2

Table AII-1: Pump properties

II.1.3 – Useful Cold, Electric Energy and Heat Rejected

These mentioned values play a big role in the performance of the facility, as they are needed to calculate some the most important KPIs. Therefore, they should be calculated very carefully.

The useful cold delivered to the building is calculated through the heat exchanger WT1. The energy output is calculated with the following equation

$$Q\ [KWh] = \sum_{i}^{n} \frac{\rho\ \dot{V}_i . Cp . \Delta T_i}{3600} \qquad \text{(AII.4)}$$

summing n times (minutes of timeframe observed) the volume flow (in m3/h – FIR-KW-1-1) the constants density and Cp (assumed constant for water between 5°C and 30°C) and the temperature difference (outlet – TIR-KW-8-1; inlet – TIR-KW-2-1; in °C) of the heat exchanger. This value is key to determine the COP of the facility.

In addition, the same concept applies for the heat rejected through the cooling tower. As it was stated before in the work, the cooling subsystem of the cooling tower will not be analyzed in detail. So the heat rejected will be considered by the heat exchanger WT2, with data from the cooling subsystem. The same formula applies to this case. The volume flow is measured by FIR-RKW-1-1, temperature outlet is measured by TIR-RKW-1-1 in °C, and inlet by TIR-RKW-2-1 also in °C.

Regarding the electrical energy consumption, there were considered mainly pumps and the cooling tower fan. In this case, the electrical power of the pumps is relevant. For the pumps' consumption, the pump speed is taken following the affinity law:

$$\frac{P_2}{P_1} = \left(\frac{n_2}{n_1}\right)^3 . \left(\frac{D_2}{D_1}\right)^5 \qquad \text{(AII.5)}$$

Moreover, the electrical power of the pumps is given by the apparent power (S), which results of the division of the active power (P) and the cos φ (see Table AII-1 for the pumps' data). Summing all the instantaneous power per minute (affected by the rotational speed ratio) and arranging the units, the electrical energy consumption can be obtained:

$$EE\ [KWh] = (\sum_{i}^{n} \frac{P_i.}{\cos\varphi_i\ .\ 60}) \ +\ EE_{Add} \qquad \text{(AII.6)}$$

EE_{add} represents additional electrical consumption, added manually in the main screen of the software. For example, it has been studied that the standby mode of the facility consumes 0.6 KWh of energy per hour. Other consumptions that are not considered in the calculations can also be added. The electrical energy consumption results of utmost importance to calculate the COP_{el}.

II.1.4 – Motive Heat

The motive heat of the facility is obtained in this work through a complete energy balance of the facility. The figure AII-1 illustrates the energy flows taken into account for its calculation. The heat and cold losses calculation is developed in a further annex, but is necessary to correctly perform this calculation. Assumptions made:

- Pipe losses only in cold (evaporator – building) and hot side (solar collector – steam drum). Tank losses calculated with daily average temperatures (see detailed calculation in annex II.2).
- All other heat calculations were shown in previous subsections.

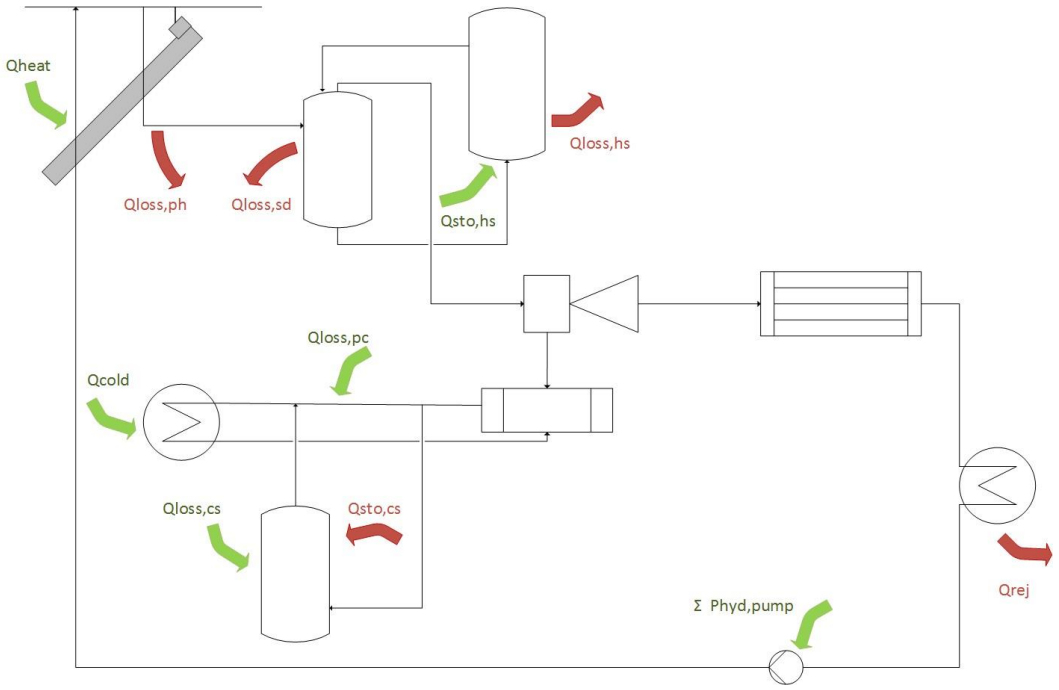

Figure AII-1: Heat Flows involved

The only pump in the figure represents the sum of the hydraulic power of all pumps in the circuit. The heat balance is done following the thermodynamic principles developed in chapter 2. The equation for the heat balance is then:

$$Q_{heat} = Q_{rej} - Q_{cold} - \sum_{i} P_{hyd,pump} + \sum_{j} Q_{loss,j} + Q_{sto,hs} - Q_{sto,cs} \quad \text{(AII.7)}$$

The development of the lost heat in pipes and storage will be developed in the corresponding annex. The value of motive heat is obtained in KWh (units coherent).

II.1.5 – Median Vapour Fraction in Solar Collectors

The median vapour fraction in collectors is calculated through a sequence of equations, presented in the following series. The assumption of saturated vapor produced in the collectors should be made. Daily average values for the sensors are considered, plus the total motive heat for the timeframe studied.

$$\dot{m}_{VRK} = \dot{V}_{VRK} . \rho(T, p) \text{ at FIR-W-15-1, TIRC-W-15-1 and PIRC-W-11-1}$$

$$h_{evap} = h_{sat,vap} - h_{sat,liq} \text{ at TIR-W-1-1}$$

$$h_{col,in} = h\,(T, p) \text{ at TIRC-W-15-1 and PIRC-W-11-1}$$

$$h_{col,out} = h\ (T, p) \text{ at TIRC-W-1-1 and PIRC-W-11-1}$$

$$\dot{m}_{vap} = \frac{Q_{heat}.3600 - \dot{m}_{tot}\ .(h_{col,out} - h_{col,in})}{h_{evap}} \quad \text{(AII.8)}$$

$$x = \frac{\dot{m}_{vap}}{\dot{m}_{tot}} \quad \text{(AII.9)}$$

II.2 – Heat and Cold losses in the facility

The losses included where the pipe losses (cold side, from condenser to building feed, and hot side, from solar collectors to steam drum) and storage losses (steam drum, heat and cold storage modules). The procedure was developed following the publication of Kumana and Kothari "Predict storage tank heat transfer precisely" (1982) and the further work from Enrico Lammers "Heat loss calculation in a vertical and horizontal storage and in a pipeline" (2011).

The importance of the losses calculation relies in the value of the motive heat through a heat balance. The balance of the losses is shown in the next equation:

$$\sum_j Q_{loss,j} = Q_{loss,cs} + Q_{loss,pc} - Q_{loss,sd} - Q_{loss,ph} - Q_{loss,hs} \quad \text{(AII.10)}$$

Each of the calculations is performed in a separate spreadsheet, and after that added manually to the input sheet in the software. The necessary data to perform the calculations are:

- Average temperatures in the timeframe selected
- Properties of the facility (pipes, materials, insulation, tank sizes)
- Properties of fluids involved (water, vapor, PE-8110, Water-Paraffin mixture)

As an introduction, the heat transfer through a wall can be modelled like the figure

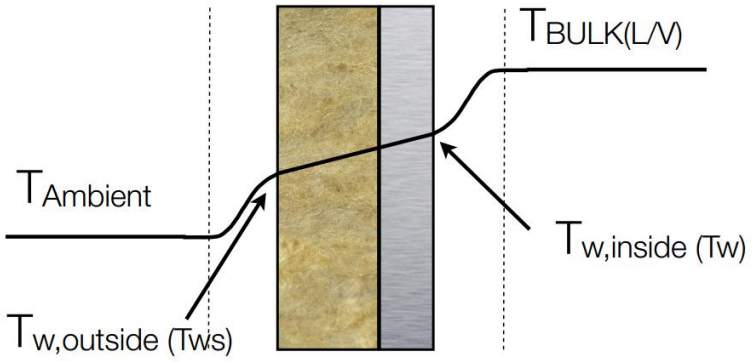

Figure AII-2: Heat transfer through an insulated wall

The heat flow is assumed to remain constant through all layers. In the inside and outside of the tank/pipe the heat is transferred via convection, while through the walls the conduction governs the heat transfer. Following Fourier's Law of conduction and Newton's law of convection, it results for tanks

$$\dot{Q}_{tank}[KW] = \frac{\sum(U\,.A\,.\Delta T)}{1000};\, U\ \left[\frac{W}{m^2\,.K}\right] \qquad \text{(AII.11)}$$

With U as the overall heat transfer coefficient, calculated like this

$$U_{tank,tot} = \left[\sum_i \frac{1}{h_i}\right]^{-1};\, h_i\ \left[\frac{W}{m^2.K}\right] \qquad \text{(AII.12)}$$

For each layer and fluid involved. In the case of the pipe losses, the U value is calculated per meter like the following formula

$$\dot{Q}_{pipe}[KW] = \frac{\sum(U\,.L.\Delta T)}{1000};\, U\ \left[\frac{W}{m\,.K}\right] \qquad \text{(AII.13)}$$

As the different diameters involved have an influence on the U value calculated

$$U_{pipe,tot} = \left[\frac{1}{h_{int}.\pi\,.D_i} + \frac{t_m}{h_{met}.\pi\,.D_{m,met}} + \frac{t_{ins}}{h_{ins}.\pi\,.D_{m,ins}} + \frac{1}{h_{air}.\pi\,.D_o}\right]^{-1} \qquad \text{(AII.14)}$$

Fouling coefficient and wind factor were neglected due to the lack of precise information. Also radiation is not considered in this study. The precise step by step can be followed in the previous mentioned papers.

II.2.1 – Heat loss in steam drum

Since the heat loss flux is different when there is liquid water in the steam drum and when there is vapour, the heat losses depend on the water level of the tank. Therefore, four different heat fluxes can be identified:

1. Q_d –through the dry wall
2. Q_w – through the wet wall
3. Q_r - through the roof
4. Q_b - through the bottom

It is important to make clear that it was assumed that the structure that holds the tank in its position can be neglected and the cylinder heads are semispherical. As stated in Kumana and Kothari (2009), "Since the Prandtl and Grashof Numbers occur repeatedly in the film heat-transfer coefficient equations and remain relatively unchanged for all the conditions of interest, let us first calculate their values".

$$Gr = \frac{L^3 \,.\, \rho^2 . g \,.\, ß \,.\, \Delta T}{\mu^2} \; ; Pr = \frac{Cp \,.\, \mu}{k} \qquad \text{(AII.15); (AII.16)}$$

- μ viscosity [Kg/m.s]
- β coefficient of volumetric expansion [1/K]
- k Thermal conductivity [W/m.K]
- ρ Density [Kg/m^3]
- g Gravity acceleration [m/s^2]
- L Length in contact with fluid [m]
- Cp Constant pressure specific heat [KJ/Kg.K]
- ΔT Temperature difference between surface and fluid [K]

Changing the values for L and ΔT for each case, the Gr is calculated and then the Nusselt number as well (variable in different situations). The surface temperature is always initially assumed as the average between the outside temperature and the inside (water or vapor, in every case). The h (convection coefficient) is calculated with the following formula

$$h_{conv,i} = \frac{Nu_i \,.\, k}{L_i} \left[\frac{W}{m^2 K}\right] \qquad \text{(AII.17)}$$

The values of The corresponding equations for the Nusselt number are

$$Nu_d = Nu_w = Nu_{air,w} = 0.138 \,.\, Gr^{0.36} . (Pr^{0.175} - 0.55) \qquad \text{(AII.18)}$$

$$Nu_r = 0.27 \,.\, (Gr.Pr)^{0.25} \qquad \text{(AII.19)}$$

$$Nu_b = Nu_{air,r} = 0.14 \,.\, (Gr.Pr)^{0.33} \qquad \text{(AII.20)}$$

The conduction coefficients for wall and insulation are obtained with the formula

$$h_{cond,i} = \frac{k_i}{t_i} \left[\frac{W}{m^2 K}\right] \qquad \text{(AII.21)}$$

with t_i the thickness of the material. Therefore, the U-value is calculated with every correspondent h coefficient. The next table illustrates and example of the variables involved (numbers calculated for an example day):

Summary				
Coefficient (W/m^2 K)	Dry wall	Wet wall	Roof	Bottom
Coefficient of vapour at wall, h_{vw}	0.00	-	-	-
Coefficient of liquid at wall, h_{Lw}	-	136.45	-	-
Coefficient of vapour at roof, h_{Vr}	-	-	0.00	-
Coefficient of liquid at the tank bottom, h_{Lb}	-	-	-	134.90
Coefficient of outside air at roof, h'_{Ar}	-	-	0.40	0.40
Coefficient of outside air at wall, h'_{Aw}	1.43	1.43	-	-
Conduction coefficients for metal wall $\mathbf{h_M}$	9000	9000	9000	9000
Conduction coefficients for insulation $\mathbf{h_I}$	1.65	1.65	1.65	1.65
Overall coefficient, U_d, U_w, U_r, U_b	0.002	0.761	0.001	0.321

Table AII-2: Summary of h coefficients for steam drum

With the calculations of the different U_i, the surface temperatures in each case are recalculated (manual iteration) in order to optimize the final value. Obviously the surface temperature will be in between the outside air temperature and the inner fluid one. The equations to optimize this are

$$T_{i,outsurf} = \left(\frac{U_i}{h_{i,air}}\right)\left(T_{fluid} - T_{air}\right) + T_{air} \qquad \text{(AII.22)}$$

$$T_{i,insurf} = T_{fluid} - \left(\frac{U_i}{h_{i,fluid}}\right)(T_{fluid} - T_{air}) \quad \text{(AII.23)}$$

The assumed value for the surface and the calculations above are iterated until its difference approaches to zero. The final U-values are then obtained. Finally, the surfaces are calculated for every case and the lost heat flux is obtained.

$$A_{w,wet} = 2.\pi\,.D\,.L_w\,; A_{w,dry} = 2.\pi\,.D\,.(L - L_w) \quad \text{(AII.24) ; (AII.25)}$$

$$A_{r,b} = \frac{\pi.D^2}{2} \quad \text{(AII.26)}$$

The heat loss in KW is calculated through equation AII.11. The total energy lost in the studied timeframe results of multiplying the KW and the amount of hours.

$$Q_{lost}[KWh] = \dot{Q}_{loss}[KW].hs \quad \text{(AII.27)}$$

Steam drum presents a total height of 1.3 m and a diameter of 0.6 m. Wall thickness is 5 mm and of steel (k = 45 W/m.K). Insulation is 20 mm thick. The water level is calculated through daily average. The variables involved are:

- Outside temperature - TIR-Aussen
- Steam Drum inside temperature - TIRC-B1-1
- Steam Drum inside pressure - PIR-B1-1
- Steam Drum Water level - FMP-B1-1.

II.2.2 – Heat and cold loss in pipes

The procedure to calculate the losses in pipes is similar to the presented one in II.2.1 for the steam drum, with some adjustments to pipes, following the work from Kumana and Kothari (2009). The only difference between both cases rely on the outside and inside flow temperatures, while the general procedure of calculation remains the same.

The first step is, like last subsection, the calculation of the Grashof and Prandtl adimensional numbers, through equations AII.15 and AII.16. Also it is necessary to obtain the Nusselt

number to calculate the h coefficients for convection (equation AII.17). For this application, the calculation of the Rayleigh and Reynolds numbers is necessary:

$$Ra = Gr \,.\, \mathrm{Pr} \;\; ; \;\; Re = \frac{\rho \,.\, v \,.\, D}{\mu} \qquad \text{(AII.28) ; (AII.29)}$$

In consequence, the Nusselt number for flowing water and outside air are:

$$Nu_{flow} = \frac{\left(\frac{f}{8}\right).(Re - 1000)Pr}{\left[1 + 12.7\,.\left(\frac{f}{8}\right)^{\frac{1}{2}}\left(Pr^{\frac{2}{3}} - 1\right)\right]} \qquad \text{(AII.30)}$$

$$Nu_{air} = \left\{\frac{0.6 + \left(0.387.Ra^{\frac{1}{6}}\right)}{\left[1 + \left(\frac{0.559}{Pr}\right)^{\frac{9}{16}}\right]^{8/27}}\right\}^{2} \qquad \text{(AII.31)}$$

With *f* as the Pethukov Single Relation as

$$f = [0.79\,.\ln(Re) - 1.64]^{-2} \qquad \text{(AII.32)}$$

As for the conduction coefficient in the pipe wall and insulation, again equation AII.21 applies. The final calculation for the U_{pipe} was shown in equation AII.14.

Coefficient (W/m^2 K)	Values
Coefficient of flowing liquid at pipe wall (convection), $h_{wi,f}$	7469.18
Outside coefficient of air at pipe wall (convenction), h'_{wo}	3.47
Conduction coefficient for metal wall $\mathbf{h_M}$	22500
Conduction coefficient for insulation $\mathbf{h_I}$	1.74
Overall coefficient,U_{tot}	1.16

Table AII.3: Summary of h coefficients for pipes

An example of the final coefficients is presented in the table AII.3. The total heat loss in KW is obtained by equation AII.13 and the total energy loss is the same as presented for the steam drum (eq. AII.27). The length considered for the pipe losses are 70 m for each pipe between evaporator and cold heat exchanger (140 m in total of cold pipes) and 100 m between solar

collector field and steam drum (hot pipes). The insulation thickness is 19 mm for cold pipes and 50 mm for hot pipes (Armacell), with a k value of 0.033 W/m.K. Flow speed is assumed 2 m/s. Pipe material is metal (k = 45 W/m.K) with 2 mm thickness and outer diameter 60.3 mm (DN 60). The variables involved are:

- Outside temperature – TIR-Aussen
- Water flow through WT1 – FIR-KW-1-1
- Temperature cold water inflow – TIR-KW-2-2
- Temperature cold water outflow – TIR-KW-8-1
- Temperature hot water outflow – TIR-W-1-1
- Water flow hot – FIR-W-15-1

II.2.3 – Heat and cold loss in storages

The last loss calculation involves the heat and cold storages. Since the storage is performed with PCM Materials, the content is sometimes in solid phase and others in liquid. When the PCM is in solid phase, the wall temperature is assumed as the same as the PCM temperature, eliminating the inner convection component. Therefore, what is only left is the conduction through walls and insulation and the convection component of the outside air.

The first step is, like stated above, the calculation of the Grashof and Prandtl adimensional numbers, through equations AII.15 and AII.16. Also it is necessary to obtain the Nusselt number to calculate the h coefficient for convection (equation AII.17). The used Nusselt numbers are AII.18 for walls, AII.19 for roof and AII.20 for the bottom. Conduction coefficients are obtained with eq. AII.21. The general procedure is identical to the one in II.2.1 (steam drum), but without the inner convection component.

One difference in this case is related to the surfaces. Since the hot storage is not a cylindrical vessel, the surfaces are calculated with length, width and height. The rest of the process remains the same as in II.2.1. The variables involved are:

- Cold Storage → V = 1.5 m^3. L = 1.9 m. D = 1 m. t = 5 mm.
- Heat Storage Module 1 & 2 → H = 0.3 m, L = 0.6 m, W = 0.18 m. t = 0.003 m.

- Insulation thickness = 100 mm
- Outside temperature – TIR-Aussen
- Cold Storage → Average of TIR-B5-1, TIR-B5-2 and TIR-B5-3
- Heat Storage Module 1 → inflow TIRC-W-7-1
- Heat Storage Module 2 → inflow TIRC-W-7-2

Annex III: Temperature sensors calibration

The calibration of two temperature sensors was performed the 29th March 2016, in the container where the facility operates. Due to some inconsistencies in the Heat Storage presented in this work, the selected sensors belong to this part of the facility.

The calibrated sensors are TIRC-W-7-1 and TIRC-W-8-7, which are respectively inlet and outlet from the Heat Storage module 1. These are resistance thermometers, which means they calculate the temperature through an electric current in two wires, which provide different ohmic resistance due to the temperature shift. The procedure was carried out with a Fluke 9142 calibrator (hot oil), which can provide exact temperatures. The device can be seen in the next picture.

Figure AIII-1: Calibration device.

Figure AIII-2: Temperature sensors

The last figure presents both examples of temperature sensors. The taken W-7-1 and W-8-7 have a short rod. To provide a better sensing, it was first attempted the measurement with an auxiliary longer rod. However, in the first attempt it was observed that the stabilization period could last hours, making impossible the correct measurement. In this case, the calibration device was set to 80°C and it took the sensor 50 minutes to raise from 33.0 to 33.9°C the measured value, without stabilizing. The fact that the rod is very short can set an influence in the measurements, and creates an error that is not measurable. Therefore, it was decided that focus would be made in the difference between the calibration curves of both sensors and the distance between the exact temperature and the measured ones.

The procedure is to set the calibration device in set temperatures (every 20°C) in the usual working range (80-150°C) and observe the returned value of the sensor, after a short temperature stabilization period (about 15 minutes for the calibration device and another 15 minutes for the sensor per measurement). Besides, an initial measurement of 20°C was also taken. With the measured values, the trendlines for both sensors are drawn, in order to obtain the calibrations' curve of both thermometers. The next figure shows both curves and the obtained values.

Gerät	W-7-1	W-8-7
20	19.3576	19.5746
80	74.4791	74.5659
100	93.0121	93.0555
120	114.4965	114.8003
140	133.4635	133.8107
150	142.7083	142.8385

Table AIII-1: Measured values for calibration

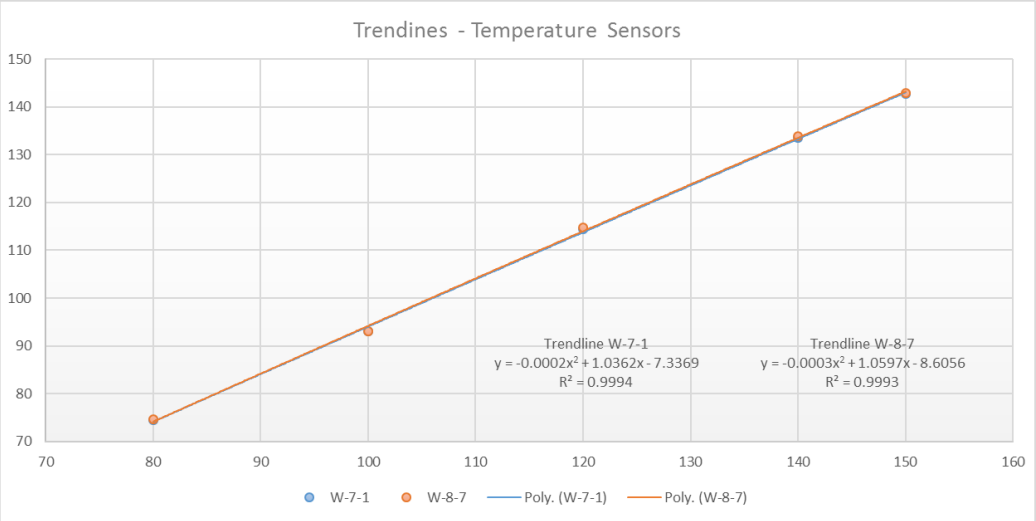

Figure AIII-3: Trendline for temperature sensors

As it can be easily seen, both curves respond to very similar equations, with a very high R^2 value. In addition, a distance of almost 6/7 degrees under the exact set value is observable for each measurement. Conclusions over this subject are discussed in the main content of the thesis.